Recombinant stimulus-responsive biomaterials to target hypoxic/ischemic perinatal brain injury

by

Abdullah K. Alshememry

A thesis submitted in partial fulfillment of the requirements for the degree of

Doctor of Philosophy

in
Pharmaceutical Sciences

Faculty of Pharmacy and Pharmaceutical Sciences
University of Alberta

Abstract

Hypoxic-ischemic brain damage (HIBD) is a major concern during the neonatal period, and can result in chronic neurological complications arising from damage to the term newborn brain. Delivering drugs at the site of brain injury is thought to be crucial to the advancement of therapy for these patients. Herein is described a two prong approach for the development of nanoparticles for delivering drugs at the site of injury, namely, temperature sensitive elastin-like polypeptide based nanoparticles and identification of peptides that can target the penumbra and ischemic core observed in HIBD. It is thought that this approach will lead to the development of a platform system that can facilitate the release of drugs at the site of injury with multiple triggers so as to prevent off-target toxic side-effects.

A novel family of leucine-containing, short, marginally soluble elastin-like polypeptides (ELPs) were developed. In order to successfully express and purify these ELPs, a novel purification method needed to be developed. The protocol described here is designed as an extension of existing techniques for creating elastin-like polypeptides. It allows for the expression and purification of ELP constructs that are poorly expressed or have very low transition temperatures. DNA concatemerization has been modified to reduce issues caused by methylation sensitivity and inefficient cloning. Linearization of the modified expression vector has been altered to greatly increase cleavage efficiency. The purification regimen is based upon using denaturing metal affinity chromatography to fully solubilize and, if necessary, pre-

concentrate the target peptide before purification by inverse temperature cycling (ITC). This protocol has been used to express multiple leucine-containing elastin-like polypeptides, with final yields 10-20 times greater than reported yields for comparable constructs. Due to the relative hydrophobicity of the tested constructs, even compared with commonly employed ELPs, conventional methods would not have been able to purify these peptides.

In order to better understand the effect of drug loading on the size and self-assembly and disassembly behaviour of ELPs particles, multiple ELPs with varying concentrations and guest amino acid hydrophobicity were tested. The results revealed that the nature and hydrophobicity of the guest amino acid position and the ratio of ELP:drug have a significant effect on the particle size and the assembly/disassembly behaviour, and the drug entrapment efficiency was increased as the hydrophobicity of the guest amino acid increased. Moreover, less ELP when mixed with the drug seemed to increase the entrapment efficiency as well. Therefore, a certain balance needs to be maintained between the ELP:drug ratio and the choice of the guest amino acid as together they will have an effect on the phase transition behaviour of ELPs and its drug entrapment capability.

Peptides that can specifically interact to the injury within the brain are promising agents for a variety of applications, including site-specific drug delivery that reduces toxic side effects and diagnostics platforms for the injured brain. To this end, in vivo phage display technology was employed where several unique peptides that home preferentially to ischemic tissue were

identified. Peptides preferentially homing for the vasculature of penumbra (PHP1), ischemic core (CHP1) and healthy brain tissue (HHP1 and HHP2) were the most frequently occurring sequences after three rounds of biopanning. These identified vasculature-homing peptides may have significant clinical applications as targeting moieties to be used in diagnostic and ligand-mediated targeted therapy for hypoxic-ischemic perinatal brain injury.

Preface

This thesis is an original work done by Mr. Abdullah Alshememry. All animal experiments were carried out in accordance with protocols that were evaluated and approved by the University of Alberta Animal Care and Use Committee. Portions of Chapters 1 – 4 were published in (Bahniuk, M.S., **A.K. Alshememry**, and L.D. Unsworth, *High-yield recombinant expression and purification of marginally soluble, short elastin-like polypeptides*. Biotechniques, 2016. 61(6): p. 297-304.). M.S.B and A.K.A had equal contribution to the work in this manuscript. A.K.A and M.S.B contributed to the development, analysis, and execution of the experiments. M.S.B., A.K.A., and L.D.U. wrote and edited the manuscript. Portions of chapter 1 was published in (**Alshememry, A.K.**, S.S. El-Tokhy, and L.D. Unsworth, *Using Properties of Tumor Microenvironments for Controlling Local, On-Demand Delivery from Biopolymer-Based Nanocarriers*. Curr Pharm Des, 2017. 23(35): p. 5358-5391.). A.K.A and S.S.E contributed equally to the manuscript. L.D.U. provided the scope for the review and editorial assistance in the writing of the manuscript and necessary revisions.

This work is dedicated to
my parents, my beloved wife Nada, and my little princess Jood

Acknowledgments

I would like to first and foremost thank my supervisor Dr. Larry D Unsworth for giving me the opportunity to join his research group. I am grateful for his guidance, encouragement and unconditional support throughout the years of my PhD. Also for his mentorship that allowed me to become an independent researcher I am today.

I would like to extend my thanks to my other main supervisor Dr. Ayman El-kadi for his advice and constant support and for giving me the opportunity to be an interdisciplinary student co-supervised by himself and Dr. Larry Unsworth and working at the national institute for nanotechnology labs. I would also like to acknowledge my supervisory committee member Dr. Dion Brocks.

Special thanks to Dr. Markian Bahniuk, together we built the Markdullah team that I will always remember, thanks for his friendship, unconditional support and for spending the time teaching me many techniques in the lab.

I would like to acknowledge our collaborators Dr. Jerome Yager and Ed Armstrong, thank you for your assistance and guidance.

I would like to thank the faculty administrative staff for their support and help during my stay in the program, with special thanks to Mrs. Joyce Johanson.

I would also want to thank current and previous Unsworth lab members, and summer students for their friendship, advice, and continuous support. Special thanks to Mehdi Ghaffarisharaf for teaching me the phage display technique, Suleiman Saleh for helping me with the HPLC method validation, and for Scott Elgersma and Tiffany Grad for helping me in data collection.

I would like to acknowledge the friends and colleagues I have made during my time at UofA and NINT, namely Ahmed Mahmoud, Eman Osman, Valentyna Semenchenko, Cathy de Guzman, Angela Brigley and Bethany Borst for sharing their expertise and for the endless support.

Finally, I am grateful for the generous financial support I received from King Saud University to pursue my graduate studies in Canada.

Table of Contents

List of Tables

List of figures

List of abbreviations

HIBD	Hypoxic-ischemic brain damage
ELPs	Elastin-like polypeptides
ITC	Inverse temperature cycling
CP	Cerebral palsy
CBF	Cerebral blood flow
BBB	Blood brain-barrier
ROS	Reactive oxygen species
DNase	Deoxyribonuclease
XO	Xanthine oxidase
NOS	Nitric oxide synthase
NOX	NADPH oxidases
ETC	Electron transport chain
MPT	Membrane permeability transition
MPTP	Membrane permeability transition pore
dATP	Deoxyadenosine triphosphate
Apaf-1	Apoptotic protease activating factor-1
MOMP	Mitochondrial outer membrane permeabilization
MMPs	Matrix metalloproteinases
GC	Glucocorticoids
DEX	Dexamethasone
VEGF	Vascular endothelial growth factor
BDNF	Brain derived neurotrophic factor
Epo	Erythropoietin
IGF-1	Insulin like growth factor 1
GCSF	Granulocyte colony-stimulating factor
RBC	Red blood cell
SHp	Stroke homing peptide
PLGA	poly(lactic-co-glycolic acid)
LEX	Lexiscan
CTX	Chlorotoxin
RDL	Recursive directional ligation
MBP	Maltose binding protein
NPs	Nanoparticles
Ni-NTA	Nickel-nitrilotriacetic acid matrix
DLS	Dynamic light scattering
PDI	Polydispersity index
E.E.	Encapsulation efficiency
HPLC	High-performance liquid chromatography
CCA	Common carotid artery

IP	Intraperitoneal
pfus	Plaque forming units
PCR	Polymerase chain reaction
IMAC	Immobilized metal ion affinity chromatography
KCC2	K^+-Cl^- co-transporter 2
PHP1	Penumbra-homing peptide 1
CHP1	Core-homing peptide 1
HHP1	Healthy-homing peptide 1
HHP2	Healthy-homing peptide 2
HUMMR	Hypoxia up-regulated mitochondrial movement regulator protein
SGLT1	Sodium/glucose cotransporter 1
BMPRII	Bone morphogenetic protein receptor type-2
EAAs	Excitatory amino acids
EPP	Exchangeable phosphate pool
NAA	N-acetylaspartate
NO	Nitric oxide
NTP	Nucleoside triphosphate
OFRs	Oxygen free radicals
RIPostC	Remote ischaemic postconditioning

1.   Introduction

Portions of this chapter have been published in:

1. Bahniuk, M.S., **A.K. Alshememry**, and L.D. Unsworth, *High-yield recombinant expression and purification of marginally soluble, short elastin-like polypeptides*. Biotechniques, 2016. 61(6): p. 297-304.

2. **Alshememry, A.K**., S.S. El-Tokhy, and L.D. Unsworth, *Using Properties of Tumor Microenvironments for Controlling Local, On-Demand Delivery from Biopolymer-Based Nanocarriers*. Curr Pharm Des, 2017. 23(35): p. 5358-5391.

1.1. Perinatal hypoxic/ischemic brain injury

Perinatal hypoxic-ischemic brain damage (HIBD) is the major cause and contributor to global infant mortality and morbidity [1]. Neonatal HIBD incidence in the United States is 2–3 per 1000 live births, with evidence of incidences being up to 6 per 1000 live births [1]. Studies in underdeveloped countries have reported an even higher incidence rate up to 26 per 1000 live births [2]. As a result, between 20%–25% of term newborn infants die early during the neonatal period and about 25% of those that survive suffer from permanent neurological disabilities.

Perinatal brain injury is responsible for a spectrum of mental and physical disabilities, the most characteristic and the primary outcome recognized as cerebral palsy (CP) [3, 4]. CP is a chronic, developmental disorder of the brain most predominantly characterized by abnormal muscle tone, reflexes, or motor development and coordination, but also encompassing cognitive and mental health disorders [3, 5]. Currently, CP has no cure, and the only available management is through physiotherapy and other rehabilitation services [6-8]. Over the past 40 years, the epidemiology of CP has not changed and remains at 1-3/1000 of term births, despite obstetric and neonatal innovations [9, 10]. Developmental disabilities resulting from CP and HIBD are chronic and lifelong and a huge emotional and financial burden for those affected, their families, and society. The estimated lifetime cost per CP affected individual is nearly $1.2 million [11, 12].

1.1.1. Pathophysiology

The Hypoxic-Ischemic Core and Penumbra HIBD

Hypoxic ischemic encephalopathy is considered to be an evolving process: following a cytotoxic cascade, apoptotic and necrotic damage develops in certain brain regions dependent on

the severity and duration of HIBD, both of which show positive correlations [13]. In young children, the severity of HIBD is highly associated with adverse neurodevelopmental outcome [14, 15]. To provide the most optimal treatment, it is crucial to discern the injury or recovery phases, as well as the location of the injury.

HIBD-related injuries are comprised of two parts: the core and the penumbra, both of which are critical to gaining a better understanding of HIBD evolution [16]. The core is the part of the brain where oxygen deprivation and cessation of blood flow take place first, resulting in necrotic cell death caused by depletion of nutrients and ATP. On the other hand, the penumbra - the hypo-perfused brain region which surrounds the core - contains not only dying but also living neurons. As a result of the aforementioned characteristics, the penumbra is considered to be a desirable target area in terms of HIBD therapy [16]. Theoretically the presence of living cells, oxygen and survival substrates could be harnessed to prevent necrotic core's expansion and neuronal death, consequently strengthening the capability of penumbral cells to overcome HIBD injury. Targeting the penumbral region is therefore crucial for functional recovery following hypoxic ischemia [17].

Very limited research has been done examining the HIBD core and penumbra. However, the core has been found to have both necrotic and apoptotic cells after HIBD, while the penumbra is mainly composed of apoptotic cells [18, 19]. Studies indicate that apoptosis increases to maximum levels 24 hours after HIBD, with a decline recorded after 48, 72 hours and 7 days following the injury, with cleaved caspase-3 being higher in the core as compared to the penumbra at all time points [19]. Furthermore, caspase-3 activation is also observed in adults following ischemia-reperfusion injuries as early as 3 hours into recovery, with a more pronounced activation occurring at the 24 hours mark. In addition, it has also been suggested that

caspase-independent mechanisms associated with cell death tend to be favored in areas marked by reduced perfusion such as in the core [20]. These data bring forth the suggestion that apoptotic and non-apoptotic damage happens differently in the penumbra and the core after the occurrence of HIBD/ischemic stroke and may even last for months if left untreated. The overall process of how the different phases of HIBD and therapeutic agents related to it differentially affect the core requires further investigation.

Initiation of the pathophysiological cascade in HIBD

The etiology of HIBD is associated with multiple maternal, placental and fetal conditions, each having different clinical manifestations. These include conditions like chronic maternal hypoxia (e.g., chronic utero-placental hypoxia or cardiopulmonary arrest), nuchal cord, pre-eclampsia, umbilical cord knotting and prolapse, shoulder dystocia and premature placental detachment [21]. Perinatal hypoxia is initiated after an interruption of oxygenated cerebral blood flow (CBF) to the fetus, which triggers systemic as well as cellular level responses. Constant energy supply to the fetal brain in the form of ATP is critical and any interruption as a result of HI injury will, as a response, trigger the uncontrolled release of excitatory neurotransmitters (e.g. glutamate), which mark the beginning of the ischemic cascade. Triggering the ischemic cascade has an extremely damaging effect on neurons and other brain cells at the cytoplasm and mitochondrial levels. Moreover, the damage also causes blood brain-barrier (BBB) disruption and activation of inflammatory responses. An illustration of the different pathological phases of cerebral injury after cerebral HI is shown in (Figure 1.1).
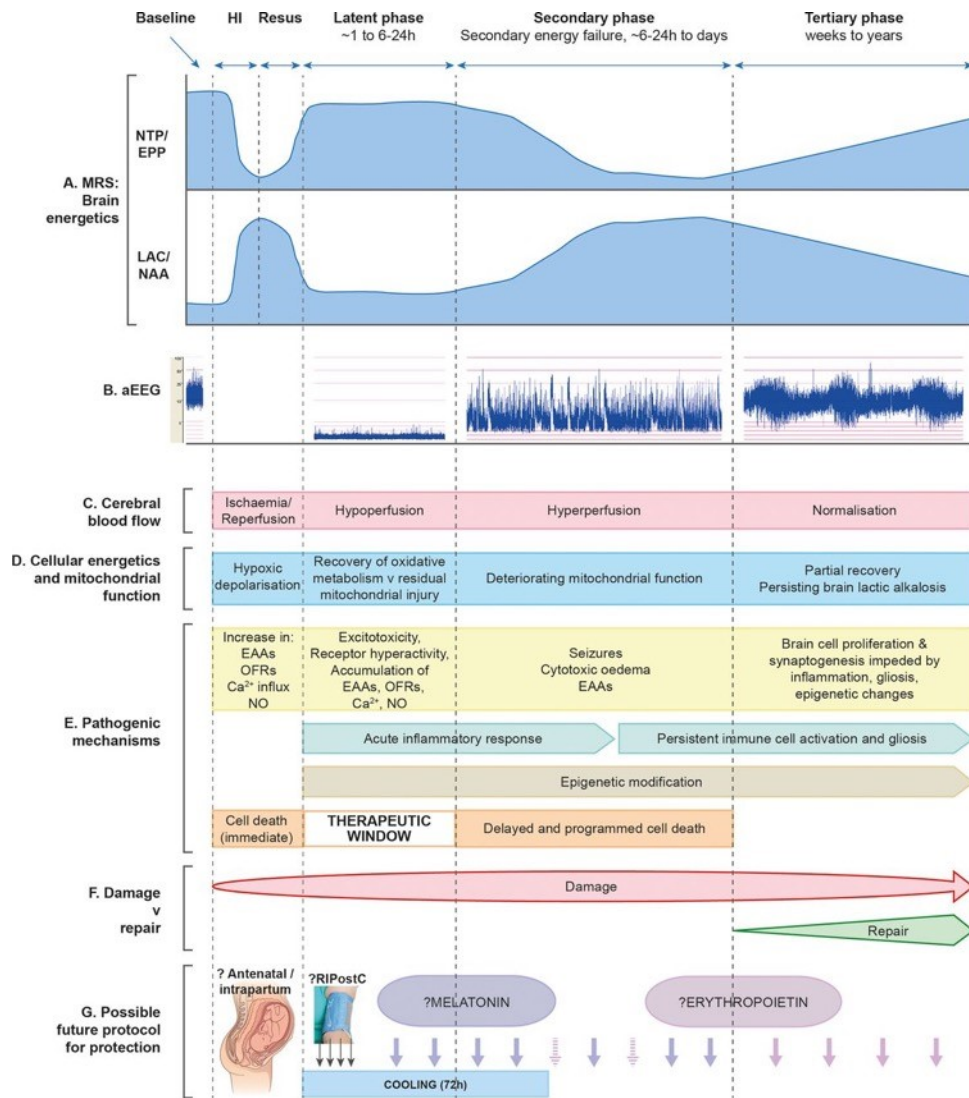
Figure 1. 1 Schematic diagram illustrating the different pathological phases of cerebral injury after cerebral HI. *Reprinted from (Hassell et al, 2015) [22] with permission from BMJ Publishing Group Ltd.*

The primary phase (acute HI), latent phase, secondary energy failure phase and tertiary brain injury phase are shown. (A) Magnetic resonance spectra showing the biphasic pattern of NTP/EPP decline and lactate/NAA increase during primary and secondary phases following HI insult. Persisting lactic alkalosis is shown in tertiary phase. (B) Amplitude-integrated EEG showing normal trace at baseline, flat tract following HI, burst-suppression pattern in latent phase, emergence of seizures in secondary phase and normalisation with sleep–wake cycling in tertiary phase. (C) Following HI, there is a period of hypoperfusion associated with hypometabolism during latent phase, followed by relative hyperperfusion in secondary phase. (D) Cellular energetics and mitochondrial function are reflected in the biphasic response shown on magnetic resonance spectroscopy (A), with a period of recovery in latent phase followed by deterioration in secondary phase. There is partial recovery in tertiary phase. (E) The most important pathogenic changes are shown for each phase, including generation of toxic free radical species, accumulation of EAAs, cytotoxic oedema, seizures and inflammation. Cell lysis occurs immediately following HI, while programmed cell death occurs in secondary phase; latent phase provides a therapeutic window. Persisting inflammation and epigenetic changes impede long-term repair. (F) Damage is maximal in the secondary phase, but persists into the tertiary phase as inflammation and gliosis evolve. (G) In the future, neuroprotective treatments are likely to involve a 'cocktail' of therapies to be administered intrapartum, in the latent phase to prevent secondary energy failure and through secondary and tertiary phases to offset evolving damage. HI, hypoxia-ischaemia; EAAs, excitatory amino acids; EPP, exchangeable phosphate pool; NAA, N-acetylaspartate; NO, nitric oxide; NTP, nucleoside triphosphate (this is mainly ATP); OFRs, oxygen free radicals; RIPostC, remote ischaemic postconditioning.

5

Excitotoxicity

The stage of gestational development primarily determines the metabolic rate of the fetal brain, which in order to meet its metabolic demands, neural tissue metabolizes lactate, ketone bodies and glucose [21]. In comparison to the developed brain, the fetal brain can adapt to the energy loss during HI and, therefore, have higher capacity to tolerate HIBD [22]. However, at prolonged HIBD, it loses the ability to adapt and eventually becomes susceptible to injury as a result of critical energy (i.e. ATP) depletion. At prolonged HIBD, cellular equilibrium is disrupted as a result of depletion of ATP and failure to maintain ionic gradients. As a response, neurons depolarize and release glutamate into the synaptic cleft [23]. Elevated extracellular glutamate concentrations result in excitotoxicity in neurons and other cells, specifically glial progenitor cells, those expressing glutamate receptors. Overactivation of glutamate receptors NMDA, AMPA, kainic acid and metabotropic glutamate receptors (i.e. C G-protein-coupled receptors that indirectly activates ion channels on the plasma membrane through a signaling cascade) causes a cytotoxic cellular influx of calcium ions [24]. Increased intracellular calcium levels in neurons and glial progenitor cells result in a series of events including the production of reactive oxygen species (ROS), activation of calcium-dependent proteases, lipases and deoxyribonuclease (DNase), cytotoxic edema, oxidative stress, mitochondrial dysfunction and the stimulation of cellular death pathways [25-29].

Oxidative stress

Oxidative stress tends to play a vital role in the pathophysiology of hypoxic ischemic encephalopathy since the developing brain contains a high amount of unsaturated fatty acids, susceptible to lipid peroxidation, metals catalyzing free radical reactions as well as low antioxidant concentrations [30]. The subsequent production of ROS and increased sensitivity to

oxidative stress cause severe damage to nucleic acids, proteins and lipids, resulting in DNA degeneration, protein oxidation, and lipid oxidation, respectively. In the event of hypoxic ischemic encephalopathy, there are numerous sources of ROS that include xanthine oxidase (XO), nitric oxide synthase (NOS), and NADPH oxidases (NOX), as well as arachidonic acid (12/15 lipoxygenase) and the mitochondrial electron transport chain (ETC). In cases of treating hypoxic ischemic encephalopathy, nitric oxide synthase (NOS) is usually targeted, with strategies aimed at inhibiting or ablating the activity of NOS invariably being neuroprotective in HIBD animal models [31].

Mitochondrial dysfunction

Mitochondria have numerous functions, such as regulation of intracellular calcium, generation of ATP, pro-cell death signaling, ROS production and biosynthesis of lipids, nucleotides and amino acids. Over the years, there have been extensive reviews on the role mitochondria play in hypoxic ischemic encephalopathy [32-34]. Generally, mitochondrial contribution to secondary brain injury in the event of HI occurs through a process termed as apoptosis which involves the regulation of the pathways associated with cell death. Cellular apoptosis following HI is activated through both intrinsic (for instance, in response to the presence of damaged DNA and mitochondrial dysfunction) and extrinsic pathways (such as response to cell death receptors like Fas and tissue necrosis factor-α) and involves the release of proteins associated with pro-cell death from mitochondria.

In cases of hypoxic ischemia, a number of processes, among them p53 activation, excitotoxicity, DNA damage, ROS production and altered mitochondrial function tend to influence the activity of pro-apoptotic Bcl-2 proteins (Bax, Bid etc.) In turn, this leads to the development of Bax-dependent mitochondrial membrane permeability transition (MPT) [35, 36].

Moreover, excessive generation of ROS by mitochondria due to the leakage from the ETC can oxidize cardiolipin - the inner mitochondrial membrane phospholipid, promoting mitochondrial membrane permeability transition pore (MPTP) opening and subsequent release of cytochrome-c. Together with deoxyadenosine triphosphate (dATP), the released cytosolic cytochrome-c interacts with the apoptotic protease activating factor-1 (Apaf-1), hence forming the apoptosome which then cleaves and ends up activating pro-caspase-9 [37]. After its activation, caspase-9 in turn activates caspase-3, which is considered to be the primary proteolytic enzyme responsible for dismantling cells during the process of apoptotic cell death. Pro-apoptotic factors, including endonuclease G, apoptosis-inducing factor, and Smac/DIABLO, are released into the cytosol in the event of further alterations to the mitochondria such as mitochondrial outer membrane permeabilization (MOMP) [38, 39]. Generally, the translocation of both Endo-G and the apoptosis-inducing factor to the nucleus mediates the fragmentation of chromatin, while DIABLO/Smac, on the other hand, interacts with apoptosis inhibitors in an effort to reduce their overall reactions on activated caspases. Tumor necrosis factor (cell death receptor) signaling mainly stimulates the extrinsic pathway by activating caspase-8, which in turn activates other caspases, including caspase-3. It is also critical to note that, in response to HI activation, other cell death pathways can occur such as autophagy, necrosis, ferroptosis and necroptosis. Furthermore, these pathways can also be activated in response to cellular disturbances such as ROS production, calcium influx, depletion of cellular energy, mitochondrial dysfunction and adenosine monophosphate-activated protein kinase cell signaling.

Inflammation

Over the years, extensive reviews on inflammatory response as a result of hypoxic ischemic encephalopathy have been conducted [40, 41]. When an injury occurs in immature

brain due to hypoxia-ischemia, innate immunity response occurs within a few minutes [42]. Concerning this, the innate response process starts with the activation of microglia present in the cerebral parenchyma; this action is usually accompanied by a systematic inflammatory response which is not only mediated by the infiltration of circulating monocytes but also T-cells, as well as neutrophils into the brain. The activated microglia, in turn, develop a number of attributes that resemble those of a macrophage. Some of these attributes include the production of cytokines, antigen presentation and development of phagocytic properties as well as the release of matrix metalloproteinases (MMPs). The integrity of the BBB is compromised by release of microglia and the consequent activation of MMPs, an action that tends to promote the invasion of peripheral leukocytes, which consequently proceeds further into the cerebral parenchyma further aggravating/worsening the existing cerebral injury.

The accumulation of amoeboid microglia inside the periventricular matter is considered as the hallmark of HIBD, which leads to production of inflammatory cytokines such as TNF-α ,IL1-β, and NO, inclusive of other ROS [42]. Together, they increase the toxic effects associated with the ischemic cascade present in not only the glial progenitor cells but also in neurons as well as the cerebral vasculature. When this occurs, neuroprotective support is provided to not only the neurons but also astrocytes primarily through the release of superoxide, glutathione and increased synaptic uptake of glutamate, inclusive of maintenance of ion channel gradients. However, to a great extent the all these protective mechanisms can be easily overrun. Similar to microglia, astrocytes also become highly hyper-activated as a result of pro-inflammatory cytokines, ROS, and dying neurons. The pro-inflammatory cytokines IL-6, TNF-α, IL-1α/β and INF-γ are also released by the activated astrocytes which, in turn, increases cell death pathways induced by HI such as in the case of apoptosis. Furthermore, chemokines secreted by astrocytes

also aggravate tissue injury by attracting existing systemic immune cells which then penetrate into the affected tissues.

1.1.2. Current clinical intervention

Window of opportunity

Brain injury following hypoxic-ischemic insult is a complex process that keeps evolving over hours to days, which allows for a unique window of opportunity for therapeutic interventions using neuroprotective treatment. The "therapeutic window", also referred to as "reperfusion window", which is the interval after reperfusion (within 6 hours of insult), during which an intervention might be efficacious in limiting the extent and severity of the brain damage. Because the cascade of biochemical and histopathological events after a brain injury can last from days to weeks after the insult is triggered, this may provide a "therapeutic window of opportunity" for therapeutic rescue intervention. However, at this time such interventions are restricted by inadequate knowledge of the time and duration of therapeutic window in newborns [11, 43].

Therapeutic hypothermia

Post-ischemic hypothermia, also referred to as the cooling of the head or full body, is the only existing independent intervention to have effectively conferred lasting neuroprotection in not only animals but also human infants with HIBD as a rescue therapy [44]. Studies have shown that therapeutic hypothermia post HI has caused significant reductions in mortality and neurological disability by 18 months of age [45]. Hypothermia is the gold-standard rescue therapy for HIBD, especially if administered within the window-of-opportunity of 6h of HIBD diagnosis after birth [45]. Although numerous drug interventions have proven to be effective in the reduction of HIBD in both cell and animal models, none of them has been as successful as

hypothermia in human neonates [46]. Unfortunately, the neuroprotection offered by hypothermia is incomplete and does not extend to the full extent of injury, nor does it benefit neonates with severe HIBD (>50% of the brain damage with large cores that extend into the gray matter), with approximately 22% of cooled neonates still presenting with mortality and neurological disabilities [11, 45]. These obstacles emphasize why more adequate and effective treatments must be developed for newborns suffering from HIBD.

1.1.3. Pharmacological neuroprotective agents

Anti-excitotoxic agents

Targeting the early phases on injury by blocking the excitotoxicity and oxidative stress was one of the earliest pharmacological strategies for injured newborn brains' neuroprotection. However, many of these attempts were not successful. The main reason was it is nearly impossible to block normal developmental processes (i.e. glutamatergic signaling), without damaging the brain. Therefore, pharmacological therapies directed towards blocking the NMDA receptor caused an increase, rather than decrease in neuronal death [47]. However, magnesium sulfate, a pharmacological agent used to stop preterm labor, showed beneficial effects even though it blocked the NMDA receptor [48]. Recent clinical trials have supported the use of magnesium before birth [48]. In a number of hospitals in Australia and New Zealand, 1062 women carrying fetuses at ages younger than 30 weeks gestation were given 8 mmol $MgSO_4$ for up to 24 h following a loading infusion of 16 mmol. Although there were no observed significant differences in mortality rate or CP in survivors, significant reduction in substantial gross motor dysfunction and combined death or substantial gross motor dysfunction in the $MgSO_4$ group was observed [48]. In another clinical study from the United States, results showed that moderate or

severe CP was significantly less likely to occur among children exposed to MgSO4 compared to placebo [48].

Another possible anti-excitotoxic agent is xenon, a well-known anesthetic noble gas. It inhibits NMDA receptors and has been shown to be an effective agent against hypoxic-ischemic insult both *in vitro* and in a number of *in vivo* models [49]. Compared to other NMDA antagonists, xenon lacks the dopamine-releasing properties and as a result it does not cause increased apoptotic cell death. The major limitations of xenon are that it is expensive and needs a specialized delivery system [73]. Because of these factors, alternative therapies are currently being evaluated.

Anti-oxidants

Targeting oxidative stress using anti-oxidants has proven to be efficacious in both preterm and term brain injury states. Allopurinol, a xanthine oxidase inhibitor, is currently being investigated as a potential treatment of HIBD. It has shown neuroprotective effects in postnatal day 7 rats after HI [50] and 3-7 days old piglets [51] whether after being administered alone or in combination with hypothermia [52]. However, in clinical trials it was not seen to improve short or long term outcome in a small trial after birth asphyxia [53]. It was hypothesized that allopurinol needed to be given before reperfusion injury set in. Clinical trials are now underway to evaluate efficacy when given to mothers at risk of intrauterine hypoxia. A randomized blinded clinical study included 53 pregnant women with evidence of fetal hypoxia assessed by lactate levels in the umbilical cord blood, S-100B (a short-term biomarker of brain injury) and non-protein-bound-iron concentrations [54]. After given either placebo or allopurinol at birth, fetuses/newborns with therapeutic allopurinol/oxypurinol concentrations in cord blood had lower

plasma levels of the S-100B. Treatment of birth asphyxia with allopurinol is promising; however, long term outcomes of this treatment are yet to be proven to be beneficial.

An alternative promising anti-oxidant agent for treatment of hypoxic brain injury is melatonin, an endogenous neuroendocrine moiety that is well known for its role in modulating the circadian rhythm. Along the injury cascade, melatonin targets apoptosis, oxidative stress, inflammation and mitochondrial failure [55-57]. The lack of significant side effects in children and term neonates is considered its major benefit of use. With a good safety profile and low toxicity risks, melatonin holds substantial promise in management of newborns with HIBD [58, 59]. However, larger randomized clinical trials need to be conducted to validate its beneficial use.

Anti-inflammatory agents

As mentioned above, melatonin has multiple targets in the injury cascade including inflammation and therefore is a promising choice for manipulating inflammation [60]. Glucocorticoids (GC) are powerful anti-inflammatory compounds frequently administered in clinical medicine [61]. The clinically available glucocorticoid drug dexamethasone (DEX) is a synthetic adrenocorticosteroid with glucocorticoid activity known to be involved in the hypothalamic-pituitary-adrenal gland pathway [62]. DEX, as the other GCs, is characterized by a carbon skeleton with four fused rings (Figure 1. 2). Chemical alterations by functional groups at various positions on the rings of the steroid molecule lead to synthetic analogous of cortisol. These analogues could have increased mineralocorticoid and/or glucocorticoid activities. DEX is approximately 30 times as potent as hydrocortisone, the main human endogenous GC [63]. A brief comparison between several GC agents including their anti-inflammatory potencies is shown in (Table 1. 1). The anti-inflammatory effect of DEX is complex, but primarily via

inhibition of inflammatory cells and suppression of expression of proinflammatory cytokines and mediators [64].
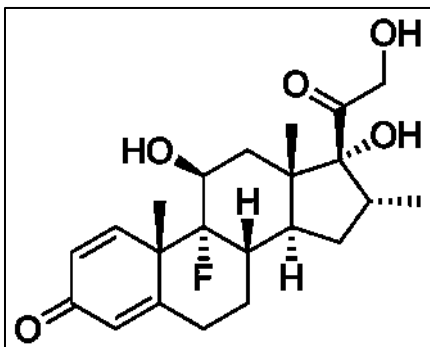
Figure 1. 2 Chemical structure of DEX

In patients with vasogenic edema, a common complication after cerebral ischemia, glucocorticoids have been used [65]. Moreover, because of its immunosuppressive properties, DEX may also prevent inflammation-related complications [66]. It was shown in previous *in vitro* studies that DEX reduces hypoxia-induced hyperpermeability of endothelial cells and decreases the expression of vascular endothelial growth factor (VEGF), a known factor to enhance endothelial permeability [67].

However, results of clinical trials showed contradicting results about the beneficial effects of DEX, when given to stroke patients [68]. This has led to great controversy, given the beneficial effects of corticosteroids observed in individual patients [65]. This contradiction is mainly caused by differences in dosing, timing, method of administration, and severity of the model used between these studies. Even though the long-term effects of DEX are controversial,

it is possibly the best choice in conjunction with clinical hypothermia treatment especially in devastating inflammatory diseases (e.g. HIBD after neonatal stroke). Glucocorticoids demonstrate serious side effects in large dosages, especially at prolonged administration [69].Therefore, new targeting strategies are needed for enhancing drug delivery efficiency of DEX at the site of the injury while minimizing its toxic side effects.

Table 1. 1 Comparison of relative corticosteroid potencies

	Approximate equivalence dose in mg	Relative anti-inflammatory potency[a]	Biological half-life (h)
Hydrocortisone	20	1	8-12
Prednisone	5	3.5-4.0	12-36
Prednisolone	5	4.0	12-36
Methylprednisolone	4	5.0	12-36
Dexamethasone	0.75	30	36-72
Betamethasone	0.6	30	36-72
Deflazacort	7.5	2.5-3.5	24-36

Adapted from SMA Anti, *et al.* [63].
[a]Relative to hydrocortisone (cortisol).

Growth Factors

Numerous growth factors have vital roles during fetal and postnatal brain development. The effects of some growth factors, such as brain derived neurotrophic factor (BDNF), are largely restricted to the brain. Others like erythropoietin (Epo), VEGF, insulin like growth factor 1 (IGF-1), and granulocyte colony-stimulating factor (GCSF) have crucial somatic effects in addition to their role in neurodevelopment. Currently, Epo is the closest to clinical use and the best studied for this purpose. Exogenously administered Epo exhibits neuroprotective effects in several animal models through the activation of anti-apoptotic, anti-oxidant and anti-inflammatory pathways as well as by stimulation of angiogenic and neurogenic events [70, 71]. Animal studies support the efficacy and safety of Epo as a therapeutic intervention for a variety

of brain insults [72]. Results from a very recent randomized controlled trial suggests that multiple high doses of Epo may provide neuroprotection against brain injury in term infants [73].

1.1.4. Potential drug delivery strategies

A series of pathological changes following the HIBD affects drug delivery. Limited blood supply to the local ischemic tissue, in addition to the BBB and the shrinkage of the extraocular space limit the administered drug from accessing the injured brain tissue. Some other pathological changes after HIBD may have the potential to be utilized as a smart sensitive trigger for controlled drug release. This will result in the development of site-specific drug delivery vehicles. One of these pathological changes is lower intracellular pH value in the ischemic brain tissue (pH<6.75) as a result of a metabolic shift towards anaerobic glycolysis, which produces lactic acid as a byproduct [74]. Another pathological change is the upregulation of matrix MMP-2 and MMP-9 after cerebral ischemia. These enzymes are involved in accelerating matrix degradation, disrupting the BBB, increasing the infarct size [75]. Also, it is well-known that after the reperfusion, toxic ROS are increased in the ischemic region, resulting in injury of neurons [76]. Therefore, from a pharmaceutical drug delivery design perspective, stimuli-responsive drug delivery systems can be designed to incorporate ROS, pH, or MMP-sensitive groups for controlled, on-demand release into the ischemic region.

An example of an ROS-responsive nanocarrier for stroke-specific delivery of a neuroprotective agent was reported by *Lv, Wei et al* [77]. The dextran biopolymer core was modified with an ROS-responsive boronic ester and a red blood cell (RBC) membrane shell in addition to a stroke homing peptide (SHp) inserted. Their results showed increased systemic circulation of the neuroprotective agent, enhanced active targeting of the ischemic area in the MCAO rats, and reduced ischemic brain damage [77].

Few studies have the utilized the immediate upregulation of MMPs after cerebral ischemia by incorporation of MMP-responsive domains for controlled release [78, 79]. For example, by using poly(lactic-co-glycolic acid) (PLGA) nanoparticles loaded with lexiscan (LEX) joined with particle surface modification using chlorotoxin (CTX), an MMP2-senstive peptide, a significant increase in the delivery efficiency of nanoparticles to the ischemic brain compared to the therapy alone was achieved [78].

There are almost no studies that have been published utilizing the potential of pH-responsiveness release strategy in the ischemic brain environment. However, many pH sensitive peptide-based biopolymers have been explored for use in targeting the tumor microenvironment which is directly translatable to brain targeting [80, 81]. Recent peptide-based pH-responsive nanocarriers are summarized in Table 1.2.

Table 1. 2 Illustrative examples of peptide-based nanocarriers that are able to respond to pH for targeting the tumor microenvironment.

Nanocarrier	Therapeutic/diagnostic payload	*In vitro* cell line(s)/ *In vivo* model	Characteristics	Ref.
Peptides; poly(L‑histidine)				
Micelles	Andrographolide	Hep3B and MDA-MB-231 cells / Hep3B tumor-bearing mice	Andrographolide-loaded micelles made of GA and pHIS conjugated with PEG and PGLA forming GA-PEG-pHIS-PLGA. Drug release undder acidic pH was attributed to the increased hydrophilicity of the system caused by partial pHIS protonation	[82]
Micelles	Doxorubicin	HeLa cells	DOX-loaded micelles made of poly(itaconic acid)–PEG–folate–pHIS released drug due to pHIS protonation, causing micelle disassembly, and lysosomal membrane disruption.	[83]
Micelles	PTX	MCF-7 and SKOV-3 cells / MCF-7 tumor-bearing mice	PTX-loaded micelles made of pHIS-b-sbPEI coated mPEG and pH sensitive PSDM released at acidic pH as PSDM loses its negative charge and dissociates from the micelle exposing the cationic surface of	[84]

			pHIS-b-sbPEI. When in the acidic endosomal compartment, pHIS is protonated, the micelle dissociates and the drug released	
Micelles	Docetaxel	MCF-7 and SGC-7901 cells	DOX-loaded cell penetrating peptides-functionalized PEG-PLA micelles were made with arginine-glycine $(RG)_5$ and histidine-glutamic acid $(HE)_5$ were conjugated to PEG or PLA to generate different micelles. Enhanced DOX release at acidic pH was attributed to protonation of (HE) which resulted in swelling of the micelles and larger amount of DOX release	[85]
Liposomes	Doxorubicin	C6 and U87-MG cells / U87-MG orthotopic tumor-bearing nude mice	DOX-loaded $H_7K(R_2)_2$ modified liposomes were prepared. Enhanced DOX-release was attributed to to the ionization of pHIS in the $H_7K(R_2)_2$ peptide and switching from hydrophobic to hydrophilic at acidic pH	[86]
Peptides; poly(L-lysine), poly(L-histidine)				
Polymersomes	Doxorubicin	CT26 cells	A series of triblock copolymers vesicles composed of $p(PEGA)_{30}$-b-$p(Lys)_{25}$-b-$p(His)_n$ were synthesized. Increased DOX release at acidic pH was triggered by the destabilization of the vesicle bilayers, caused by the protonation of the pHIS	[87]
Peptides; STP (SKDEEWHKNNFPLSP)				
Liposomes	Doxorubicin	HUVEC cells	DOX-loaded liposomes functionalized with pH sensitive STP peptide and at acidic pH, the Lys-Asp-Glu-Glu forms an α-helix resulting in improved recognition ability and enhance penetrability.	[88]
Peptides; poly(L-glutamic acid) PGA				
Chimaeric Polymersomes (pepsomes)	Doxorubicin	RAW 264.7, MCF-7/ADR and L929 cells	DOX-loaded copolymers PEG-b-poly(L-leucine)-b-poly(L-glutamic acid) showed greater release of DOX at acidic pH due to protonation of COOH groups changing PGA from random to α-helix. This change disrupts pepsome structure and causes drug release.	[89]
Peptides; Collagen				
Biopolymer-drug conjugate; dendrimer/collagen hybrid gels/DOX	Doxorubicin	MCF-7 and MDA-MB-231 / SL4-GFP	Dendrimer-DOX prodrugs embedded in collagen gel showed enhanced release under acidic conditions due to cleavage of hydrazone linkages.	[80]

(prodrug)		tumor-bearing nude mice		
Peptides; Elastin or Elastin-like biopolymers				
Biopolymer-drug conjugate; ELP NPs/DOX	Doxorubicin	Colon cancer; *In vitro*: C26 cells In vivo: BALB/c	DOX-conjugated *via* hydrazone linker to elastin-like polypeptide (ELP) fused with tumor-homing peptide (F3) and a cysteine-rich segment (C8) showed DOX release at low pH from degraded hydrazone.	[90]
Micelles	Iodine-125 (^{125}I)	HCT-15 tumor-bearing nude mice	Iodine-125 (^{125}I)-loaded and histidine-rich ELPs were designed to undergo phase-transition and disassembly in response to drop in pH of the medium	[91]
Peptides; Silk or silk-like biopolymers				
Silk NPs	Doxorubicin	MCF-7/WT and MCF-7/DOX cells	DOX-loaded silk NPs showed enhanced DOX release at acidic pH.	[92]
Hydrogels	Doxorubicin	MDA-MB-231 / MDA-MB-231 tumor-bearing nude mice	DOX-loaded silk hydrogels showed enhanced DOX release at acidic pH by adjusting the hydrogel silk content	[93]

1.2.   Elastin-like polypeptides

Elastin-like polypeptides (ELPs) are protein-based biopolymer analogs of mammalian elastin [94]. The general architecture of an ELP sequence is any number of repeats of the amino acid sequence valine-proline-glycine-X-glycine (VPGXG), where X can be any amino acid except proline [95]. In elastin, this guest amino acid is typically valine. What makes this particular sequence of amino acids distinct is that it can reversibly undergo self-assembly in reaction to changes in local environmental factors such as temperature and salinity [94].

The exact environmental conditions under which ELPs change their conformation and solubility depend greatly upon the number of repeats of the VPGXG sequence and the side chain chemistry of the amino acid in the guest amino acid position [95]. This effectively means that ELPs can be customized to aggregate under very specific conditions and can be employed in a

variety of situations. ELPs are being used in a number of applications, including protein purification, environmental sensing, customizable drug delivery vehicles, and as a method of targeting the delivery of drugs to specific areas [96-99]. In addition to their flexibility, the preliminary biocompatibility of ELPs has been favorable and because they are made up of amino acids, there are few concerns about toxic degradation products [100]. Another advantage of using protein-based polymers such as ELPs is that they can be produced recombinantly by inserting a DNA gene encoding an ELP into *Escherichia coli*, using the bacteria as molecular factories. Making these types of molecules using recombinant methods allows for an unprecedented level of control over the final product compared with traditional polymer synthesis and can allow for the straightforward incorporation of various biofunctional moieties, including targeting, cell penetrating, and enzymatically cleavable sequences.

Despite the widespread development of ELP-based biomaterials, the behaviour of ELPs is still not fully understood. For instance, the mechanism responsible for the reversible phase transition of ELPs is still an area of active investigation. The most recent models suggest that ELPs are intrinsically disordered and capable of momentarily adopting local beta-turn and polyproline structures both below and above their transition temperatures and that sudden decreased backbone solvation may cause ELP aggregation without affecting the structural fluidity of the individual ELP chains [101-107]. Some systematic studies have been carried out examining the effects of guest amino acid, chain length, concentration and pH on the transition temperature of ELPs but the scopes of these studies have been limited either by the limited fidelity of early ELP synthetic techniques or by a focus on a narrow range of ELP constructs and particle characteristics [108-117]. While this information may be somewhat useful for designing a construct for a specific temperature or pH trigger using the studied characteristics, these

models are still limited in scope and there are other key parameters for which there is no systematic understanding.

The purification of recombinantly produced proteins is typically the largest bottleneck in their production, but with ELPs, their reversible solubility can be exploited to partially simplify purification under the correct conditions. This approach is known as inverse temperature cycling (ITC) and was first demonstrated by Meyer and Chilkoti [118]. While ELPs and their potential applications are attractive and worth pursuing, there has until now been no published systematic protocol for expressing and purifying marginally soluble, short ELPs, and in our experience, standard protocols are inadequate for this subset of ELPs.

DNA sequences encoding for ELPs are by their very nature highly repetitive and are often rich with G-C base pairs. These two characteristics makes it difficult to work with these types of sequences in the lab and also prohibitively expensive to synthesize large ELP genes commercially. Techniques such as PCR, which depends on the melting and re-annealing of double-stranded DNA, may not function well, if at all, for ELP-encoding DNA sequences. Fortunately, through the clever application of specific restriction enzymes, short commercially sourced ELP genes can be concatemerized together. This process is known as recursive directional ligation (RDL) [119]. Here, we describe a protocol featuring modifications to RDL designed to address technical bottlenecks experienced in our lab, including inefficient restriction enzyme cleavage due to DNA methylation, significant numbers of incorrect vector-only clones during attempted ELP sequence concatemerization, and minimal *Sfi*I cleavage when using only one cleavage site in the expression vector modifying sequence. Our modifications greatly increase the overall efficiency of the RDL process while minimizing time- and reagent-intensive steps, such as modified-expression-vector linearization and mass colony screening.

The protein sequences created from these difficult-to-process DNA sequences can also be troublesome to deal with. Given that ELPs are generally hydrophobic regardless of their conformation, even routine lab procedures such as spin concentration, dialysis, and long-term storage become more complicated. Care must also be taken to not lose ELPs due to non-specific adsorption to sample tubes during routine handling. The ELPs covered here are highly repetitive, typically uncharged, relatively hydrophobic, and can spontaneously precipitate out of solution when stored at high concentrations at temperatures as low as 4°C for long periods of time. While these characteristics are integral to the unique reversible solubilization of ELPs, they also make their purification and downstream sample handling a delicate affair.

When ELPs have been purified successfully, for the most part the guest amino acids in these constructs fall toward the middle of Urry's ELP hydrophobicity scale [114]. While ITC purification has been sufficient for these types of constructs, it is not applicable to all ELPs. Successfully employing an ITC-only purification procedure means the ELP construct and its expression have to meet certain criteria: The ELP must not end up in the insoluble fraction of the cell lysate during the lysis procedure; the ELP must be in its soluble monomer form in the cell lysate; the phase transition needs to be triggered in the cell lysate under reasonable temperature and salinity conditions; and the protein must be expressed at a concentration high enough for a phase transition to be possible under reasonable conditions but must also be low enough to avoid significant depression of the transition temperature as well as the formation of inclusion bodies. Not all ELP purifications meet these criteria. If an ELP is poorly expressed, or if it contains guest amino acids that are significantly more hydrophilic or hydrophobic than those commonly employed in the literature, or if the ELPs are significantly longer or shorter than what is

commonly used, the transition temperature of the ELP construct may be too high or too low for an ITC-only approach.

Some work has been carried out on shorter, hydrophobic ELPs using maltose binding protein (MBP) as a solubility and affinity-purification partner as a way to circumvent the above issues [120]. This has, however, introduced another complication in that the MBP must then be separated from the hydrophobic ELP, an approach with varying levels of success depending on the ELP construct in question [120]. More recently an ITC-only purification approach has been used to produce the ELPs without the interfering MBP, but the yields of purified protein severely limit the applications of such an approach [121].

1.3.   *In vivo* **phage display screening**

Phage display technology was first created in 1985 by George P. Smith as a method for presenting foreign polypeptides as fusions on the surface of pIII minor coat protein of lysogenic filamentous bacteriophage particles [122]. Since then, this technology has become one of the most effective ways of producing large amounts of peptides, proteins, and antibodies for high-
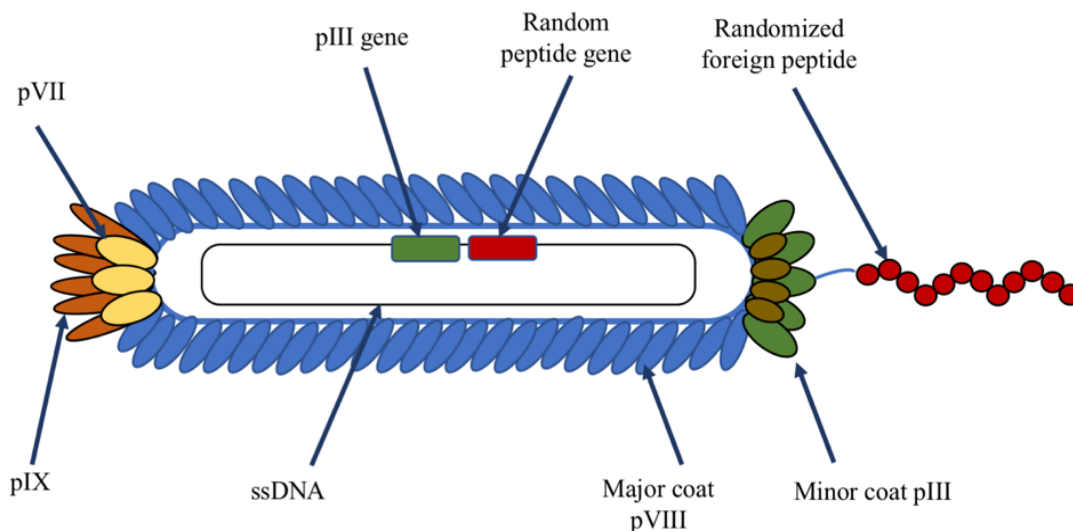
Figure 1. 3 The M13 non-lytic filamentous phage display system. The inserted sequence is shown as a fusion peptide with the minor coat protein III

throughput screening applications. The principle of this method is in the cloning of variable foreign DNA inserts into a specific site in the coat protein of a bacteriophage. These inserts will then be expressed alongside the coat protein of the phage, resulting in a fusion protein with the desired randomized peptide displayed on the surface of the phage, while still maintaining viability and physiological functions of the bacteriophage (Figure 1.3). Such fusion enables the peptide to interact with external molecules.

The most common application of the concept phage display constructs is the creation of random peptide libraries. A phage library is a collection of phages carrying on their surface foreign and completely random proteins or peptides encoded by the inserted DNA in the phage genome. Although each individual phage displays only a single type of peptide or protein on its surface, the library as a whole will have a vast number of phages with many different proteins in total, around 10^6–10^{11} different ligands in a population of 10^9-10^{12} phage molecules [123]. The phage-based libraries are highly advantageous as bacteriophages can tolerate a wide range of experimental screening conditions, including environments of extreme acidity or temperatures range and in the presence of DNAse or proteolytic enzymes [124, 125].

Several bacteriophage types such as filamentous phages, lambda, T4 and T7 have been used to develop foreign displayed peptides phage libraries. However, filamentous phages (M13, fd, f1) have long been the most frequently used vehicle [126, 127]. Moreover, bacteriophage T7-based libraries are gaining more and more attention for their unique features [128]. The length of displayed peptides in these random libraries usually ranges from 5 to 20 amino acids. However, because of their commercial availability, heptapeptide and dodecapeptide displaying libraries are the most broadly used peptide libraries.

Compared to other library screening methods, including *in vitro* and *ex vivo*, *in vivo* phage display screening offers advantages in that phage are exposed to the target molecules present and intact in their native environment. Besides, phage clones displaying peptides that bind to non-target molecules, such as plasma proteins, are depleted from the phage population and will be washed out in the bloodstream. Only peptides that survive the degradative environment of the vascular system and the ones that can access their targets are selected and propagated [129]. The unique advantage of *in vivo* biopanning that it causes the clustering of highly specific peptide ligands on the vasculature of a particular tissue whereas the non-specific phages turn to be distributed through the whole body of the animal.

The first *in vivo* phage display screening approach to target selective vasculature was performed by Pasqualini and Ruoslahti in 1996 and has since been reviewed [130-132]. Their work described the use of phage display technology to differentiate, for the first time, between the endothelial layer in the brain and kidney of Balb/c mice [133]. The resultant peptides containing consensus motifs were shown to be selective to the organ they were isolated from. Their work demonstrated a proof of principle and that opened the door to many subsequent studies to utilize the advantages of *in vivo* biopanning.

During the *in vivo* phage display selection process, phage libraries are administrated to the animal through different routes including, intravenous [134], intraperitoneal [135], intranasal [136], and trans-dermal [137] phage administration. The phages are then allowed to circulate in the body for a certain period of time for the phage clones to be distributed in the vascular system followed by systemic perfusion that clears the bloodstream of the unbound phage. After the harvest of the organ of interest, the recovered phages are then amplified through *E. coli* infection and undergo additional binding/amplification rounds to enrich the pool in favor of binding

sequences. Three to five enrichment rounds of *in vivo* phage display are usually enough to obtain peptides with considerable high affinity against the organ of interest. Therefore, screening for organ/tissue-homing peptides using *in vivo* biopanning is a direct and rapid method of identifying novel peptide sequences suitable for drug-targeted delivery applications.

Experimental evidence has indicated that the vasculature in each individual normal and diseased tissue is unique and highly specialized [130, 138]. These unique "Zip codes" in blood vessels can be utilized by using affinity ligands for organ-specific delivery of therapeutic molecules [130, 133, 139, 140]. Affinity-based physical targeting (e.g. active targeting) makes use of these vascular ZIP codes to achieve selective targeting of systemically administered drugs to the target organ [139]. The desired outcome of the organ-specific targeting is increased local accumulation of the therapeutic payload while lowering systemic concentration [139].

There are few phage display studies directed against brain microvasculature reported [133, 136, 141-145]. However, there is a very limited number of ligands that have been characterized for targeted drug delivery to the microvasculature of the ischemic brain. In fact, there is only one article published where a peptide has been identified (CLEVSRKNC) that can home to ischemic stroke brain vasculature in an adult rat MCAO model [145]. This peptide was screened from a CX7C peptide displaying library based on a T7 415-1b phage vector. This peptide was incorporated onto nanoliposomes for localized drug delivery to ischemic brain tissue [146]. A summary of brain vasculature-homing peptides identified using *in vivo* phage display is in Table 1.3 Identifying peptides that accumulate at the site of HI injured cerebrovasculature through the use of phage display techniques will allow us to develop a targeted drug delivery platform to target this region.

Table 1. 3 Brain vasculature-homing peptides derived from *in vivo* phage display.

Sequence	Animal model	Phage library	Route of administration	Ref.
		Healthy brain vasculature		
SRL	Balb/c	Two library pools: Pool I $CX_{5-7}C/CX_9$ Pool II $X_2CX_{14}CX_2/X_2CX_{18}$	Intravenous	[133]
LGG	C57Bl/6	CX_7C	Intravenous	[144]
CAGALCY	Balb/c	$CX_{10}C$	Intravenous	[143]
ACTTPHAWL	Adult male Wistar rats	CX_7C	Intranasal	[136]
GLAHSFSDFARDFVA and GYRPVHNIRGHWAPG	C57Bl/6	f3-15mer	Direct perfusion via the heart	[142]
CTSTSAPYC	ICR mice	CX_7C	Intravenous	[141]
		Pathological brain vasculature		
CLEVSRKNC	MCA rat	CX_7C	Intravenous	[145]

1.4. Hypothesis and objectives

Hypothesis

Developed self-assembling nanoparticles (NPs), carrying neuroprotective agents (e.g. DEX) will target and release these agents as a result of changes in the brain vasculature and brain microenvironment.

Objectives:

(1) Use *in vivo* phage display techniques to identify novel vasculature-homing brain targets at early onset HI events.

(2) Engineer a recombinantly expressed self-assembling peptides with two domains: one for targeting the penumbral tissue and another for forming environmentally-triggered hydrophobic core nanoparticles for carrying neuroprotective agents.

(3) Characterize the self-assembling behavior of the NPs in the presence and absence of the drug.

2. Materials and Methods

Portions of this chapter have been published in:

1. Bahniuk, M.S., **A.K. Alshememry**, and L.D. Unsworth, *High-yield recombinant expression and purification of marginally soluble, short elastin-like polypeptides*. Biotechniques, 2016. 61(6): p. 297-304.

2. Bahniuk, M.S., **A.K. Alshememry**, S.V. Elgersma, and L.D. Unsworth, *Self-assembly/disassembly hysteresis of nanoparticles composed of marginally soluble, short elastin-like polypeptides*. J Nanobiotechnology, 2018. 16(1): p. 15.

2.1.   Materials

Ph.D.™-12 Phage Display Peptide Library Kit (New England Biolabs, Beverley, MA), Luria-Bertani (LB) medium (ThermoFisher, Waltham, Massachusetts, USA), LB agar (Sigma-Aldrich, St. Louis, Missouri, USA), Dulbecco's Modified Eagle's Medium (1000 mg/L glucose) (DMEM) (Gibco, Invitrogen, Carlsbad, California, USA), Pierce Protease Inhibitor Mini Tablets (ThermoFisher, Waltham, Massachusetts, USA), Tetracycline (Sigma-Aldrich, St. Louis, Missouri, USA), Polyethylene glycol-8000 (PEG) (Sigma-Aldrich, St. Louis, Missouri, USA), Isopropyl thiogalactoside (IPTG) (ThermoFisher, Waltham, Massachusetts, USA), X-gal (ThermoFisher, Waltham, Massachusetts, USA), Tris-buffered saline (TBS) (ThermoFisher, Waltham, Massachusetts, USA), Sodium chloride (NaCl) (ThermoFisher, Waltham, Massachusetts, USA), Tween 20 (Sigma-Aldrich, St. Louis, Missouri, USA), Escherichia coli (ER2738) (New England Biolabs, Ipswich, Massachusetts, USA), Dexamethasone (Sigma-Aldrich, St. Louis, Missouri, USA), Glycerol (Invitrogen, Carlsbad, CA).

2.2.   ELP synthesis

A complete listing of the materials used in this study and a detailed protocol are provided in **Appendix 1**.

Method summary:

This efficient and dependable method for the high-yield production and purification of short, marginally soluble, elastin-like polypeptides (ELPs) involves increasing the reliability of DNA concatemerization procedures and utilizing denaturing metal affinity chromatography to ensure these ELPs are fully soluble and recoverable from insoluble cell debris. If the ELPs are poorly expressed, this also serves as a pre-concentration step to maximize the ELP concentration before temperature cycling purification.

2.3.   ELP gene concatemerization and cloning

A synthetic oligonucleotide encoding for 10 repeats of VPGLG (L_{10}) was purchased from Integrated DNA Technologies (Coralville, IA). Due to its length the oligonucleotide was provided in a pIDT-blue plasmid. This plasmid was transformed into XL10 Gold competent *E. coli* cells (Agilent Technologies, Santa Clara, CA), and the cells were grown in liquid culture to produce large amounts of the ELP-containing plasmid. The ELP gene was obtained from the plasmid by double digesting it with the *EcoR*I and *HinD*III restriction enzymes (all restriction enzymes were purchased from New England BioLabs, Ipswich, MA) and purified by agarose gel electrophoresis. The gene was ligated into a pUC19 vector (Bio Basic, Ontario, Canada) that was also digested by the same restriction enzymes. Correct gene insertion was confirmed by double digestion with restriction enzymes *Bgl*I and *Nde*I.

Oligomerization of the ELP gene was carried out using a modified RDL scheme (Figure 2. 1). Vector DNA was linearized using *PflM*I, purified using gel electrophoresis, digested again with *PflM*I, and dephosphorylated using Antarctic phosphatase (New England Biolabs). Insert DNA was double-digested with *PflM*I and *Bgl*I and purified using gel electrophoresis. The two ELP-containing genes were ligated together and transformed into XL10 Gold cells. A double digest using *PflM*I and *Bgl*I confirmed successful gene concatemerization. This RDL process was repeated to generate ELP genes with increasing numbers of repeats.

For the RDL-generated ELP genes to be inserted into a pET-25b(+) expression vector (EMD Millipore, Ontario, Canada), a short modifying sequence containing two *Sfi*I cleavage sites along with the N- and C-terminal sequences of the ELP was first added. As with the L_{10} gene above, the synthetic oligonucleotide was purchased commercially (Integrated DNA Technologies), supplied in a vector, transformed into XL10 *E. coli*, and the sequence of interest

was isolated using the *EcoR*I and *Nde*I restriction enzymes. The expression vector was similarly linearized and then ligated with the isolated modifying sequence. A post-ligation digest with *BamH*I before transformation was used to greatly reduce the number of vector-only clones. Vector modification was confirmed by single digests with either *BamH*I or *Sfi*I.
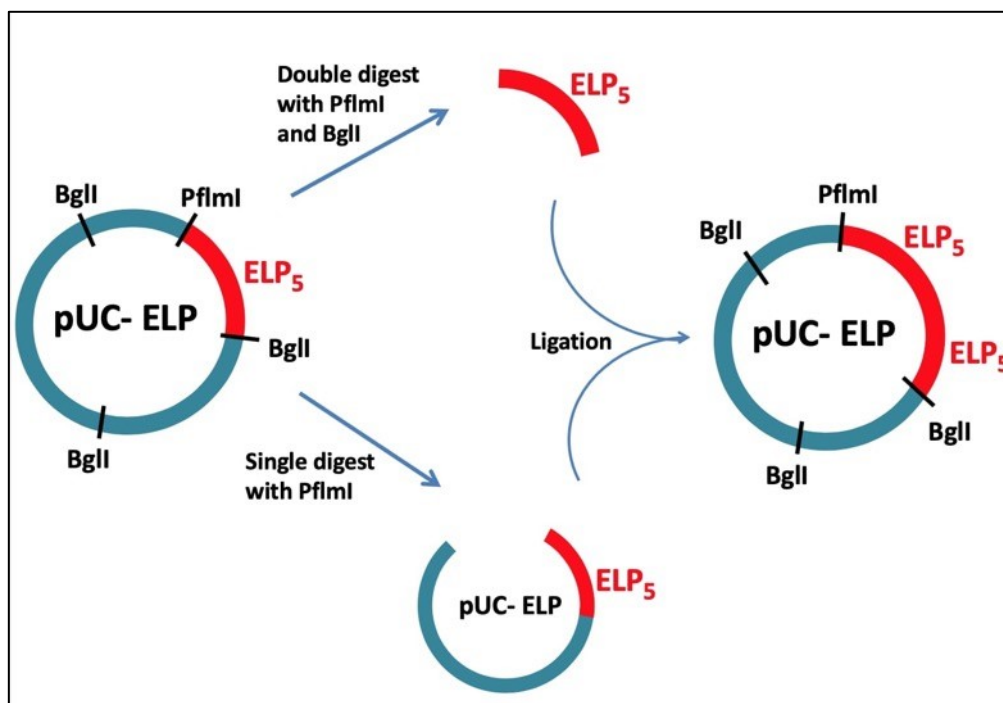
Figure 2. 1 Schematic illustration of Recursive Directional Ligation (RDL) method.

To prepare for insertion of the ELP gene into the modified expression vector, the vector was digested with *Sfi*I, purified by gel electrophoresis, digested again, and then dephosphorylated. The insert was prepared in the same manner as the inserts for RDL. The two were ligated together, and a post-ligation *Sfi*I digest was performed before transformation to reduce the number of incorrect colonies observed after cloning. Restriction enzyme digestions and DNA sequencing confirmed the final plasmid sequences. Example of the DNA sequencing results is available in Appendix 1.

2.4.   Expression and purification

ELP expression vectors were transformed into OneTouch BL21 (DE3) *E. coli* (Invitrogen, Carlsbad, CA) cells, and 1 L cultures of these cells were grown in Terrific Broth (TB) (Thermo Fisher Scientific, Waltham, MA) supplemented with 100 μg/mL ampicillin (Thermo Fisher Scientific) and 10 mM L-proline (Sigma-Aldrich, St. Louis, MO). Expression was induced for 24 h using 2 mM isopropyl β-D-1-thiogalactopyranoside (Thermo Fisher Scientific).

Purification was achieved by first performing denaturing metal-affinity chromatography and eluting the ELPs using an imidazole step gradient. Briefly, cleared cell lysates are loaded onto the nickel-nitrilotriacetic acid matrix (Ni-NTA). His-tagged proteins bind strongly to the column while most other proteins that do not bind or bind weakly pass through the matrix. Following washing of the matrix material, peptides containing polyhistidine sequences can be easily eluted with either buffered imidazole solutions, which competes with the polyhistidine tag for binding to the column, or by a decrease in the matrix pH, which consequently decreases the affinity of the tag for the resin (Figure 2. 2). Buffered 8 M urea (Thermo Fisher Scientific) was used to lyse the cells and ensure the ELPs were fully soluble and free from any inclusion bodies. The urea was removed during the extensive column washing. Eluents were screened for the presence of ELPs by gel electrophoresis or by heating them to room temperature or 37°C, depending on the construct, and observing which samples turned reversibly cloudy. Samples confirmed to contain ELPs were combined and then subjected to one round of ITC for final purification. An illustration of the ITC method can be found in Figure 2. 3. The temperature used to cause ELP aggregation varied depending on the construct. The purification was confirmed

with denaturing PAGE (SDS-PAGE) and the ELP concentrations were measured by sample absorbance at 280 nm.
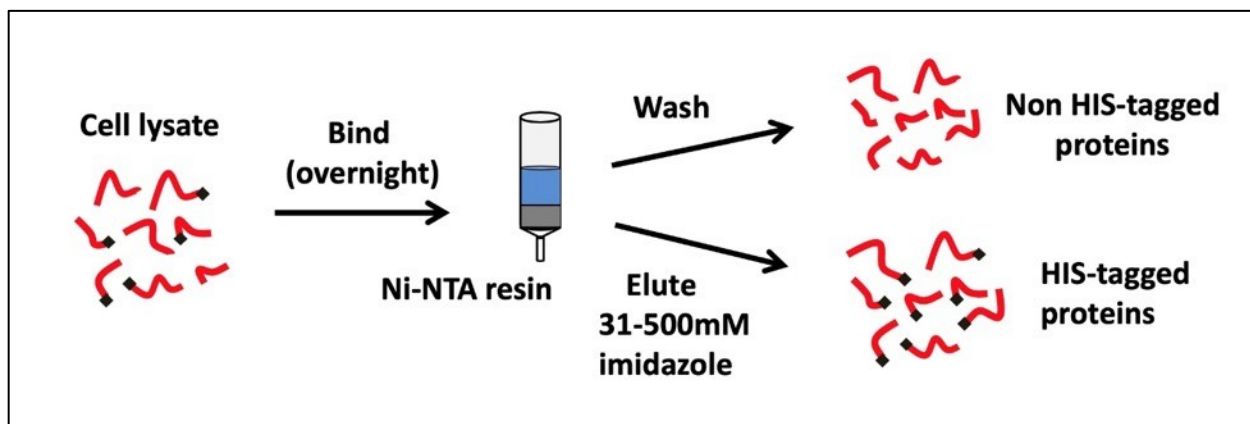
Figure 2. 2 Schematic illustration of Ni-NTA affinity column chromatography method.
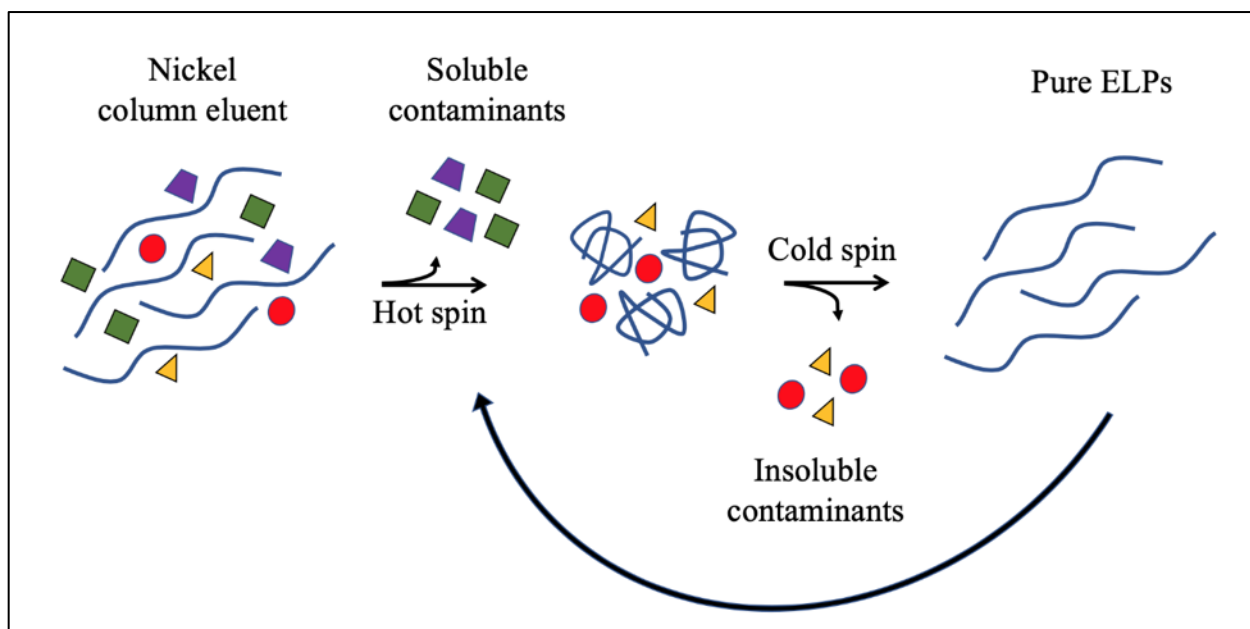
Figure 2. 3 Schematic illustration of ITC method.

2.5.   Dynamic light scattering measurements

Thermal behavior of Leucine-containing ELP construct with 40 repeats (L40), and Valine-containing ELP construct (V40) at two concentrations was studied with and without the presence of the drug using dynamic light scattering (DLS) (Malvern Zetasizer Nano ZS, Malvern

Instruments Ltd, Malvern UK). Low ELP concentration at 0.1 mg/mL was used in this experiment and compared to a 10x higher concentration at 1.0 mg/mL to study the effect of concentration on the thermal behavior of the ELP particles. Frozen ELP aliquots were thawed and diluted on ice with PBS pH 7.4 to the desired concentration. After the addition of DEX, 100 µL final volume of ELP+DEX mixture was placed in a 40 µL minimum volume DLS cuvette and kept cold on ice until measurement. ELP samples were equilibrated within the zetasizer at 5°C before starting measurements. Samples were heated from 5°C to 50°C and subsequently cooled back to 5°C. Size was measured at 5°C intervals. A two-minute interval at each measurement temperature was programmed to allow for thermal equilibration of the sample. There was about 10 mins gap between the heating the cooling runs as the sample is taken out immediately after the end of the heating cycle for visual check of any perpetration and after initiating the cooling cycle the instruments take extra minutes to equilibrate and start the measurements. Two measurements, each with >10 subruns were recorded at each temperature during heating and cooling. Absorbance, refractive index and viscosity of the PBS and ELP were calculated using Malvern's zetasizer software 7.03. Protein analysis mode was used for all measurements. Measurement settings were automatically optimized at each temperature interval. All DLS data represents the peak position of the distribution of particle sizes. All aggregate distributions had polydispersity index (PDI) values <0.2 unless the samples were actively undergoing a substantial change in particle diameter or the sample had been affected by particle precipitation.

2.6. Dexamethasone loading

DEX was used in this experiment as a model drug because it is hydrophobic, safe, and has higher anti-inflammatory potency compared to most commonly used corticosteroids [63].

ELP nanoparticles were loaded with DEX, during the formation of the particles. DEX at a fixed concentration of 0.2 mg/mL was chosen to keep a close ratio of polymer:drug (1:2) when mixed with low concentration ELP at o.1 mg/mL and also to test the effect of higher ratio of polymer:drug on the drug E.E. when mixed with a higher concentration of ELPs at 1.0 mg/mL. Briefly, DEX was added at a concentration of 0.2 mg/ml to ELP solutions at 4°C and incubated in ice for 10 mins. Then the solution was warmed up above the ELPs transition temperature entrapping the DEX inside the self-assembling ELP NPs.

2.7.   Determination of encapsulation efficiency

The ELP nanoparticle encapsulation efficiency (E.E.) was determined upon their separation from the aqueous preparation medium containing the free DEX by centrifugation (10,000 ×g, 40°C, 10 min). The amount of free DEX in the supernatant was determined in the supernatant by high-performance liquid chromatography (HPLC) (Agilent 1100 Series). The ELP NPs encapsulation efficiency was calculated using the following equation:

$$E.E.(\%) = \frac{Total\ drug\ amount\ (\mu g) - Free\ drug\ amount\ (\mu g)}{Total\ drug\ amount} \times 100$$

2.8.   HPLC analysis of Dexamethasone

2.8.1.   Chromatographic condition

Reversed phase HPLC system was performed using an Agilent 1100 instrument (Palo Alto, CA) with a diode array absorbance detector. The column was an Agilent ZOBRAX SB-C18 column (4.6 X 250 mm, particle size 5μm). The mobile phase for the DEX assay was a

mixture of 5 mM phosphate buffer, acetonitrile and methanol (35:50:15 %v/v, respectively) adjusted to pH 3.5 and injected at a flow rate of 1 ml/min. The effluent was monitored at wavelength 244 nm. The injection volume was 20 µl and the run time per sample was 5 minutes at ambient temperature. The elution time for the DEX was approximately 3.2 minutes.

2.8.2. Preparation of stock solution

The stock solution of DEX was prepared by weighing a suitable amount of DEX powder and dissolving it in methanol. The final concentration of the stock solution of DEX was 10 mg/ml.

2.8.3. Preparation of calibration standard

The stock solution was diluted with the solvent system consisting of a mixture of 5 mM phosphate buffer, acetonitrile and methanol (35:50:15 % v/v, respectively) adjusted to pH 3.5 to prepare seven working solutions with concentrations of 0.25, 0.5, 1, 3, 5, 10 and 25 µg/ml.

The resulting solutions were vortexed well for 20 seconds and transferred to clean HPLC vials and then 20 µl were injected into the HPLC autosampler.

A calibration curve was obtained by plotting the theoretical concentrations of working solutions (x axis) against average peak areas (y axis).

2.8.4. Method validation procedure

Linearity and Range

The linearity of the analytical method is its ability to obtain test results which are directly proportional to the concentration of the analyte in the samples within a given range [147].

The range of the analytical method is the interval between the upper and lower levels of analyte that have been demonstrated to be determined with a suitable level of accuracy, precision and linearity using the procedure as written [147].

The linearity of the analytical method is evaluated by visual inspection of a plot of test result as a function of analyte concentration. If a linear relationship exists, test results should be evaluated by appropriate statistical methods, for example, by calculation of a regression line by the method of least squares. Data from the regression line itself may be helpful to provide mathematical estimates of the degree of linearity [148].

In practice, linearity of an HPLC method can be demonstrated *via* visual examination of the calibration curve (peak areas as a function of drug concentrations of working solutions). If it shows a linear relationship, the correlation coefficient, y-intercept and slope of the regression line should be reported and used in all calculations.

Accuracy and Precision

Accuracy of an analytical method is the closeness of test results obtained by that procedure to the true value. Precision of an analytical method is the degree of agreement among individual test results when the procedure is applied repeatedly to multiple samplings of a homogeneous sample [147].

Accuracy and Precision should be assessed using a minimum of nine determinations over a minimum of three concentration levels, covering a specified range (three concentrations and three replicates of each concentration) [147].

Accuracy is expressed as the percentage of recovery of the analyte, while the precision is expressed as the standard deviation or relative standard deviation (coefficient of variation) [147].

In practice, accuracy and precision are determined by assaying three selected concentrations of DEX working solution each of three replicates. The percentage of recovery and standard deviation were calculated.

Selectivity

Selectivity describes the ability of an analytical method to distinguish various substances in the sample and is related to methods in which two or more compounds are separated and quantitated in the complex matrix. Thus, the term selectivity is suitably applied to chromatographic techniques in which the components of the mixture are physically separated from each other. The selectivity of the method is compromised by the presence of potential interferences including related compounds (impurities) and components of the matrix (formulation excipients, endogenous substances) [147].

Therefore, the mentioned HPLC method of analysis should be selective for measuring DEX in the presence of formulation excipients and substances used in the analytical methods.

In practice, selectivity of HPLC can be demonstrated by comparing representative chromatograms of standard and study samples to ensure that the results (peaks) are unaffected by the presence of any extraneous materials.

Limit of Quantitation (LOQ)

The limit of quantitation is the lowest amount of the analyte in a sample which can be quantitively determined with suitable precision and accuracy [149]. It can be determined by a signal:noise ratio of 10:1 or by using the following equation:

$$\textbf{LOQ=10*SD}_{\textbf{intercept}}\textbf{/Slope} \quad [148]$$

where, LOQ is the Limit of Quantitation and SD is the standard deviation. This equation was adopted in the current study.

Limit of Detection (LOD):

The detection limit is the lowest amount of the analyte in a sample which can be detected, but not necessarily quantitated as an exact value [149]. It can be determined by a signal:noise ratio of 3:1 or using the following equation

$$\textbf{LOQ=3.3*SD}_{\textbf{intercept}}\textbf{/Slope} \qquad [148]$$

where, LOQ is the Limit of Quantitation and SD is the standard deviation. This equation was adopted in the current study

2.9.   Animals

Long-Evans rats were purchased from Charles River and were kept on a 12 h light/dark cycle and allowed access to food ad libitum. Two females and 1 male rat were placed in a cage for 2 weeks for breeding. After this time the females were placed in individual cages to give birth. The day of delivery was recorded as postnatal day 1. Both males and females were represented from each litter, and were randomly selected. Litters were culled to 10 pups to ensure relative equalization across the pups of weight gain and attendance by their dam. The animal experiments were carried out in accordance with protocols that were evaluated and approved by the University of Alberta Animal Care and Use Committee. The standard Rice-Vannucci model of neonatal HIBD was performed on PD7 Long-Evans rat pups (12-16 g) [150]. Briefly, this model is accomplished as follows: 7-day-old rats were anesthetized with isoflurane (4% induction; 2% maintenance) in 70% nitric oxide-30% oxygen. The right common carotid

artery (CCA) was isolated from the vagal nerve and ligated twice with double-knots using 5-0 surgical silk (Harvard Apparatus). The right CCA was then permanently cut between the two ligations to stop blood flow. Once the CCA was successfully ligated the incision sutured with 5-0 silk. Pups were kept in an incubator at 35°C before and after surgery to maintain body temperature. When all surgeries were completed, pups were returned to their dam to recover for 2 hours. The pups were then individually placed in covered glass jars (with inlet and exit ports) floating and partially submerged in a pre-heated water bath (36.5-37°C) and exposed to a hypoxic environment of 8% O_2 and 92% N_2 for 60 (mild HIBD) or 150 mins (severe HIBD). The combination of cerebral ischemia and hypoxia act together to produce mild to severe brain damage in the right hemisphere of the brain (ipsilateral to the CCA ligation) [150]. Mortality was 0% and 10% for mild and severe HIBD, respectively. After hypoxia animals were returned to their dams.

Injection Protocol

After animals were removed from their dams after 3 hours and placed in a 35°C incubator. They were given an intraperitoneal (IP) injection of $1x10^{11}$ Phage in 100 ul. They were placed in the incubator for 15 min. The pups were anesthetized as described above. An incision was made through the integument and abdominal wall, just below the rib cage. A cut was made in the diaphragm and a cut was made from the rib cage to the collarbone. The sternum was lifted up and away from the pleural cavity and held in place with forceps. A 25-gauge needle was placed in the left ventricle and the right atria was cut. Normal saline was then pumped through the heart at a flow rate of 1 ml/min until 9 ml of saline had been perfused through the pup. The brain was removed, and the posterior aspect of the cortex removed and washed and used for growing phage.

2.10.   Phage display library

A Ph.D.^{TM}-12 phage library was used for all *in vivo* biopanning experiments. This library represents over 10^9 unique genotypes encoding random linearized peptides fused to the pIII coat protein of the filamentous phage M13. Displayed peptides share the general motif $^{N'}$S-**XXXXXXXXXXXX**-GGGS^{C,} where X12 represents a unique and random 12-mer peptides followed by a short amino acid spacer GGGS that links the C-terminus of the peptide to the N-terminus of the phage pIII coat protein.

2.11.   *In vivo* biopanning

A phage display high throughput screening strategy was employed for the identification of hypoxic ischemic brain homing peptides involving three rounds of *in vivo* selection. Three
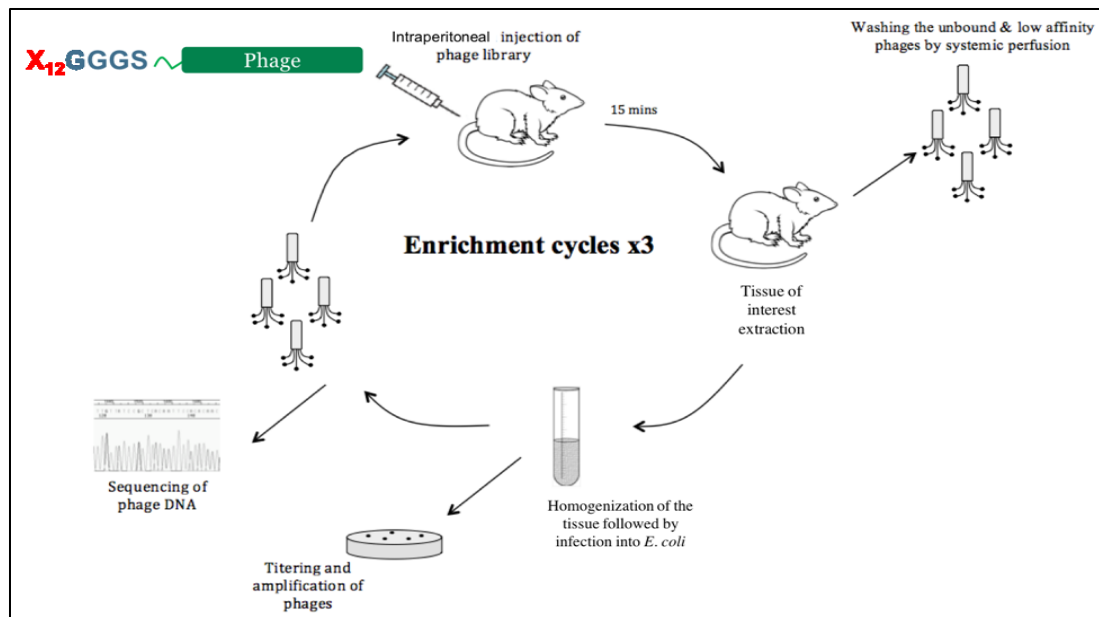
Figure 2. 4 Schematic diagram of the in vivo phage display processes to identify vasculature-homing peptides.

phage display experiments were undertaken against three animal groups to study if there would be any overlapping between peptides acquired from each injury type and further confirm the selectivity of those peptides. The first group was animals with ischemia and 60 min hypoxia. The

second group had ischemia and 150 min hypoxia. The third group was a control in healthy rats. The protocol used herein was adapted from the work of Work LM *et al* and modified to be appropriate for P7 rats instead of adult rats [151]. Briefly, P7 rats were anaesthetized and injected intraperitoneally with 100 µL PBS containing 1×10^{11} plaque forming units (pfus) of the Ph.D.™-12 library. After 15 mins circulation period, unbound phages were washed out by systemic perfusion through the heart with 9 ml normal saline (0.9% NaCl) while under anesthesia. Posterior cortex from each animal group was then harvested and washed three times with ice-cold DMEM containing protease inhibitor cocktail (DMEM/PI) in addition to 0.1-0.3% Tween-20. Tissues were then snap-frozen in liquid N_2 and kept at -80°C freezer (Figure 2. 4).

2.12.   HI Brain homing phage recovery, amplification and titration

Harvested tissues were homogenized with a tissue homogenizer (Power Gen 125, Fisher Scientific, Pittsburg, PA, USA) and washed three times in ice-cold DMEM/PI. The homogenates were then centrifuged, and the pellet was washed and incubated with early-log phase ER2738 in LB media and centrifuged to remove residual bacteria. The supernatant was mixed with PEG/NaCl incubated on ice for 1 hr and centrifuged to collect the amplified phage pellet. Pelleted phages were resuspended in TBS, precipitated again with PEG/NaCl on ice overnight, and resuspended in TBS for the next round. Phage titering was performed through plating a mixture of phage and mid-log phase ER2738 in LB media on agar plates containing X-gal and IPTG. As the library phage are derived from the common cloning vector M13mpl9, which carries the lacZa gene, phage plaques appear blue when plated on IPTG/X-gal-containing LB-agar media. Amplified phages are then re-injected in new animals for the next round.

2.13.   Peptide sequences and amplification of phage clones

Phage clones recovered after each round of biopanning were sequenced for the peptide insert. To determine the peptide sequences displayed by the selected phage, individual clones were amplified and DNA isolated. Then the DNA inserts in the integrated section of the phage were amplified by polymerase chain reaction (PCR) and sequenced using Sanger DNA Sequencer using 5'-CCCTCATAGTTAGCGTAACG-3' primer provided with the library kits. The peptide sequences were translated from DNA sequence and analyzed for their frequency of occurrence using Clustal W program in order to align amino acid sequences and shared motifs, together with NCBI protein BLAST search to identify proteins from the protein with homologous motifs.

3.   Results

Portions of this chapter have been published in:

1. Bahniuk, M.S., **A.K. Alshememry**, and L.D. Unsworth, *High-yield recombinant expression and purification of marginally soluble, short elastin-like polypeptides*. Biotechniques, 2016. 61(6): p. 297-304.

3.1.   ELP Synthesis

The basic workflow of RDL has been based on the work of Meyer and Chilkoti [119]. Modifications have been introduced to both maximize restriction enzyme digest efficiency by minimizing interference by methylation and significantly decrease the likelihood of incorrect background colonies by maximizing vector linearization and purity. This drastically reduced the number of colonies that must be screened in order to find the correct RDL product. We found that methylation was less of a concern when using XL10-Gold *E. coli* as opposed to the XL1-Blue strain. Before switching host cell lines, restriction enzyme digests were usually only 30%–40% efficient. This drastically reduced the yield of linearized vector and correctly digested inserts necessary for RDL. The number of background colonies was decreased by gel purifying the digested vectors, repeating the linearization procedure, and then dephosphorylating the vector. These precautions reduced the proportion of incorrect clones from ~95% to <5%. Figures 3.1 to 3.4 shows the results of colony screening procedure for the successful doubling of leucine-containing ELPs with 10 repeats inserts to 20 repeats, then to 40, 80, 160 repeats using RDL and clearly demonstrates the complete lack of empty vector clones. The time required to screen clones to find a correct ligation is greatly reduced by performing all of the steps above to reduce both uncut vector and religated DNA. Useful controls for the RDL cloning procedure consisting of DNA ligation reactions where the ELP insert and/or ligase enzyme are replaced by water can be used to assess the amount of empty vector that makes it through the ligation procedure.

Figure 3. 1 Successful doubling of an elastin-like polypeptide (ELP) L$_{10}$ insert to L$_{20}$.

Plasmids were digested with PflMI and BglI for 1 h and then run on a 2% agarose gel before being stained with ethidium bromide. This digest should yield 170, 1118 and 1371 bp bands from the vector, plus an ELP band whose size will vary. In this instance, the L10 gene was 165 bp long, the L20 gene was 330 bp, and the L$_{30}$ gene was 495 bp. Lane 1 is a positive control digest of pUC19-L10, Lane 2 is the molecular weight ladder, and Lanes 3–7 are clones from the RDL reaction concatemerizing L$_{10}$ to L$_{20}$. Based on the increase in band sizes, Lanes 3–6 contain the genes for L$_{20}$, while Lane 7 likely contains an L$_{30}$ gene. Note that the 170 bp vector-derived fragment is clearly visible in Lanes 3–7 but overlaps the L$_{10}$ gene in Lane 1. The L$_{30}$ is the result of a double insertion of the ELP L$_{10}$ gene into a single cloning vector. This is not an uncommon occurrence while performing RDL using the recommended molar ratios of insert to vector and may actually be beneficial in some cases.
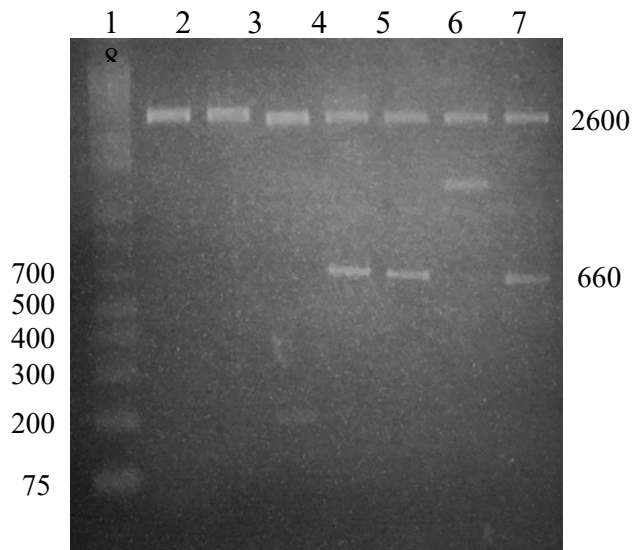
Figure 3. 2 Successful doubling of an elastin-like polypeptide (ELP) L$_{20}$ insert to L$_{40}$.

Plasmids were digested with *EcoRI* and *HindIII* for 1 h and then run on a 2% agarose gel before being stained with ethidium bromide. This digest should yield 2635 bp bands from the vector, plus an ELP band whose size will vary. In this instance, the L40 gene was 660 bp long. Lane 1 is the molecular weight ladder, Lane 2 is clone#1 from the RDL reaction concatemerizing L$_{20}$ to L$_{40}$, single digested with EcoRI, and Lanes 3 is clone#1 single digested with HindIII, Lane 4-8 are double digested clones 1-5. Based on the increase in band sizes, Lanes 5,6, and 8 contain the genes for L$_{40}$, while Lane 7 likely contains an L$_{80}$ gene. The L$_{80}$ is the result of a double insertion of the ELP L$_{20}$ gene into a single cloning vector. This is not an uncommon occurrence while performing RDL using the recommended molar ratios of insert to vector and may actually be beneficial in some cases

47
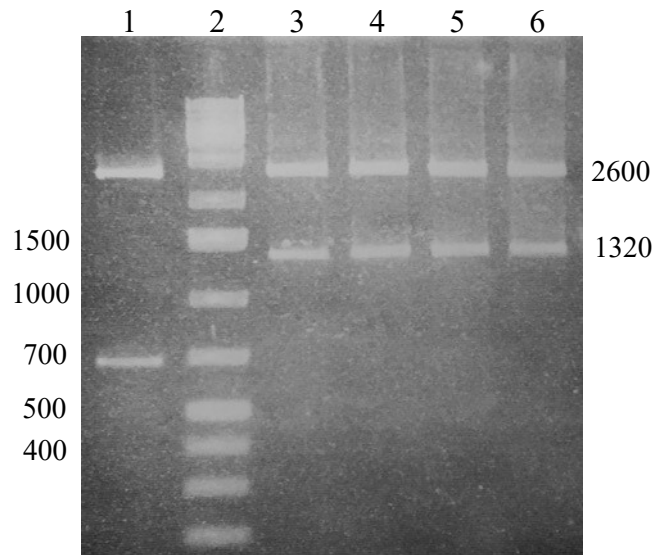
Figure 3. 3 Successful doubling of an elastin-like polypeptide (ELP) L_{40} insert to L_{80}.

Plasmids were digested with *EcoRI* and *HindIII* for 1 h and then run on a 2% agarose gel before being stained with ethidium bromide. This digest should yield 2635 bp bands from the vector, plus an ELP band whose size will vary. In this instance, the L_{80} gene was 1320 bp long. Lane 1 is a positive control digest of pUC19-L_{40}. Lane 2 is the molecular weight ladder, Lane 3-6 clones from the RDL reaction concatemerizing L_{40} to L_{80}. Based on the increase in band sizes, Lanes 3-6 contain the genes for L_{80}.
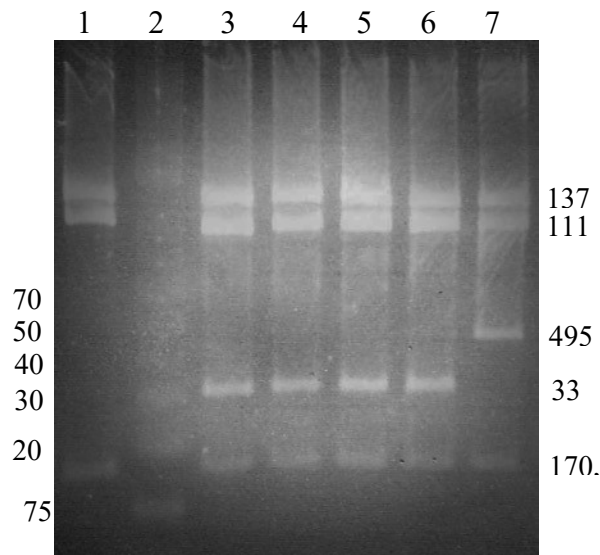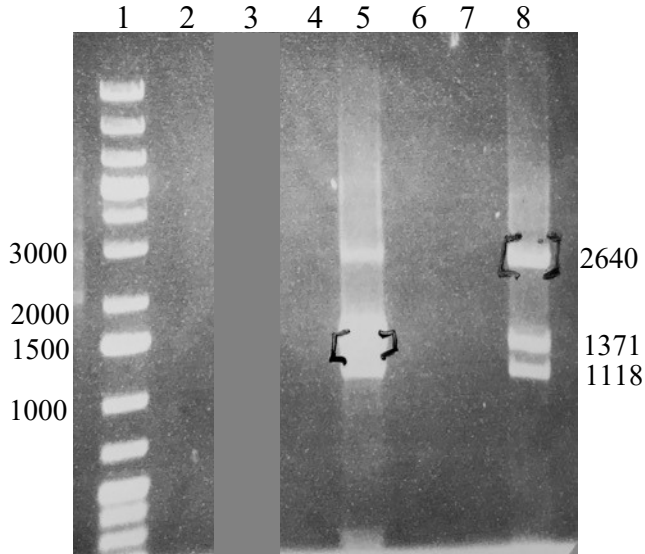

Figure 3. 4 Successful doubling of an elastin-like polypeptide (ELP) L_{80} insert to L_{160}.

Plasmids were digested with *PflmI* and *BglI* for 1 h and then run on a 0.8% agarose gel before being stained with ethidium bromide. This digest should yield 170, 1118 and 1371 bp bands from the vector, plus an ELP band whose size will vary. In this instance, the L_{160} gene was 2640 bp long. Lane 1 is the molecular weight ladder. Lanes 2-4, 6, and 7 are empty. Lane 5 is a positive control digest of pUC19-L_{80}. Lanes 8 is a clone from the RDL reaction concatemerizing L_{80} to L_{160}. Note that the 170 bp vector-derived fragment is too small to be visible on this gel. Based on the increase in band sizes, Lane 8 contain the genes for L_{160}.

Two *Sfi*I sites and a spacer of appropriate length were added to the pET-25b(+) vector so that the RDL-derived ELP gene can be inserted into the expression vector. A vector with a single *Sfi*I site was only cleaved with ~10% efficiency, whereas a vector with two *Sfi*I sites and a spacer had a cleavage efficiency of ~100%. Using a vector with a single *Sfi*I site and doping the digest reaction with a short double-stranded DNA oligonucleotide also containing an *Sfi*I cut site did not significantly improve vector linearization in our experience. The modification sequence we designed contained the DNA for the N- and C-terminal amino acids of the ELP gene, the two *Sfi*I restriction sites and their spacer, a tobacco etch virus protease recognition site, and a polyhistidine tag.

We have found that IPTG induction of these constructs and a 24 h expression period dramatically increased expression yields. Numerous parameters were tested, including expression time, OD_{600} at time of induction, incubation temperature, IPTG concentration, and uninduced expression. The expression conditions described here represent those that worked well for the corresponding constructs; however, they may not be ideal for the expression of other ELPs, and some sequence-specific optimization may be required.

In most circumstances, standard Tris-glycine SDS-PAGE was sufficient unless small ELPs such as L_{20} were being produced. In this case, Tris-tricine electrophoresis allowed for superior resolution of the low molecular weight products. The tricine SDS-PAGE method has been modified in order to scale down the gel sizes for a Bio-Rad Mini-Protein Tetra Cell system (see protocol in Appendix 1). In all cases, gels were negatively stained with $CuCl_2$ [152] as some literature suggests conventional Coomassie staining does not work on ELPs [153].

The first method we used to purify the ELPs was denaturing nickel affinity chromatography. We found that an overnight binding of the crude cell lysate to the nickel

affinity column beads is crucial to recovering large amounts of ELP. In other ELP purification protocols polyethyleneimine is used to remove DNA; however, it is not necessary for denaturing nickel affinity chromatography, and in our experience, polyethyleneimine actually precipitated the hydrophobic ELPs as well as the DNA. Other ELP constructs may elute at different imidazole concentrations, so gradient elutions may need to be optimized for ELP constructs not used in this study. Figure 3. 5 illustrates the elution of a leucine-containing ELP and the revers   the protein.
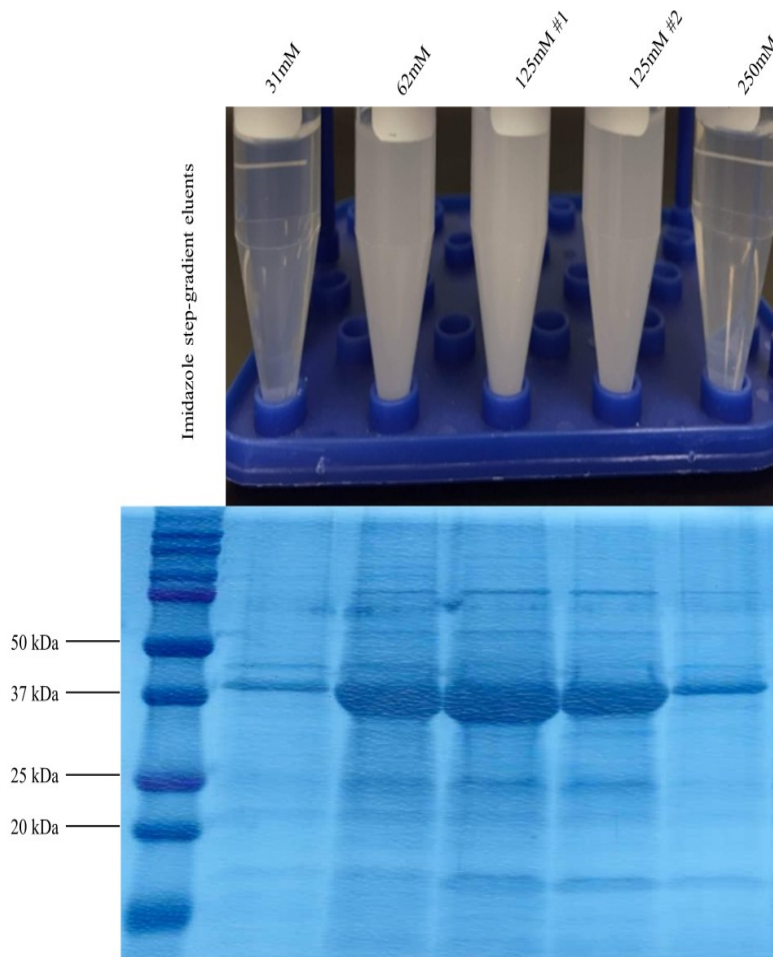
Figure 3. 5 Demonstration of the concentration effects for elastin-like polypeptide (ELP) L$_{80}$–containing metal-affinity eluents.
The sample tubes represent various imidazole step-gradient eluents from a purification of ELP L$_{80}$ from the Ni-NTA column left at room temperature for a few minutes. From left to right, the tubes and their corresponding lanes on a CuCl$_2$-stained 12% SDS-PAGE gel are the 31 mM, 62 mM, 125 mM #1, 125 mM #2, and 250 mM imidazole eluents in 25 mM Tris, 50mM NaCl, pH 8.0. This ELP has a molecular weight of 39.7 kDa; 125 mM #1 and 125 mM #2 refer to sequential fractions of the same eluent. Sample volumes of 15 μL were loaded onto the SDS-PAGE gel. The cloudiness was easily reversed simply by placing the tubes at 4°C for a few minutes.

ITC was then used to purify the ELPs from any contaminating proteins left over from the metal affinity chromatography. This is a common method for purifying ELPs, and it is readily employed throughout the literature. ITC will only work, however, if the ELPs are sufficiently concentrated so that they can undergo a phase transition under reasonable conditions and they are not so hydrophobic as to have a mass aggregation temperature below the freezing point of water. For our hydrophobic proteins, the transition temperatures can fall below room temperature and as such, supplementary NaCl and heated centrifugation were not always necessary. Because of the immobilized metal affinity chromatography, only one round of ITC (in most cases) was necessary to fully purify the ELPs. Figures 3. 6 to 3 .9 shows the affinity chromatography eluents and their subsequent purification using ITC. Determining the appropriate conditions for purifying an ELP using ITC may require some optimization. Mass spectrometry was carried out on the purified ELPs, and we found that most leucine-containing ELPs did not elicit a strong signal. L_{40}, however, did respond well, and its measured molecular weight was 21,155 Da, which matches with the expected molecular weight of 21,125, within the margin-of-error of the spectrometer. Because all of the leucine-containing ELPs were derived from the same DNA sequence, this result suggests there are no reasons to doubt the identity of the other ELPs. Our hybrid purification approach has been used to successfully purify as much as 660 mg of marginally soluble, short ELPs per liter of cells. While this value varied depending on the specific length of the construct, observed yields ranged 250–660 mg/L.

Our newly developed protocol was then utilized to clone Valine-containing ELPs made of 20, 40, 80, and 160 repeats using RDL DNA concatemerization method (Figures 3. 10 to 3. 13). Two of these sequences, V20 and V40, were successfully expressed and purified using our hybrid purification approach (Figures 3. 14 and 3. 15). Additionally, more hydrophilic ELP

constructs were made using our protocol and then expressed and purified using an ITC-only method. Constructs containing Alanine (A) and Valine (V) at the guest amino acid position at a ratio of 1:1. Using RDL method, multiple lengths of the AV-ELP construct were successfully cloned including 20, 40, 80, 100, 120, 140, and 160 repeats (Figures 3. 16 to 3. 22). One construct, AV_{120} was picked and successfully expressed and purified (Figure 3. 23).
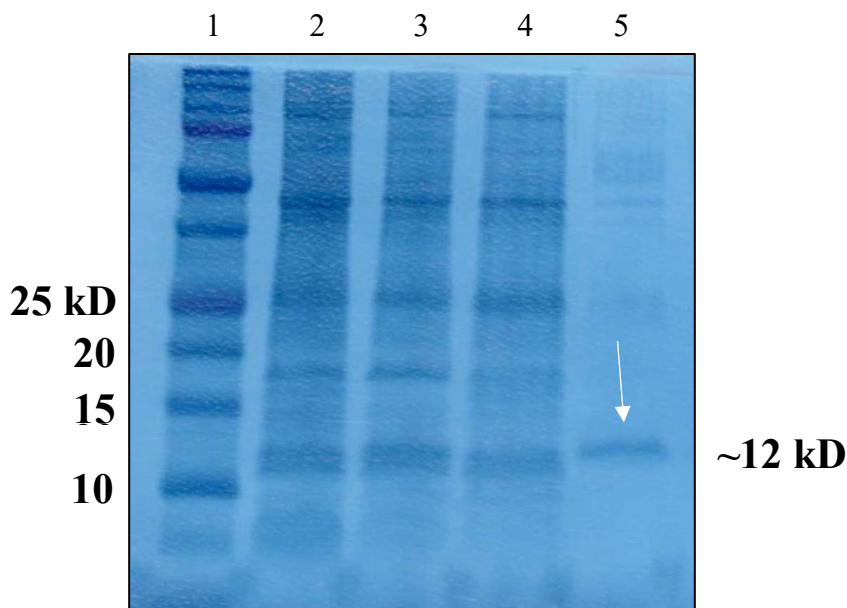
Figure 3. 6 Polyacrylamide gel demonstrating the results of metal-affinity and inverse temperature cycling (ITC) purification of elastin-like polypeptide (ELP) L_{20}.

Lane 1 was loaded with 5 μL of the molecular weight ladder. Lanes 2 and 3 were loaded with 15 μL samples of eluents from the metal-affinity purification eluted with 62 mM imdiazole (Lane 2) and 125 mM imidazole (Lane 3) and showing the ELP band at 12 kDa. Lane 4 shows the impurities from 15 μL eluent collected after the hot spin in the ITC procedure, and Lane 6 was loaded with 15 μL of the final purified ELP sample after the cold spin. Samples were run on a Tris-tricine gel and stained with CuCl2.
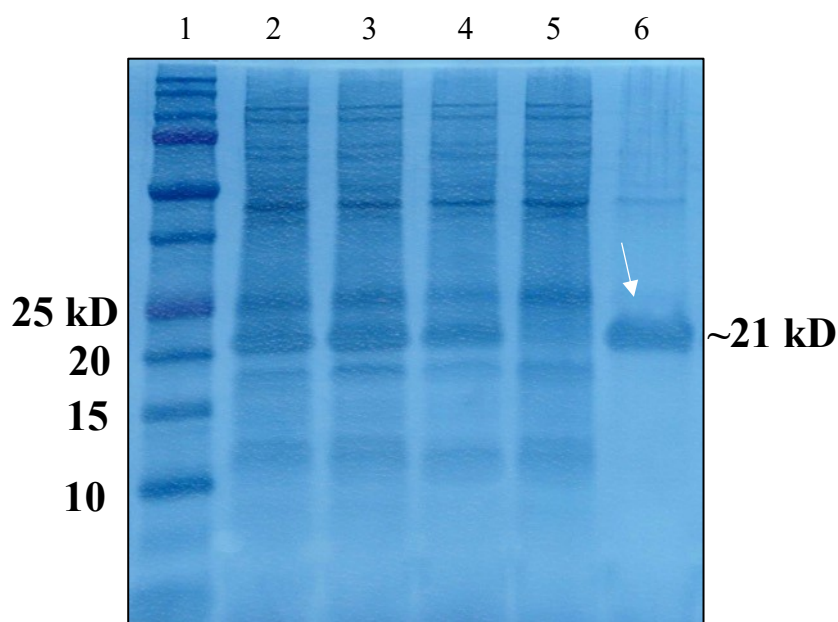
Figure 3. 7 Polyacrylamide gel demonstrating the results of metal-affinity and inverse temperature cycling (ITC) purification of elastin-like polypeptide (ELP) L$_{40}$.

Lane 1 was loaded with 5 µL of the molecular weight ladder. Lanes 2-4 were loaded with 15 µL samples of eluents from the metal-affinity purification eluted with 62 mM imdiazole (Lane 2 and 3) and 125 mM imidazole (Lane 4) and showing the ELP band at 21 kDa. Lane 5 shows the impurities from 15 µL eluent collected after the hot spin in the ITC procedure, and Lane 6 was loaded with 15 µL of the final purified ELP sample after the cold spin and shows the ELP primarily as a monomer but with a small amount of dimer as well. Samples were run on a Tris-tricine gel and stained with CuCl2

Figure 3. 8 Polyacrylamide gel demonstrating the results of metal-affinity and inverse temperature cycling (ITC) purification of elastin-like polypeptide (ELP) L$_{80}$.

Lane 1 was loaded with 5 µL of the molecular weight ladder. Lanes 2 is the crude lysate. Lanes 3-6 were loaded with 15 µL samples of eluents from the metal-affinity purification eluted with 62 mM imdiazole (Lanes 3 and 4) and 125 mM imidazole (Lanes 5 and 6) and showing the ELP band at 40 kDa. Lane 7 shows the impurities from 15 µL eluent collected after the hot spin in the ITC procedure, and Lane 8 was loaded with 15 µL of purified ELP sample after the cold spin in round 1 ITC. Lane 9 loaded with 15 µL of the final purified ELP sample after the cold spin after round 2 ITC. Samples were run on a 12% SDS-PAGE gel and stained with CuCl2.

Figure 3. 9 Polyacrylamide gel demonstrating the results of metal-affinity and inverse temperature cycling (ITC) purification of elastin-like polypeptide (ELP) L$_{160}$.

Lane 1 was loaded with 5 µL of the molecular weight ladder. Lanes 2-6 were loaded with 15 µL samples of eluents from the metal-affinity purification eluted with 31 mM imdiazole (Lane 2) and 62 mM imdiazole (Lane 3) and 125 mM imidazole (Lanes 4 and 5) and showing the ELP band at 76 kDa. Lane 6 shows the impurities from 15 µL eluent collected after the hot spin in the round 1 ITC procedure, and Lane 7 shows the impurities after the hot spin in round 2 ITC. Lane 8 was loaded with 15 µL of the final purified ELP sample after the cold spin. Samples were run on a 12% SDS-PAGE gel and stained with CuCl$_2$.

Figure 3. 10 Successful doubling of an elastin-like polypeptide (ELP) V$_{10}$ insert to V$_{20}$.

Plasmids were digested with *PflmI* and *BglI* for 1 h and then run on a 2% agarose gel before being stained with ethidium bromide. This digest should yield 170, 1118 and 1371 bp bands from the vector, plus an ELP band whose size will vary. In this instance, the V$_{20}$ gene was 300 bp long. Lane 1 is the molecular weight ladder. Lanes 2-9 are clones from the RDL reaction concatemerizing V$_{10}$ to V$_{20}$. Based on the increase in band sizes, Lanes 8 and 9 contain the genes for V$_{20}$.

Figure 3. 11 Successful doubling of an elastin-like polypeptide (ELP) V_{20} insert to V_{40}.

Plasmids were digested with *PflmI* and *BglI* for 1 h and then run on a 2% agarose gel before being stained with ethidium bromide. This digest should yield 170, 1118 and 1371 bp bands from the vector, plus an ELP band whose size will vary. In this instance, the V_{40} gene was 600 bp long. Lane 1 is a positive control digest of pUC19-V_{20}. Lane 2 is the molecular weight ladder. Lanes 3-7 are clones from the RDL reaction concatemerizing V_{20} to V_{40}. Based on the increase in band sizes, Lanes 3-7 contain the genes for V_{40}.

Figure 3. 12 Successful doubling of an elastin-like polypeptide (ELP) V_{40} insert to V_{80}.

Plasmids were digested with *PflmI* and *BglI* for 1 h and then run on a 1% agarose gel before being stained with ethidium bromide. This digest should yield 170, 1118 and 1371 bp bands from the vector, plus an ELP band whose size will vary. In this instance, the V_{80} gene was 1200 bp long. Lane 1 is the molecular weight ladder. Lane 2 is a positive control digest of pUC19-V_{40}. Lanes 3-10 are clones from the RDL reaction concatemerizing V_{40} to V_{80}. Based on the increase in band sizes, Lanes 3-5, and 9 contain the genes for V_{40}, while Lane 10 likely contains an V_{160} gene. The V_{160} is the result of a double insertion of the ELP V_{40} gene into a single cloning vector. This is not an uncommon occurrence while performing RDL using the recommended molar ratios of insert to vector and may actually be beneficial in some cases.
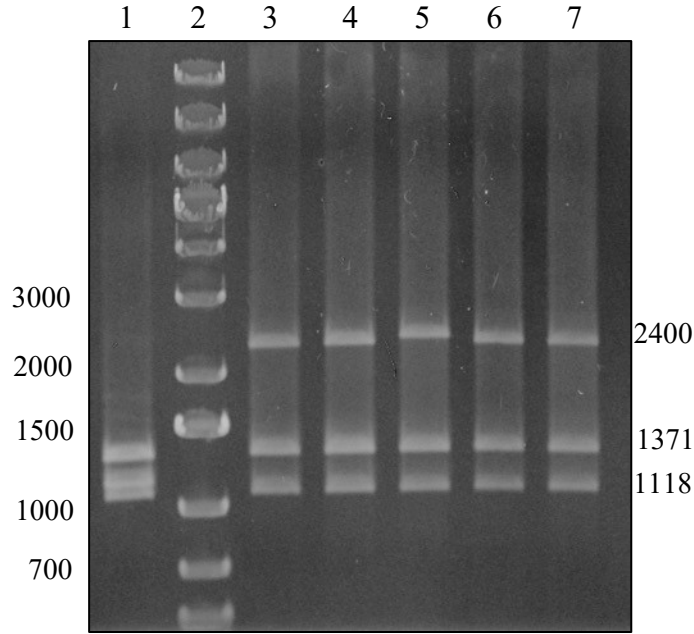
Figure 3. 13 Successful doubling of an elastin-like polypeptide (ELP) V$_{80}$ insert to V$_{160}$.

Plasmids were digested with *PflmI* and *BglI* for 1 h and then run on a 0.8% agarose gel before being stained with ethidium bromide. This digest should yield 170, 1118 and 1371 bp bands from the vector, plus an ELP band whose size will vary. In this instance, the V$_{160}$ gene was 2400 bp long. Lane 1 is a positive control digest of pUC19-V$_{80}$. Lane 2 is the molecular weight ladder. Lanes 3-7 are clones from the RDL reaction concatemerizing V$_{80}$ to V$_{160}$. Based on the increase in band sizes, Lanes 3-7 contain the genes for V$_{160}$.
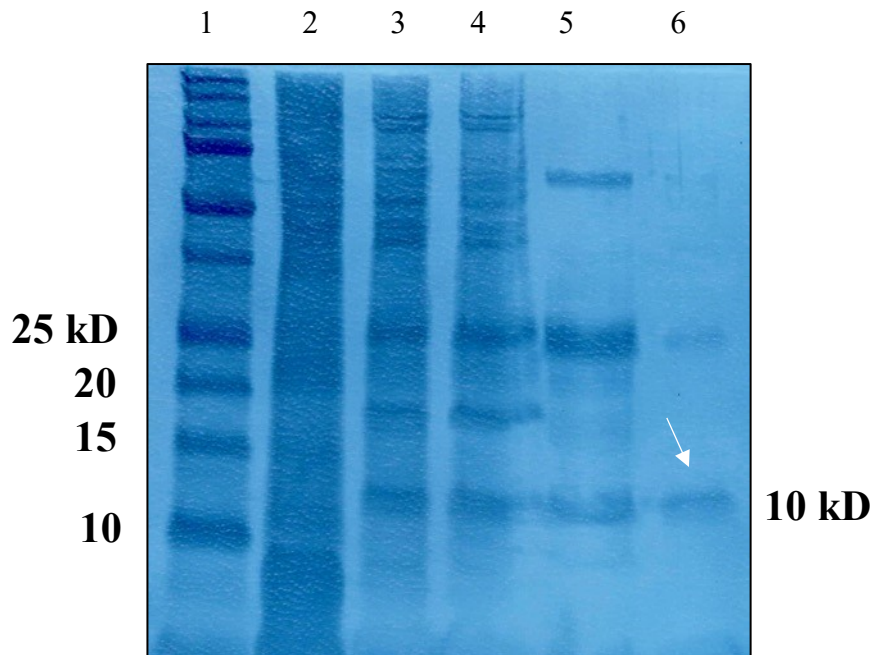
Figure 3. 14 Polyacrylamide gel demonstrating the results of metal-affinity and inverse temperature cycling (ITC) purification of elastin-like polypeptide (ELP) V$_{20}$

Lane 1 was loaded with 5 µL of the molecular weight ladder. Lanes 2 is crude lysate. Lanes 3 and 4 were loaded with 15 µL samples of eluents from the metal-affinity purification eluted with 62 mM imdiazole (Lane 3) and 125 mM imidazole (Lane 4) and showing the ELP band at 10 kDa. Lane 5 shows the impurities from 15 µL eluent collected after the hot spin in the ITC procedure, and Lane 6 was loaded with 15 µL of the final purified ELP sample after the cold spin and shows the ELP primarily as a monomer but with a small amount of dimer as well. Samples were run on a Tris-tricine gel and stained with CuCl$_2$.
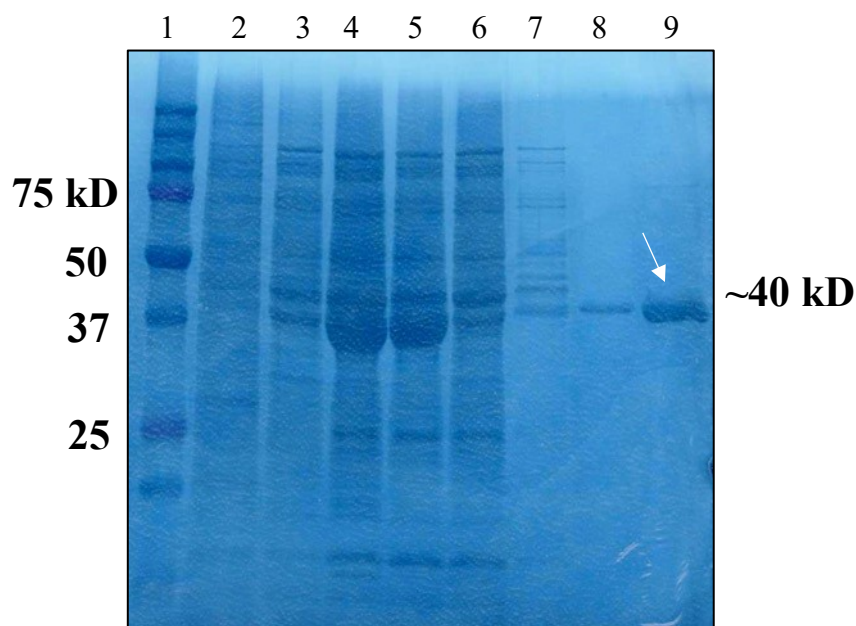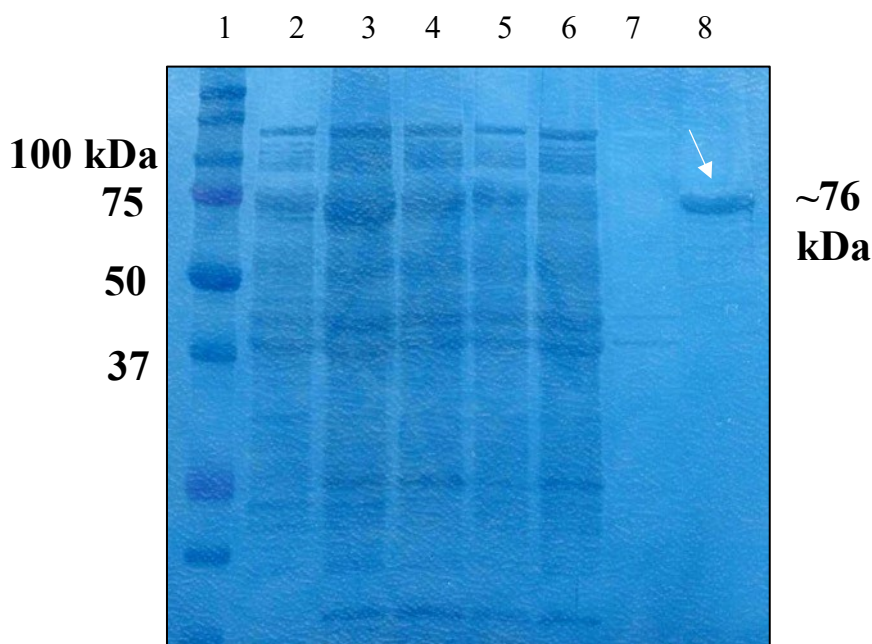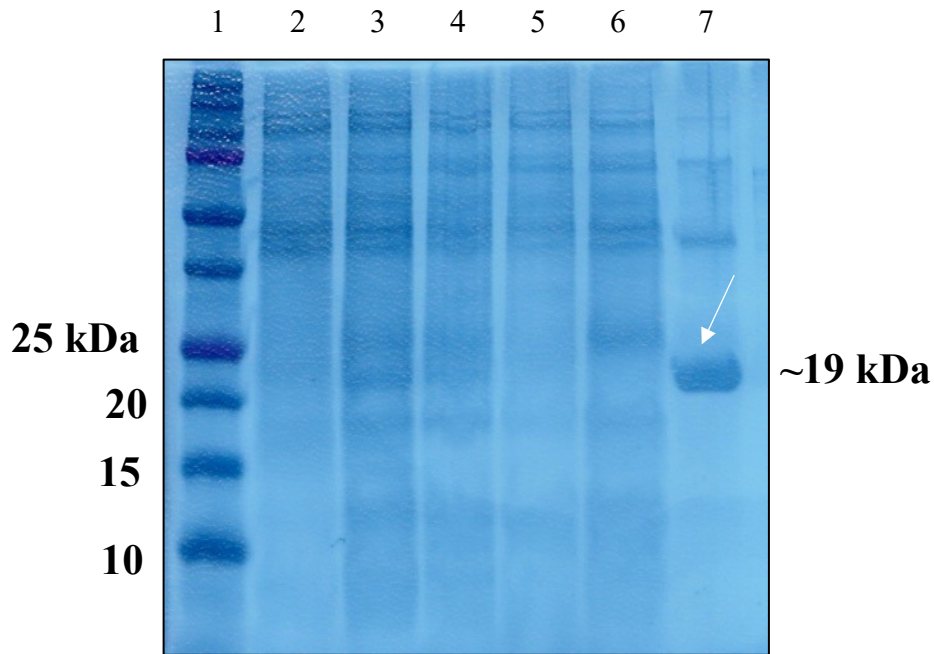
Figure 3. 15 Polyacrylamide gel demonstrating the results of metal-affinity and inverse temperature cycling (ITC) purification of elastin-like polypeptide (ELP) V$_{40}$.

Lane 1 was loaded with 5 µL of the molecular weight ladder. Lanes 2-5 were loaded with 15 µL samples of eluents from the metal-affinity purification eluted with 31 mM imdiazole (Lane 2) and 62 mM imdiazole (Lane 3) and 125 mM imidazole (Lanes 4 and 5) and showing the ELP band at 19 kDa. Lane 6 shows the impurities from 15 µL eluent collected after the hot spin in the ITC procedure, and Lane 7 was loaded with 15 µL of the final purified ELP sample after the cold spin and shows the ELP primarily as a monomer but with a small amount of dimer as well. Samples were run on a Tris-tricine gel and stained with CuCl$_2$.
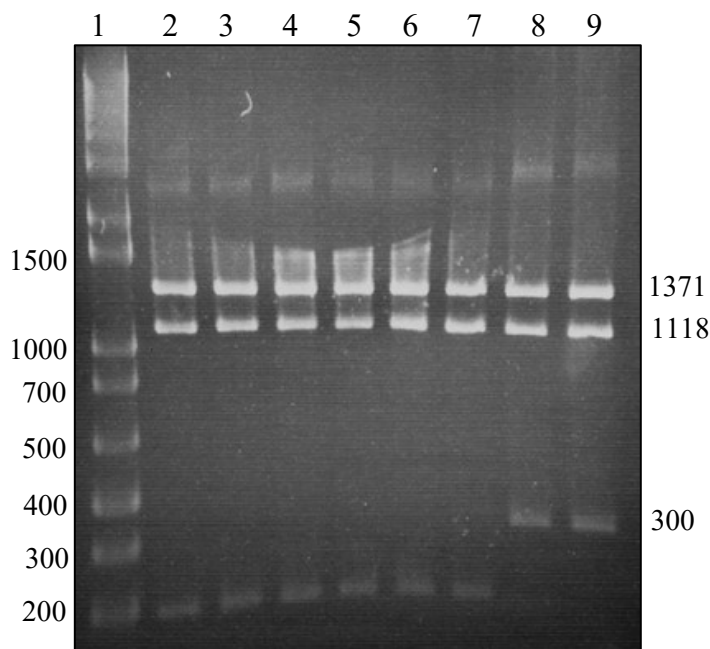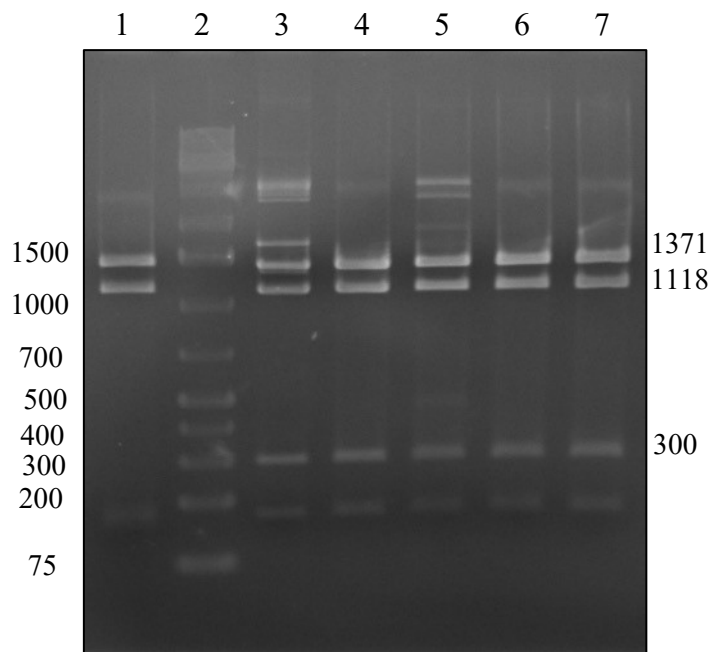

Figure 3. 16 Successful doubling of an elastin-like polypeptide (ELP) AV$_{10}$ insert to AV$_{20}$.

Plasmids were digested with *PflmI* and *BglI* for 1 h and then run on a 2% agarose gel before being stained with ethidium bromide. This digest should yield 170, 1118 and 1371 bp bands from the vector, plus an ELP band whose size will vary. In this instance, the AV$_{20}$ gene was 300 bp long. Lane 1 is a positive control digest of pUC19-AV$_{10}$. Lane 2 is the molecular weight ladder. Lanes 3-7 are clones from the RDL reaction concatemerizing AV$_{10}$ to AV$_{20}$. Based on the increase in band sizes, Lanes 3-7 contain the genes for AV$_{20}$. Note that the 170 bp vector-derived fragment is clearly visible in Lanes 3–7 but overlaps the AV$_{10}$ gene in Lane 1.
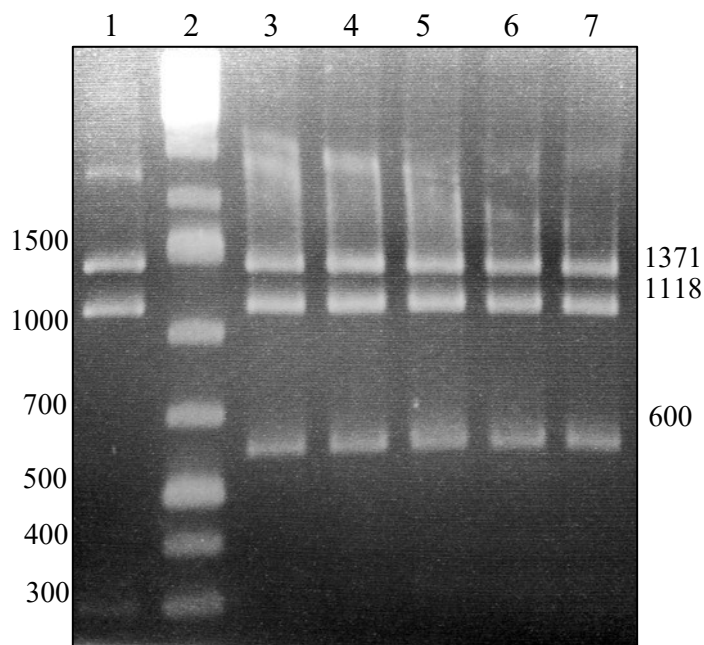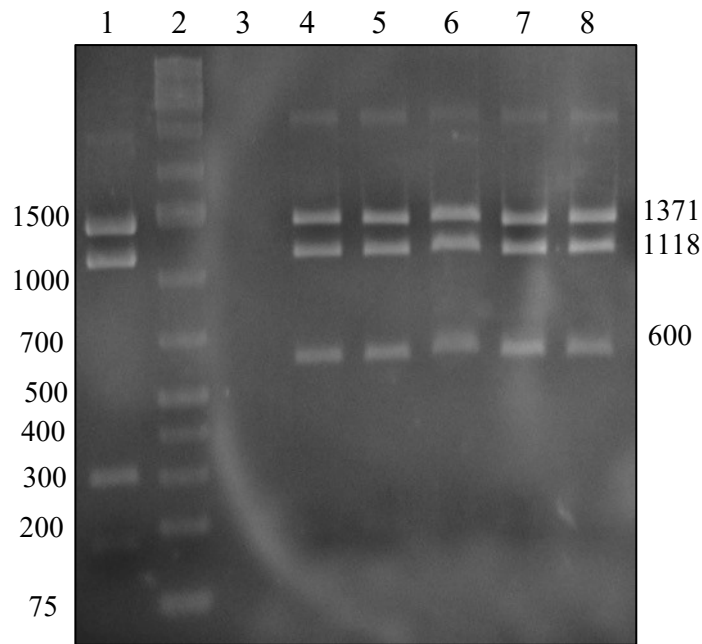
Figure 3. 17 Successful doubling of an elastin-like polypeptide (ELP) AV$_{20}$ insert to AV$_{40}$.

Plasmids were digested with *PflmI* and *BglI* for 1 h and then run on a 2% agarose gel before being stained with ethidium bromide. This digest should yield 170, 1118 and 1371 bp bands from the vector, plus an ELP band whose size will vary. In this instance, the AV$_{40}$ gene was 600 bp long. Lane 1 is a positive control digest of pUC19-AV$_{10}$. Lane 2 is the molecular weight ladder. Lane 3 is empty. Lanes 4-8 are clones from the RDL reaction concatemerizing AV$_{20}$ to AV$_{40}$. Based on the increase in band sizes, Lanes 4-8 contain the genes for AV$_{40}$.
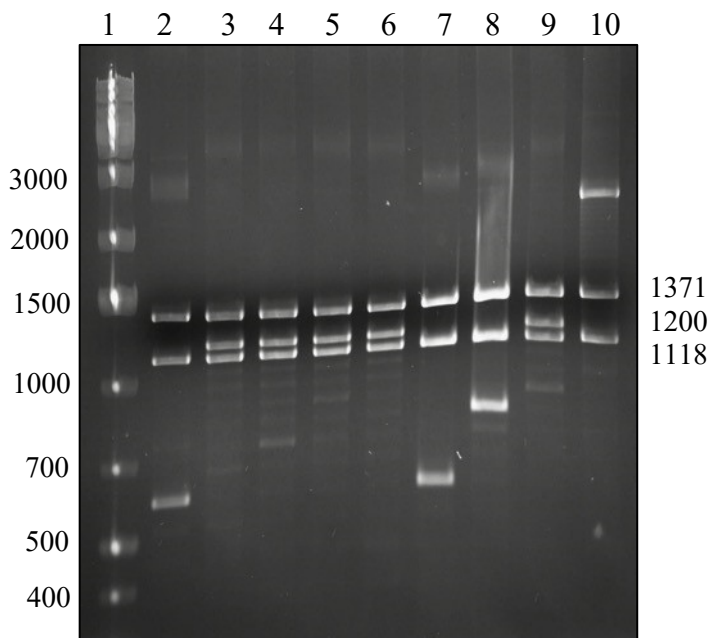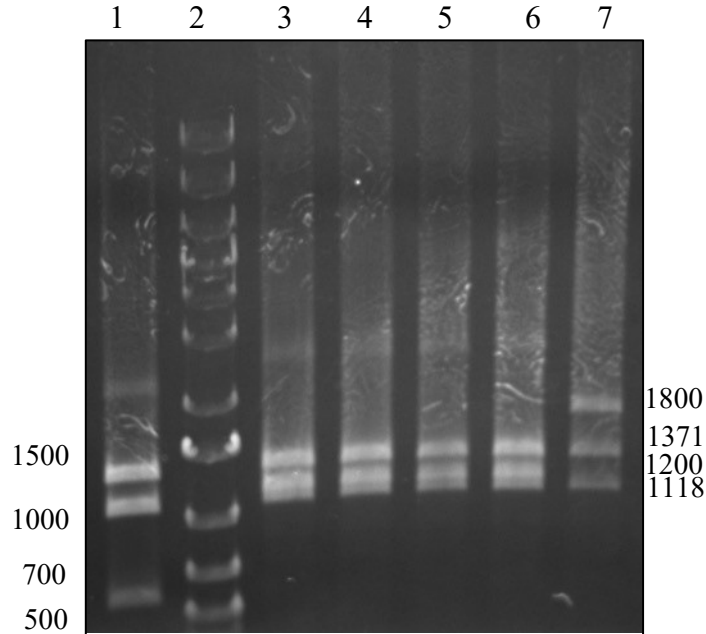

Figure 3. 18 Successful doubling of an elastin-like polypeptide (ELP) AV$_{40}$ insert to AV$_{80}$.

Plasmids were digested with *PflmI* and *BglI* for 1 h and then run on a 0.8% agarose gel before being stained with ethidium bromide. This digest should yield 170, 1118 and 1371 bp bands from the vector, plus an ELP band whose size will vary. In this instance, the AV$_{80}$ gene was 1200 bp long. Lane 1 is a positive control digest of pUC19-AV$_{40}$. Lane 2 is the molecular weight ladder. Lanes 3-7 are clones from the RDL reaction concatemerizing AV$_{40}$ to AV$_{80}$. Based on the increase in band sizes, Lanes 3-6 contain the genes for AV$_{80}$, while Lane 7 likely contains an AV$_{120}$ gene. The AV$_{120}$ is the result of a double insertion of the ELP AV$_{40}$ gene into a single cloning vector. This is not an uncommon occurrence while performing RDL using the recommended molar ratios of insert to vector and may actually be beneficial in some cases.

58
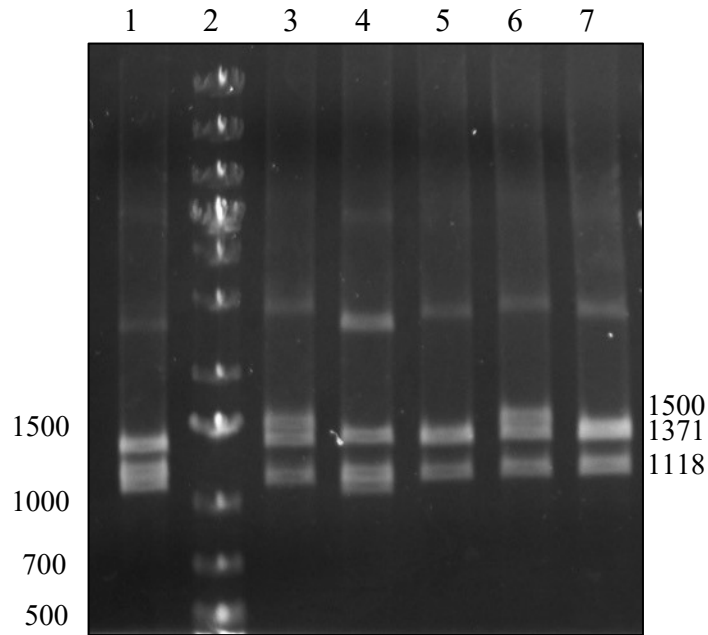
Figure 3. 19 Successful cloning of an elastin-like polypeptide (ELP) AV$_{100}$ by combining AV$_{80}$ open vector and AV$_{20}$ inserts.

Plasmids were digested with *PflmI* and *BglI* for 1 h and then run on a 0.8% agarose gel before being stained with ethidium bromide. This digest should yield 170, 1118 and 1371 bp bands from the vector, plus an ELP band whose size will vary. In this instance, the AV$_{100}$ gene was 1500 bp long. Lane 1 is a positive control digest of pUC19-AV$_{80}$. Lane 2 is the molecular weight ladder. Lanes 3-7 are clones from the RDL reaction concatemerizing AV$_{80}$ to AV$_{100}$. Based on the increase in band sizes, Lanes 3 and 6 contain the genes for AV$_{100}$.
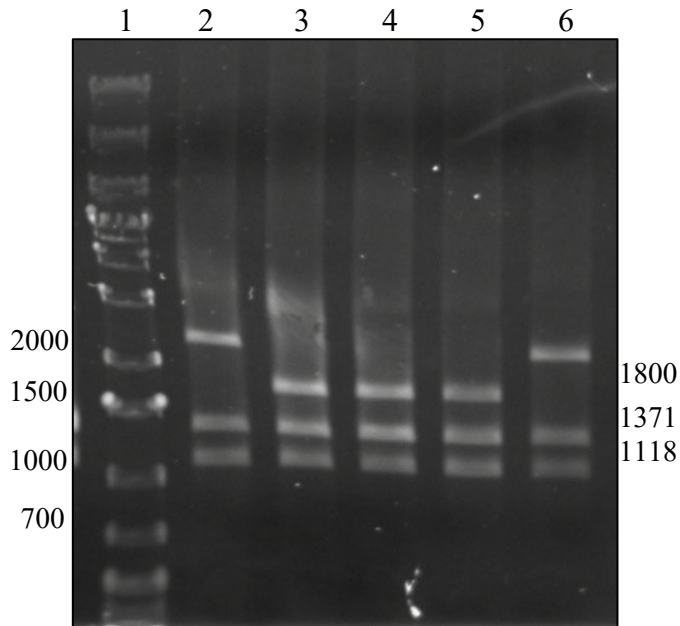
Figure 3. 20 Successful cloning of an elastin-like polypeptide (ELP) AV$_{120}$ by combining AV$_{80}$ open vector and AV$_{40}$ inserts.

Plasmids were digested with *PflmI* and *BglI* for 1 h and then run on a 0.8% agarose gel before being stained with ethidium bromide. This digest should yield 170, 1118 and 1371 bp bands from the vector, plus an ELP band whose size will vary. In this instance, the AV$_{120}$ gene was 1800 bp long. Lane 1 is the molecular weight ladder. Lanes 2-6 are clones from the RDL reaction concatemerizing AV$_{80}$ to AV$_{120}$. Based on the increase in band sizes, Lanes 3-5 contain the genes for AV$_{120}$, while Lanes 2 and 6 likely contains an AV$_{160}$ gene. The AV$_{160}$ is the result of a double insertion of the ELP AV$_{40}$ gene into a single cloning vector AV$_{80}$. This is not an uncommon occurrence while performing RDL using the recommended molar ratios of insert to vector and may actually be beneficial in some cases.

59
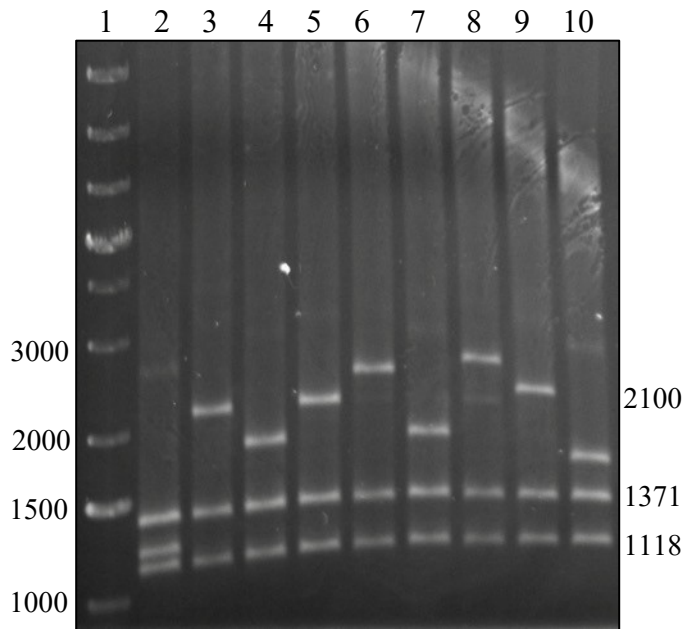
Figure 3. 21 Successful cloning of an elastin-like polypeptide (ELP) AV$_{140}$ by combining AV$_{120}$ open vector and AV$_{20}$ inserts.

Plasmids were digested with *PflmI* and *BglI* for 1 h and then run on a 0.8% agarose gel before being stained with ethidium bromide. This digest should yield 170, 1118 and 1371 bp bands from the vector, plus an ELP band whose size will vary. In this instance, the AV$_{140}$ gene was 2100 bp long. Lane 1 is the molecular weight ladder. Lane 2 is a positive control digest of pUC19-AV$_{80}$. Lanes 3-10 are clones from the RDL reaction concatemerizing AV$_{120}$ to AV$_{140}$. Based on the increase in band sizes, Lanes 3, 5, and 9 contain the genes for AV$_{140}$, while Lanes 6 and 8 likely contains an AV$_{160}$ gene. The AV$_{160}$ is the result of a double insertion of the ELP AV$_{20}$ gene into a single cloning vector AV$_{120}$. This is not an uncommon occurrence while performing RDL using the recommended molar ratios of insert to vector and may actually be beneficial in some cases.
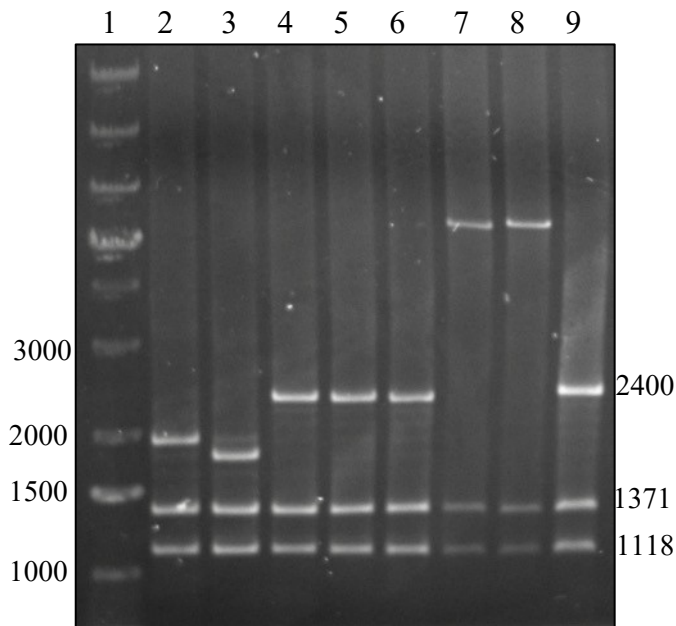
Figure 3. 22 Successful cloning of an elastin-like polypeptide (ELP) AV$_{160}$ by combining AV$_{120}$ open vector and AV$_{40}$ inserts

Plasmids were digested with *PflmI* and *BglI* for 1 h and then run on a 0.8% agarose gel before being stained with ethidium bromide. This digest should yield 170, 1118 and 1371 bp bands from the vector, plus an ELP band whose size will vary. In this instance, the AV$_{160}$ gene was 2400 bp long. Lane 1 is the molecular weight ladder. Lanes 2-9 are clones from the RDL reaction concatemerizing AV$_{120}$ to AV$_{160}$. Based on the increase in band sizes, Lanes 4-6, and 9 contain the genes for AV$_{160}$.

60
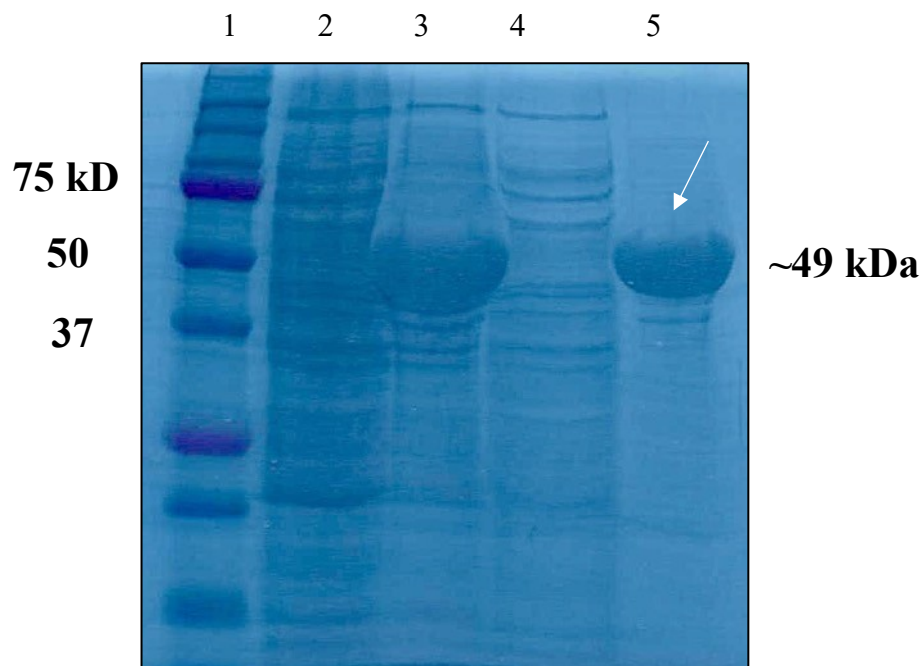
Figure 3. 23 Polyacrylamide gel demonstrating the results of inverse temperature cycling (ITC) purification of elastin-like polypeptide (ELP) AV$_{120}$.
Lane 1 was loaded with 5 μL of the molecular weight ladder. Lane 2 shows the impurities from 15 μL eluent collected after the hot spin in the round 1 ITC procedure, and Lane 3 was loaded with 15 μL of ELP sample after the round 1 cold spin. Lane 4 shows the impurities from 15 μL eluent collected after the hot spin in the round 2 ITC procedure, and Lane 5 was loaded with 15 μL of of the final purified ELP sample after the cold spin. Samples were run on a 12% SDS-PAGE gel and stained with CuCl$_2$.

3.2. Drug entrapment effect on ELP assembly/disassembly behavior

The behavior of ELP L40 at various temperatures and concentrations in the presence and absence of the drug is summarized in Figure 3. 24 The low ELP concentration, 0.1 mg/mL without the drug showed that the particle size drastically changed from approximately 1 to 400 nm at 20°C (Figure 3. 24a). Upon further heating, the diameter increased to about 685 nm. As the sample was subsequently cooled, the diameter of the L40 particles steadily decreased from about 700 to 400 nm until cooled to 5°C, at which point the ELP aggregates returned to the pre-heated sample sizes.
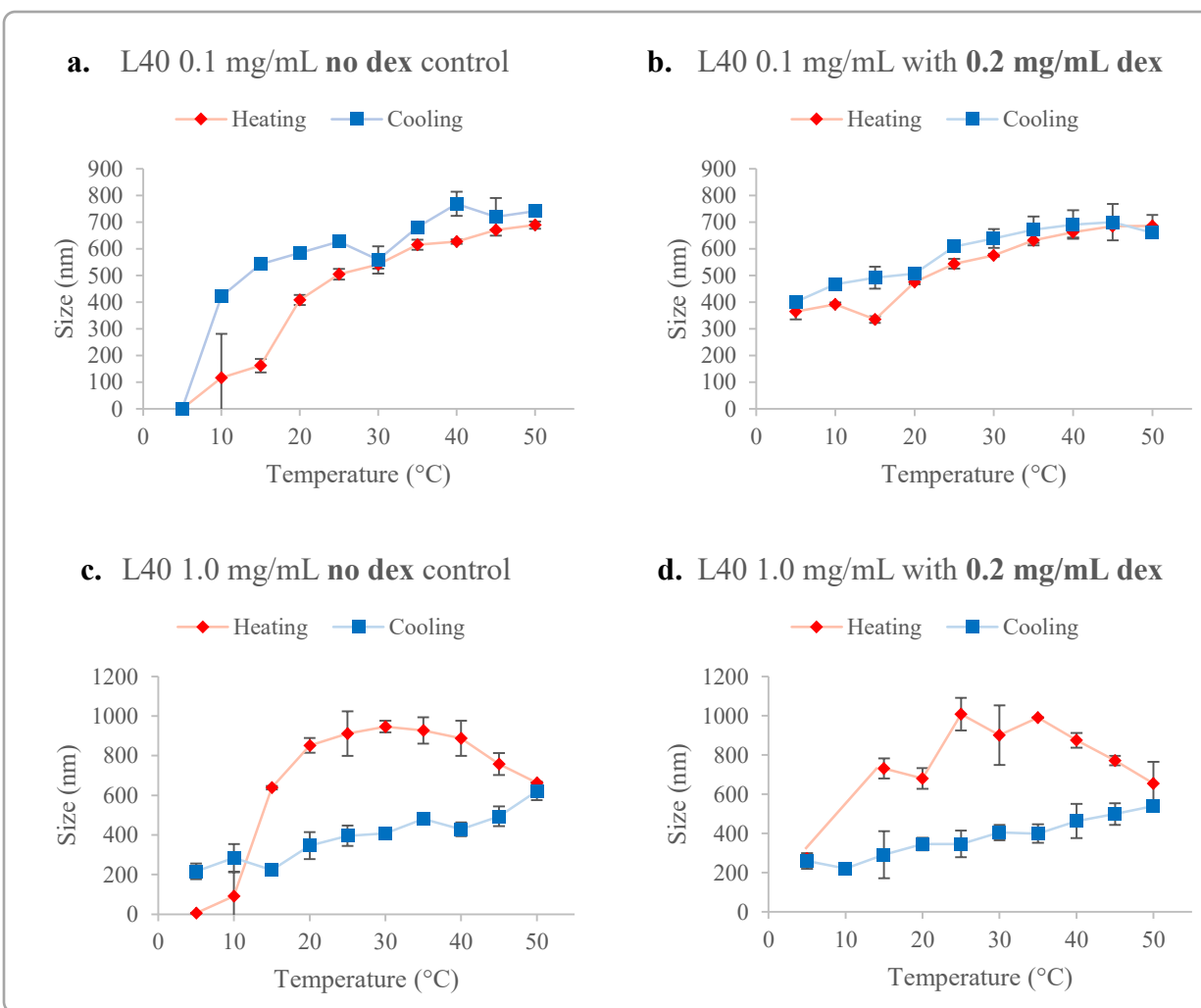
Figure 3. 24 Effect of dexamethasone entrapment on assembly and disassembly behavior of L$_{40}$.
L$_{40}$ diameters as measured using DLS in 1X PBS pH 7.4, upon heating (♦) and cooling (■). Solution temperature was altered in 5°C increments with a 2 minute equilibration period prior to taking readings. ELP solution concentrations were A) 0.1 mg/ml B) DEX+0.1 mg/ml, C) 1.0 mg/ml and D) DEX+1.0 mg/ml. Missing temperature points were considered unreliable and removed. Trend lines are presented only to guide the eye; each data point represents the average ± SD, n≥10.

The size of the particles as they were cooled was slightly higher than the diameters observed while the sample was being heated. However, after mixing the ELP solution with the drug, different assembly/disassembly behavior was observed (Figure 3. 24b). At 5°C, ELP particles at size around 365 nm were already formed. Upon heating to 15°C, the diameter slightly dropped to 330nm followed by relatively stable increase in size until reached 685nm at 50°C

before steadily decreasing in diameter upon cooling until it reached 400nm again at 5°C with no observed particles assembly or disassembly behavior.

At 1.0 mg/mL without the drug, L40 underwent a transition in particle size at 15°C which saw the diameter sharply increase to about 850 nm at 20°C before steadily decreasing in diameter as the temperature increased to 50°C where the particle size became 660nm (Figure 3. 24c). Cooling the sample back down continued the trend of a steadily decreasing particle diameter. At 5°C, the size of the L40 reached 200 nm but did not reach a value small enough to indicate a complete return to pre-heated size for the ELPs. At the same ELP concentration but after the addition of the drug, ~270 nm particles were observed at 5°C, a similar pre-formed particle behavior of the L40 0.1 mg/ml in combination with the drug. ELP particle size was then drastically increased at 15°C to reach about 730 nm followed by a fluctuation of the particle size when increased from 15 to 35°C until it started to steadily decrease to reach ~650nm at 50°C (Figure 3. 24d).

The results of altering solution temperature and ELP concentration on V40 in the presence and absence of the drug are shown in Figure 3. 25. At 0.1 mg/mL, the sample underwent a temperature-triggered increase in diameter at 40°C to ~380 nm (Figure 3. 25a). Once heated to 50°C a drastic reduction in diameter to ~500 nm occurred. This behavior was also observed in reverse when the sample was cooled, with the diameter increasing as the temperature was decreased to 40°C, and a complete return to pre-heated sizes was seen at 30°C. The presence of the drug in ELP solution resulted in pre-formed particles at 5°C in a size about 380 nm (Figure 3. 25b). Unlike the 0.1 mg/mL drug-free ELP run, no ELP phase transition was observed upon heating and particle size increased up to 1 micron as the temperature increased until a sharp reduction in diameter occurred at 50°C to reach ~420 nm. Upon cooling, similar

behavior was observed in reverse. The particles diameter increased when the temperature cooled to 40°C and then gradually decreased until it reached ~ 480 nm when it hit 5°C, with an apparent loss of particle disassembly behavior.
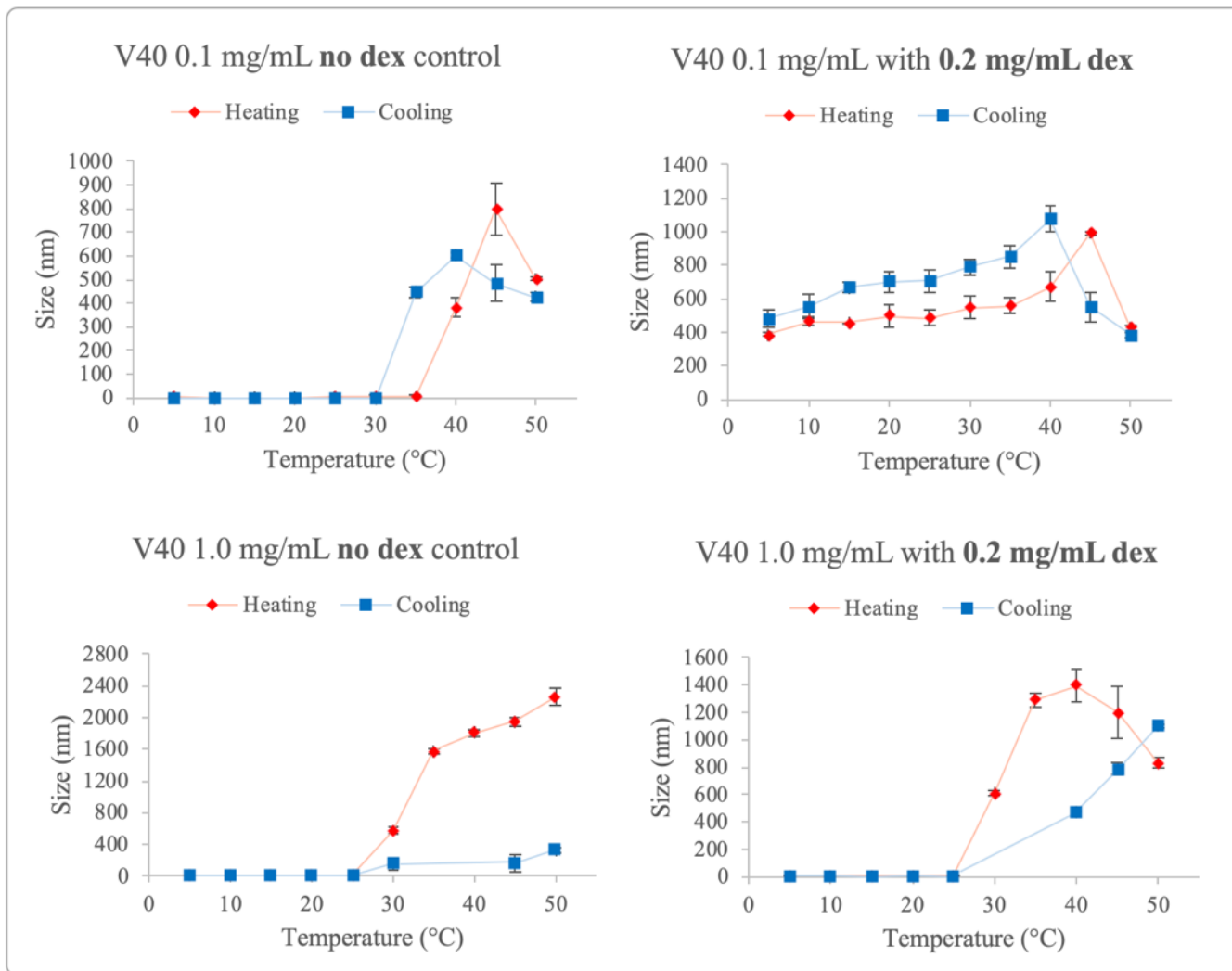
Figure 3. 25 Effect of dexamethasone entrapment on assembly and disassembly behavior of V_{40}
ELP V_{40} diameters as measured using DLS in 1X PBS pH 7.4, upon heating (♦) and cooling (■). Solution temperature was altered in 5°C increments with a 2 minute equilibration period prior to taking readings. ELP solution concentrations were A) 0.1 mg/ml B) DEX+0.1 mg/ml, C) 1.0 mg/ml and D) DEX+1.0 mg/ml. Missing temperature points were considered unreliable and removed. Trend lines are presented only to guide the eye; each data point represents the average ± SD, n≥10.

ELP V40 at a concentration of 1.0 mg/ml began to exhibit unusual behavior (Figure 3.25c). It transitioned at a temperature of 30°C, but the initial particle size at that temperature was already 570 nm. As the temperature increased, the diameter rose into the micron range (~2.2 microns). Visual observations made on V40 samples after heating to 50°C showed the presence of some precipitation in the bottom of the DLS cuvette. Once the sample was cooled back to 5°C, no precipitated material was visible in the bottom of the cuvette. This is consistent with the particle diameter for V40 decreasing to <10 nm as the sample was cooled. Interestingly, in the presence of the drug, the ELP V40 at a concentration of 1.0 mg/ml maintained its assembly/disassembly behavior (Figure 3. 25d). Upon heating, a sharp transition in size from 1 to ~600 nm was observed after raising the temperature from 25 to 30°C, which is closely similar to the behavior observed from the control. However, when the temperature reached 50°C, the particle undergone a huge drop in diameter from 1.2 microns to about 800 nm. When the sample was cooled, a consistent decrease in particle size was observed until a complete return to pre-heated sizes was seen at 25°C.

3.3. HPLC Method Validation

The analytical method explains in detail the steps necessary to perform an analysis. The objective of validation of an analytical method is to prove that the method is suitable for the proposed use. Typical analytical characteristics used in method validation are selectivity, linearity, range, accuracy, precision and stability [148].

3.3.1. Linearity and Range

The linearity was demonstrated by multiple analyses (n=9) of six working solutions containing DEX between 0.25 to 25 µg/ml. The linear data are given in Table. 3. The calibration curve was linear in the range of concentrations between 0.25 to 25 µg/ml (Figure 3. 26).

Table 3. 1 Linearity data for analytical method of DEX.

DEX Conc. (µg/ml)	Peak area Mean ± SD	%RSD
0.25	15.4 ± 0.75895	0.049282
0.5	23.9 ± 0.8579	0.035896
1	46.31667 ± 1.28128	0.027663
3	127.23 ± 1.98863	0.01563
5	212.78 ± 1.2703	0.00597
10	436 ± 1.71581	0.003935
25	1105.2 ± 2.35372	0.00213

SD is Standard Deviation; %RSD is Relative Standard Deviation; n=9.

The linear regression equation of the standard curve between average peak areas of DEX (Y) versus DEX working solutions concentrations (X) is shown in equation (1)

$$Y = 44.122 \ (\pm 0.0937) \ X - 1.0892 \ (\pm 0.2935) \ \dots (1)$$

here, Y is the peak area and X is the DEX concentration (µg/ml). It shows a good linear relationship with the correlation coefficient (R^2=0.9999).
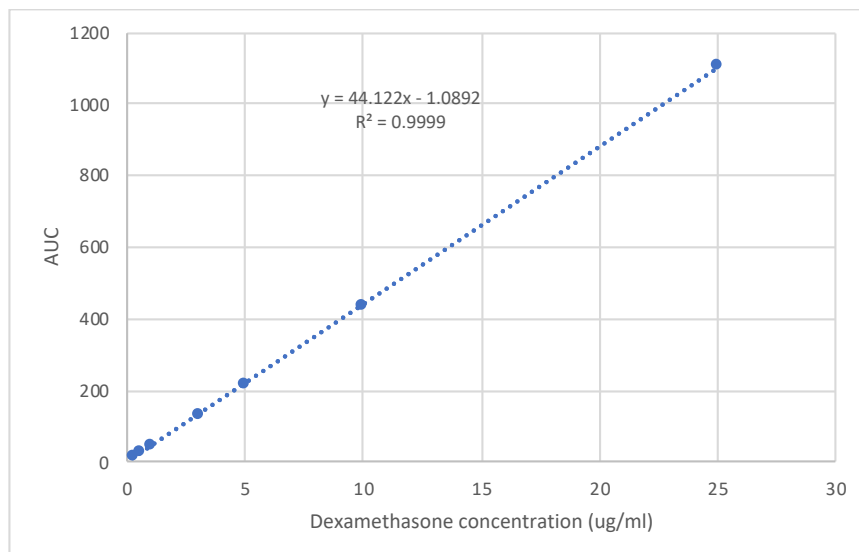
Figure 3. 26 Standard calibration curve of average peak areas versus corresponding DEX concentration from 9 independent replicates

This concludes that the method is linear throughout the range selected (from 0.25 to 25 µg/ml).

3.3.2. Accuracy and Precision

The accuracy and precision were verified by multiple analyses (n=3) of four working solutions containing DEX at 0.375, 3.75, 8 and 17.5 µg/ml. The data are given in Table 3. 2.

Table 3. 2 Accuracy and precision data for analytical method of DEX

Nominal Conc. (µg/ml)	Found Conc. Mean ± SD (µg/ml)	%RSD (%)	Percentage Recovery (%)
0.375	0.380 ± 0.01	1.502	101.27
3.75	3.74 ± 0.002	0.061	99.84
8	7.98 ± 0.01	0.171	99.80
17.5	17.46 ± 0.01	0.084	99.79

SD is Standard Deviation; %RSD is Relative Standard Deviation; n=3.

The result shows that the %RSD is not more than 2% that confined between 0.084% and 1.502% and the percentage recovery lies between 99.635 and 102.680. This confirms that the result is within the acceptable limit and hence the method is accurate and precise.

3.3.3. Selectivity

DEX with HPLC grade purity ≥98% purchased from (Sigma-Aldrich, St. Louis, Missouri, USA) was used in this work. The peak purity for sample solutions and working drug solutions were found to be similar, which means that there is no interference from mobile phase, diluents, dissolution medium or excipients. From the results it can be concluded that the method is selective for the analysis of DEX in its various solutions by this HPLC method of analysis.

3.3.4. Limit of Quantitation (LOQ) and Limit of Detection (LOD)

To determine the LOQ the following equation was used: **$LOQ = 10 * SD_{intercept}/Slope$**

The LOQ was found to be **0.6360** µg/ml.

And to determine the LOD the following equation was used: **$LOQ = 3.3 * SD_{intercept}/Slope$**

The LOD was found to be **0.2099** µg/ml.

Finally, Table 3. 3 summarizes the validation parameters of the HPLC method designed in the present study.

From the results achieved, it can be concluded that the HPLC method established in this study is precise, accurate and selective to successfully determine DEX in sample solutions and the method is validated for analysis of DEX in sample solutions in this study.

Table 3. 3 Summary of validation parameters for analytical method of DEX

Parameter	Validation Data
Linearity Range	0.25 –25 µg/ml
Accuracy	99.635 - 102.680
Precision	0.084% and 1.502%
Selectivity	No interference with extraneous materials
LOQ	0.6360 µg/ml
LOD	0.2099 µg/ml

3.4. Encapsulation efficiency

The E.E. of DEX into the ELP particles was measured at a fixed drug concentration of 0.2 mg/mL with varying ELP concentrations. Leucine-containing ELPs, L40, showed E.E. of 45 ± 5.8% and 37 ± 3.4%, per total amount of DEX added during the preparation of the particles at ELP concentrations of 0.1 and 1.0 mg/mL, respectively. E.E. of valine-containing ELPs was 39 ± 4.2% and 30 ± 1.6% at ELP concentrations of 0.1 and 1.0 mg/mL, respectively.

3.5. Screening of a phage-displayed peptide library

In vivo phage display was carried out using a commercial linear 12-mer peptide phage library and involved IP administration of phage library in consecutive three rounds of tissue selection. IP was chosen as the method of phage administration as it is the most commonly used method for small species for which intravenous access is challenging or not possible and it can be used to administer large volumes of fluid safely. Animals were divided into three groups, ischemic penumbra, ischemic core, and healthy/control and were exposed to moderate, severe, or no HI, respectively. The injury in animals with ischemia and 60min hypoxia will result in an all-

penumbra posterior cortex while animals with ischemia and 150min hypoxia should have a posterior cortex that is all core injury. After three rounds of screening, 12 clones from rounds 1 and 2 and 25 clones from round 3 from each experimental group were randomly picked. The peptide-coding DNA inserts were sequenced and then translated into corresponding peptide sequences. An alignment analysis of the peptide sequences was accomplished using the Clustal W program and revealed frequently occurring sequences (Tables 3. 1, 3. 2, 3. 3). In the ischemic penumbra group, 25 of 25 randomly picked clones from the third round had the sequence ANDTSPMMTKSW (designated as PHP1) with occurrence rate of 100%. Similarly, in the ischemic core group, there was a 100% occurrence rate of DSPEYLRMSSRA sequence (designated as CHP1), which appeared in 25 of 25 sequenced clones. In the healthy/control group, 12 of 25 sequenced clones had WTLDYTFHSMNM (48%) sequence (designated as HHP1), and 11 clones had GERPPSLPASPL (44%) sequence (designated as HHP2). To identify any homologies with known rat proteins, an NCBI-BLAST protein search against the rat genome was performed. Tables 4. 2, 4. 3 and 4. 4 list examples of rat proteins containing homologous motifs to the identified peptides revealed by searching the Swissprot database. The phage-displayed peptides may mimic one or more of these proteins in homing and binding to stroke or healthy brain tissues. The identified peptides were screened against SAROTUP "Scanner And Reporter Of Target- Unrelated Peptides" tool and no previous hit sequences similar to the peptides identified in this work were achieved.

Table 3. 4 Alignment of penumbra group peptide sequences after three rounds of biopanning.

	#	Round 1	Round 2	Round 3	Round 3 analysis:	Frequency	Percentage %
Penumbra injury animals	1	TGSAKFLQRDTH	GSWNTFRAQPTI	ANDTSPMMTKSW	ANDTSPMMTKSW	25/25	100%
	2	NO INSERT	ANDTSPMMTKSW	ANDTSPMMTKSW			
	3	TGSAKFLQRDTH	ANDTSPMMTKSW	ANDTSPMMTKSW			
	4	TNPLDARFHEPT	GSWNTFRAQPTI	ANDTSPMMTKSW			
	5	KIMAAYNNISVE	SYQRLPQFWAPT	ANDTSPMMTKSW			
	6	NO INSERT	ANDTSPMMTKSW	ANDTSPMMTKSW			
	7	TGSAKFLQRDTH	GSWNTFRAQPTI	ANDTSPMMTKSW			
	8	VPVVNVQLAMGW	ANDTSPMMTKSW	ANDTSPMMTKSW			
	9	NO INSERT	GSWNTFRAQPTI	ANDTSPMMTKSW			
	10	ANDTSPMMTKSW	ANDTSPMMTKSW	ANDTSPMMTKSW			
	11	NO INSERT	THRVEGSAQKYL	ANDTSPMMTKSW			
	12	APNGDESIRHDS	GSWNTFRAQPTI	ANDTSPMMTKSW			
	13			ANDTSPMMTKSW			
	14			ANDTSPMMTKSW			
	15			ANDTSPMMTKSW			
	16			ANDTSPMMTKSW			
	17			ANDTSPMMTKSW			
	18			ANDTSPMMTKSW			
	19			ANDTSPMMTKSW			
	20			ANDTSPMMTKSW			
	21			ANDTSPMMTKSW			
	22			ANDTSPMMTKSW			
	23			ANDTSPMMTKSW			
	24			ANDTSPMMTKSW			
	25			ANDTSPMMTKSW			

Table 3. 5 Alignment of core group peptide sequences after three rounds of biopanning.

	#	Round 1	Round 2	Round 3	Round 3 analysis:	Frequency	Percentage %
Core injury animals	1	AYLHVPNMTRTD	DSPEYLRMSSRA	DSPEYLRMSSRA	DSPEYLRMSSRA	25/25	100
	2	IPQRYAPVSNLP	DSPEYLRMSSRA	DSPEYLRMSSRA			
	3	IPQRYAPVSNLP	DSPEYLRMSSRA	DSPEYLRMSSRA			
	4	TIQPSFRPPYFF	DSPEYLRMSSRA	DSPEYLRMSSRA			
	5	EALTVNIKREME	DSPEYLRMSSRA	DSPEYLRMSSRA			
	6	GPTADHFHNRHE	DSPEYLRMSSRA	DSPEYLRMSSRA			
	7	QSNHMRPLNMLQ	DSPEYLRMSSRA	DSPEYLRMSSRA			
	8	DSPEYLRMSSRA	DSPEYLRMSSRA	DSPEYLRMSSRA			
	9	QSNHMRPLNMLQ	DSPEYLRMSSRA	DSPEYLRMSSRA			
	10	TIQPSFRPPYFF	DSPEYLRMSSRA	DSPEYLRMSSRA			
	11	APMFTPMLSANA	DSPEYLRMSSRA	DSPEYLRMSSRA			
	12	TIQPSFRPPYFF	DSPEYLRMSSRA	DSPEYLRMSSRA			
	13			DSPEYLRMSSRA			
	14			DSPEYLRMSSRA			
	15			DSPEYLRMSSRA			
	16			DSPEYLRMSSRA			
	17			DSPEYLRMSSRA			
	18			DSPEYLRMSSRA			
	19			DSPEYLRMSSRA			
	20			DSPEYLRMSSRA			
	21			DSPEYLRMSSRA			
	22			DSPEYLRMSSRA			
	23			DSPEYLRMSSRA			
	24			DSPEYLRMSSRA			
	25			DSPEYLRMSSRA			

Table 3. 6 Alignment of healthy group peptide sequences after three rounds of biopanning.

	#	Round 1	Round 2	Round 3	Round 3 analysis:	Frequency	Percentage %
Healthy/Control animals	1	LEGFEGHTHAQH	GERPPSLPASPL	WTLDYTFHSMNM	**WTLDYTFHSMNM**	12/25	48
	2	KTWPETRIAALT	WTLDYTFHSMNM	GERPPSLPASPL	**GERPPSLPASPL**	11/25	44
	3	GHESYSRSLSNP	GERPPSLPASPL	GERPPSLPASPL	LEGFEGHTHAQH	1/25	4
	4	LEGFEGHTHAQH	GERPPSLPASPL	GERPPSLPASPL	DGAPIYDAYVAV	1/25	4
	5	GGGSAETVESCL	GERPPSLPASPL	WTLDYTFHSMNM			
	6	LEGFEGHTHAQH	GERPPSLPASPL	WTLDYTFHSMNM			
	7	WTLDYTFHSMNM	LEGFEGHTHAQH	DGAPIYDAYVAV			
	8	WTLDYTFHSMNM	WTLDYTFHSMNM	WTLDYTFHSMNM			
	9	WTLDYTFHSMNM	WTLDYTFHSMNM	WTLDYTFHSMNM			
	10	NO INSERT	GERPPSLPASPL	WTLDYTFHSMNM			
	11	LEGFEGHTHAQH	GERPPSLPASPL	WTLDYTFHSMNM			
	12	EALTVNIKREME	WTLDYTFHSMNM	WTLDYTFHSMNM			
	13			WTLDYTFHSMNM			
	14			GERPPSLPASPL			
	15			WTLDYTFHSMNM			
	16			GERPPSLPASPL			
	17			GERPPSLPASPL			
	18			GERPPSLPASPL			
	19			WTLDYTFHSMNM			
	20			GERPPSLPASPL			
	21			GERPPSLPASPL			
	22			GERPPSLPASPL			
	23			WTLDYTFHSMNM			
	24			GERPPSLPASPL			
	25			LEGFEGHTHAQH			

4.   Discussion

Portions of this chapter have been published in:

1. Bahniuk, M.S., **A.K. Alshememry**, and L.D. Unsworth, *High-yield recombinant expression and purification of marginally soluble, short elastin-like polypeptides*. Biotechniques, 2016. 61(6): p. 297-304.

4.1. ELP synthesis

Many of the design considerations for new ELP sequences have been discussed in detail previously [119]. Briefly, the design of the initial DNA sequences should take into account *E. coli* codon bias; that is, the frequency of the employed triplet codons should reflect the naturally occurring frequency of their corresponding tRNAs. The ends of the ELP DNA sequences should be designed such that oligomerization of the DNA eliminates the *PflM*I and *Bgl*I cleavage sites without introducing another cut site for a restriction enzyme employed downstream. While these restriction enzymes are used here to facilitate ELP gene oligomerization, they are not the only two that could be used. In addition to the published guidelines, if individual oligonucleotides are being used, rather than genes already contained in plasmids, the oligonucleotides should be ordered in a semi-purified state. If the oligonucleotides are ordered with only standard desalting as the purification method, there is a high probability that an undesirable heterogeneous product will be obtained because of the highly repeated sequence. Gel purification of the digested vectors, repeating the linearization procedure, and then dephosphorylating the vector are additional introduced steps that helped reducing the number of background colonies resulting from both uncut vector DNA and re-closed empty vectors. Without this additional effort, the number of clones containing only the vector completely eclipsed the number of correctly ligated clones.

Modification of the expression vector before insertion of the ELP gene is a necessary step of RDL [119]. In order for the RDL strategy to generate complete repeats of an ELP gene, some of the DNA encoding for N- and C-terminal amino acids cannot be included in the original ELP oligonucleotide and must be added in the expression vector. This also allows for the introduction of various N- and C-terminal modifications without needing to redo the entire RDL procedure.

The introduction of two *Sfi*I sites and a spacer of appropriate length to the pET-25b(+) vector is a subtle but very significant departure from previous RDL methods [119]. The *Sfi*I restriction enzyme is quite uncommon in its structure, and the majority of the literature on this enzyme states that efficient cleavage of DNA by *Sfi*I only occurs when 2 of its recognition sites are present and separated by roughly 200–300 bp [154-157]. The *Sfi*I enzyme works by simultaneously cleaving at both recognition sites, which results in one compatible set of sticky ends in the vector. Some RDL literature suggests that a single *Sfi*I recognition site is sufficient [118, 119]; however, efficient and reproducible cleavage was only observed in our work when two appropriately spaced recognition sites were located in the same stretch of DNA.

ELPs were expressed by a conventional IPTG induction method. There are other protocols that suggest uninduced expression yields more ELP [158]; however, 24 h expression period dramatically increased expression yields. Then, denaturing nickel affinity chromatography was the first method used to purify the ELPs. Immobilized metal ion affinity chromatography (IMAC) is a purification method commonly employed to purify recombinant proteins containing a short affinity tag consisting of polyhistidine residues. Proteins which have affinity towards certain metals can be used for separating out target protein from a mixture of proteins. Metals like nickel or copper are used to charge the purification resins. Compared to cobalt and other ligands used for IMAC, nickel provides greater capacity for his-tagged protein purification and therefore used in this study [159]. Histidine has several electron donor groups on its imidazole ring that readily form coordination bonds with the immobilized transition metal, which makes histidine exhibit the strongest interaction with immobilized metal ion matrices [159]. The nickel affinity chromatography method was chosen because it can act as a pre-concentration step for poorly expressed ELPs and also because the use of urea helps to ensure

that individual ELPs, as well as any inclusion bodies, are fully solubilized. Especially with very hydrophobic ELPs, there is a chance their transition temperature is below room temperature and that they would end up being inadvertently removed from solution when centrifuging away insoluble cellular contaminants. If the ELPs are poorly expressed, their low concentration could potentially cause the mass aggregation temperature to be prohibitively high, thus making an exclusively ITC-based purification impossible.

Existing ITC purification approaches depend on triggering an ELP phase transition in the *E. coli* cellular lysate. This requires the solubility, transition temperature, and concentration of the ELP to fall within a certain range of values for a successful transition to be possible. For ELPs with a small number of repeats, and thus a high transition temperature, this approach may not be feasible. Additionally, constructs with strongly hydrophobic guest amino acids may have transition temperatures near or below the freezing point of water and, as such, the ITC-only approach may not be viable. In this case, the ELP may be inadvertently removed from the cell lysate when it undergoes centrifugation to remove the insoluble cell debris from the soluble fraction. The result could be the same if the ELPs are overexpressed and end up in inclusion bodies. Preliminary purifications of the leucine-containing ELPs using conventional non-denaturing tip sonication and ITC-only purifications yielded minimal amounts of protein. As such, a new purification approach was necessary.

The advantage of our method is that it is applicable to a wider range of ELP constructs than ITC-only purification procedures. The protocol uses denaturing metal affinity chromatography as the first step in purification. This ensures the ELPs are fully soluble upon cell lysis, in case they have very low transition temperatures or are expressed as inclusion bodies. Should there be an additional, chaotrope-sensitive domain appended to the ELP, non-denaturing

metal affinity chromatography may be an acceptable substitute. The chromatography can also be used to concentrate the ELPs in order to lower their transition temperature to more reasonable levels should they be poorly expressed or have high transition temperatures at moderate concentrations. For instance, this hybrid method was used to successfully purify a conventional hydrophilic ELP construct in our lab that was so poorly expressed (0.35 mg per liter of cells) that standard ITC-only purification failed because the phase transition could not be triggered due to such a low ELP concentration. The chromatography was key to successful purification because it allowed us to significantly pre-concentrate the ELP before attempting ITC. Our hybrid purification approach has been used to successfully purify as much as 660 mg of marginally soluble, short ELPs per liter of cells. While this value varied depending on the specific length of the construct, observed yields ranged from 250 to 660 mg/L. These results are a significant improvement over our in-house attempts to apply conventional ITC-only purification methods to this class of ELPs as well as previously reported yields of comparable marginally soluble, short ELPs that produced roughly 10 and 35 mg per liter of cells, respectively [120, 121]. The first purification step serves to remove a large number of contaminating proteins that would otherwise be carried over into the subsequent ITC step. These contaminating proteins typically would require multiple rounds of ITC to be removed, but by employing affinity chromatography first, a pure product can be obtained after one round of ITC. Furthermore, by using a small polyhistidine tag for the affinity purification, rather than a larger multi-kilodalton partner such as MBP or glutathione S-transferase, it may not be necessary to remove the affinity tag. This reduces the amount of sample preparation and eliminates potential complications if the ELP complexes with its purification partner after the two are cleaved from one another.

Two more ELP series have been developed using this protocol, Valine-containing ELPs and Alanine/Valine containing ELPs. The latter is relatively more hydrophilic and therefore it was designed without the addition of a histidine tag and an ITC-only method was sufficient to obtain a pure ELP in high quantities. Table 4. 1 summarizes all the ELP constructs that have been generated in this work and their detailed information.

Table 4. 1 Summary of ELP constructs generated using our protocol.

Construct name	Complete Amino Acid Sequence	Number of amino acids residues	Charge at pH 7.4	Isoelectric point (pI)	Molecular weight (Da)	DNA made	Protein expressed and purified
L20	MHHHHHHGGENLYFQGGGGGPGVG(VPGLG)$_{10}$VPGVG(VPGLG)$_{10}$VPGWP	133	-0.5	7.14	11835.95	Yes	Yes
L40	MHHHHHHGGENLYFQGGGGGPGVG[(VPGLG)$_{10}$VPGVG]$_3$(VPGLG)$_{10}$VPGWP	243	-0.5	7.14	21125.17	Yes	Yes
L80	MHHHHHHGGENLYFQGGGGGPGVG[(VPGLG)$_{10}$VPGVG]$_7$(VPGLG)$_{10}$VPGWP	463	-0.5	7.14	39703.61	Yes	Yes
L160	MHHHHHHGGENLYFQGGGGGPGVG[(VPGLG)$_{10}$VPGVG]$_{15}$(VPGLG)$_{10}$VPGWP	903	-0.5	7.14	76860.50	Yes	Yes
V20	MHHHHHHGGENLYFQGGGGGPGVG(VPGVG)$_{19}$VPGWP	123	-0.5	7.14	10326.92	Yes	Yes
V40	MHHHHHHGGENLYFQGGGGGPGVG(VPGVG)$_{39}$VPGWP	223	-0.5	7.14	18926.15	Yes	Yes
V80	MHHHHHHGGENLYFQGGGGGPGVG(VPGVG)$_{79}$VPGWP	423	-0.5	7.14	35305.47	Yes	No
V160	MHHHHHHGGENLYFQGGGGGPGVG(VPGVG)$_{159}$VPGWP	823	-0.5	7.14	68064.22	Yes	No
AV20	MSKGPG-(XGVPG)$_{20}$-WP X: Alanine/Valine, ratio 1:1	108	0.8	8.5	8768.19	Yes	No
AV40	MSKGPG-(XGVPG)$_{40}$-WP X: Alanine/Valine, ratio 1:1	208	0.8	8.5	16677.36	Yes	No
AV80	MSKGPG-(XGVPG)$_{80}$-WP X: Alanine/Valine, ratio 1:1	408	0.8	8.5	32495.71	Yes	No
AV100	MSKGPG-(XGVPG)$_{100}$-WP X: Alanine/Valine, ratio 1:1	508	0.8	8.5	40404.89	Yes	No
AV120	MSKGPG-(XGVPG)$_{120}$-WP X: Alanine/Valine, ratio 1:1	608	0.8	8.5	48314.07	Yes	Yes
AV140	MSKGPG-(XGVPG)$_{140}$-WP X: Alanine/Valine, ratio 1:1	708	0.8	8.5	56223.24	Yes	No
AV160	MSKGPG-(XGVPG)$_{160}$-WP X: Alanine/Valine, ratio 1:1	808	0.8	8.5	64132.42	Yes	No

ELP Parameters were calculated using ProtParam. (ExPASy), and PROTEIN CALCULATOR v3.4 by Scripps Research Institute (http://protcalc. sourceforge.net/).

4.2. Drug entrapment effect on ELPs' self-assembly and disassembly behaviour

Two ELP constructs, Valine and Leucine-containing ELPs at 40 repeats, were used to examine the influence of the drug loading on the self-assembly/disassembly behavior of ELPs. Having the length of both constructs held constant at 40 repeats, the effect of guest amino acid hydrophobicity on the ELP phase transition behavior in presence and absence of the drug can also be evaluated.

In the absence of the drug, the concentration of L40 was shown to affect the size of the particles both in the heating and cooling phases. During the heating phase, the average particle sizes increased from ~ 400 – 850 nm as the ELP concentration increased. During cooling, the average particle size was in good agreement with the heating sizes when the ELP was tested at low concentration whereas higher ELP concentration exhibited smaller particles around 200 nm. At no point were micron-sized particles observed. This can also be inferred by comparing the particle size measurements at 50°C unlike cases when the sample underwent precipitation (i.e. V40). The assembly transition temperature was not affected as the ELP concatenation increased, showing a phase transition around 10°C. However, ELP concentration did affect the disassembly behaviour. At 0.1 mg/ml ELP particles showed a complete return to the pre-heated size upon cooling at 5°C and an apparent thermal hysteresis (i.e. discrepancies in the transition temperature when heating and cooling the system) of 5°C. Conversely, at increased concentration, samples did not fully disassemble, and a numerical value cannot be determined.

ELP concentration had a significant effect on the particle size on the Valine-containing ELP (V40) during both heating and cooling cycles. Once above their transition temperature, V40 formed particles ranging from 380 nm to 2 microns in diameter as the concentration of ELP increased. At a concentration of 0.1 mg/ml, a self-assembly behavior was observed when the

temperature reached 40°C followed by an apparent hysteresis upon cooling as particles returned to its pre-heated sizes at 30°C. Notably, at higher concentration, ELP transitioned at 30°C and very large aggregates were formed quickly and precipitation was observed once the samples had been heated to 50°C. This is consistent with the disagreement between sample diameters at 50°C during heating and cooling. However, V40 precipitates resolubilized upon cooling to 5°C and visible settling was no longer apparent. That this construct readily resolubilized was consistent with its observed behavior during purification. Inverse temperature cycling procedures were able to precipitate and resolubilize the V40 normally.

After the addition of drug, Leucine-containing ELPs at low concentration showed a complete loss of their assembly and disassembly behaviour compared to controls as particles were already formed at 5°C and even upon cooling there was no particle disassociation as the diameter remained in the 400 nm range. Similarly, at higher concentration and unlike the control, pre-formed particles were observed at 5°C. However, consistent particle diameters were obtained during the cooling phase similar to controls.

Valine-containing ELPs (V40) behaved a little differently in the presence of the drug. At low concentration, the particle sizes were not in agreement with the control during both heating and cooling phases as pre-formed particles were detected at 5°C during heating and remained as particles over the course of the heating and cooling runs with an apparent loss of assembly and disassembly behaviour. However, increasing the concentration from 0.1 to 1.0 mg/ml changed the ELP behaviour considerably. In the absence of the drug, the particle sizes during the heating run at 50°C reached ~ 2.2 microns before dropping to ~ 400 nm range at the same temperature after the initiation of the cooling cycle. As per the procedure described in the method section, there was a gap of about 10 mins between the heating and cooling runs that could suggest the

incubation time effect at elevated temperatures on the stability of highly concentrated hydrophobic ELP NPs. This could provide an insight on the colloidal stability of valine-containing ELPs at high concentrations and it may be possible that the diameters recorded during the cooling phase and potentially the dissolution temperature may have been affected by sample instability especially since visual observations made on V40 samples after heating to 50°C showed the presence of some precipitation in the bottom of the DLS cuvette. Incubation at 50C for over 10 mins (roughly the time gap between the end of the heating and cooling runs) was enough to cause the protein to precipitate. However, in the presence of the drug, particle sizes reached around 1.4 microns, which is about 1 micron smaller in particle diameter compared to the controls. Moreover, the ELP maintained its assembly and disassembly behavior. This might suggest that the addition of drug improved the colloidal stability of the ELP particles over the course of the measurement.

4.3.   Dexamethasone Entrapment Efficiency

Only few studies have utilized the unique phase transition property of ELPs to physically entrap therapeutic molecules into ELP NPs [160, 161]. None of these studies have explored the effect of the drug loading on the ELP NPs size change, and their self-assembly/disassembly behaviour. The mean entrapment efficiency of the DEX into ELP NPs was found to be increased on lowering the concentration of the ELP from 1.0 to 0.1 mg/ml while the concentration of DEX was held constant at 0.2 mg/ml in both cases. This was observed when L40 concentration was lowered from 1.0 mg/ml to 0.1 mg/ml to yield E.E. of 37 ± 3.4%, and 45 ± 5.8%. Similar results were obtained from the Valine-containing ELPs (V40) that showed higher E.E. of 39 ± 4.2% at 0.1 mg/ml compared to 30 ± 1.6% when the concentration was increased to 1.0 mg/ml. This might be because after increasing ELP concentration roughly 10 times, ELP molecules favor

intramolecular hydrophobic interaction, allowing less chance for DEX to hydrophobically interact with its molecules. This favor interaction was detected as significant increase in ELP NPs sizes in the 1.0 mg/ml samples compared to 0.1 mg/ml after being mixed with the drug (Figure 3. 24b and d, Figure 3. 25b and d). It might also be due to the entrapment of DEX happening at the outer layer of the ELP particles, especially since 0.1 mg/ml ELP particles are relatively smaller than 1.0 mg/ml particles, which suggests they might have higher surface area, which might lead to more pronounced surface interactions. On the other hand, leucine-containing ELPs showed a higher E.E. than the valine-containing ELPs, which might be due to the fact that leucine is more hydrophobic than valine and, therefore, more hydrophobic interactions are initiated whether on the surface or core of the ELP particles.

4.4.   *In vivo* phage display against ischemic brain vasculature

In the current work *in vivo* phage biopanning was employed in the rat to identify peptide sequences exhibiting preferential cerebrovasculature-homing capabilities. These experiments were done on 7-day old rats exposed to either moderate, severe or no HI injury. It is widely accepted that the 7-day-old rat has brain maturity equivalent to that of an early third trimester human fetus [162]. Our biopanning approach used peptide-phage clones based upon 12-mer linear peptides injected into either healthy, moderate HI, or severe HI animals to identify homing peptides for healthy vasculature, penumbra, and core, respectively.

We found the 12-mer peptides showing the highest brain selectivity displayed hydrophilicity between 42-76% and pIs between 5 and 6 (Teble 4. 5). No overlapping has been observed when comparing the identified peptides between all animal groups, which strongly implies the selectivity of those peptides against their intended target tissues. Three biopanning

cycles were sufficient to observe significant enrichment of phage library for high affinity binders. The high correlation between abundances after the second and third rounds suggests that further rounds of enrichment might not be necessary. Our results demonstrate that this screen yielded novel peptides that preferentially bind to the ischemic and heathy brain. Although the precise mechanism by which these peptides bind to their receptors remains unclear, they might mimic natural ligands that bind to receptors exposed by the ischemic injury.

Examples of candidate proteins potentially mimicked by the penumbra-homing peptides are listed in Table 4. 2 In the ischemic penumbra group, PHP1 sequence (ANDTSPMMTKSW) shares homology with several rat proteins such as the ^{76}DTSPM^{80} sequence of the K^+-Cl$^-$ co-transporter 2 (KCC2) protein. This protein is only expressed in central nervous system neurons and it plays a key role in the regulation of neuronal excitability and development of the postnatal brain. In animal models of traumatic and ischemic brain injury, expression levels of KCC2 protein have been reported to be down-regulated [163, 164]. Therefore, increasing KCC2 expression/activity has a strong potential as a neuroprotective strategy [165]. The identified penumbra-homing peptide also shares homology with the ^{440}NDTSP^{444} sequence of the ionotropic receptors (also known as ligand-gated ion channels) of glutamate, NMDA 1 receptors. Under ischemic conditions, NMDA receptors are over-activated and induce neuronal toxicity and ultimately cell death [166, 167]. Penumbra-homing peptide may bind to penumbral vasculature at ischemic brain by mimicking the NMDARs and could be used as a target to deliver NMDA receptor antagonists. Moreover, the ANDTSPMMTKSW sequence also shares homology with the ^{2069}DTSPM^{2073} sequence of the voltage-dependent calcium channel, P/Q-type, alpha-1 A and mimics this protein and shares its receptor.

Table 4. 3 shows several examples of rat proteins containing homologous motifs to the core-homing peptides. For example, the identified core-homing peptide CHP1 (DSPEYLRMSSRA) shares homology with the [32]RMSSR[36] sequence of hypoxia up-regulated mitochondrial movement regulator protein (HUMMR). HUMMR protein abundance is known to be enhanced under hypoxic conditions [168]. HUMMR protein impacts directional movement of mitochondria in neuronal axons and likely plays an important role in these changes. Core-homing peptide may mimic this protein and share its receptor [169]. Moreover, the core-homing peptide also shares the [129]PEYLR[133] sequence of the sodium/glucose cotransporter 1 (SGLT1) rat protein. SGLT1 is a sodium-dependent glucose transporter which plays a role in blood-to-brain movement of glucose during pathophysiological conditions, including HI stroke [170].

Identified healthy brain vasculature-homing peptides HHP1 (WTLDYTFHSMNM) and HHP2 (GERPPSLPASPL) are homologous with several rat proteins detailed in Table 4. 4. HHP1 shares homology with the [184]HSMNM[188] sequence of bone morphogenetic protein receptor type-2 (BMPRII), membrane-bound receptors which are known to be abundantly expressed in the rat brain [171]. Lastly, the second promising healthy brain-homing peptide, HHP2, has shared homology with rat proteins; for example, it aligns with the [185]GERPPAL[191] sequence of Neurexin-2-alpha. Neurexins are transmembrane synaptic proteins and have been localized in the presynaptic membrane [172]. Moreover, HHP2 also shares homology with the [250]ERPPALP[256] sequence of Synaptotagmin-3 protein, which is a membrane-trafficking protein expressed primarily in brain and enriched and highly concentrated in synapses and synaptic plasma membranes [173].

To determine the possible existence of off-target sequences, due to non-specific binding, we analyzed our sequences using SAROTUP [174] (http://immunet.cn/sarotup/) and PepBank

[175] (http://pepbank.mgh.harvard.edu/). These tools were developed for cleaning the output data of phage display selections and determining if false positive sequences such as target-unrelated (e.g., plastic or BSA) are present in your sequences. Since we got no hits on these tools for the peptides identified in this work, this further confirms the novelty of these sequences.

Table 4. 2 Penumbra-homing peptide sequences and example of rat proteins containing homologous motifs.

	Example of homologues	Alignment	Comments	Identity (%)	E-value	Accession number
Penumbra	Electroneutral K$^+$/Cl$^-$ Cotransporter 2 (KCC2) (^{76}**DTSPM**^{80})	Query 3 DTSPM 7 DTSPM Sbjct 76 DTSPM 80	AN**DTSPM**MTKSW peptide may bind to penumbral cells at ischemic brain tissue by mimicking the potassium-chloride cotransporter 2 an could be used as a neuroprotection target to either increase KCC2 expression/activity or KCC2 inhibition	100	27	Q91V14.2
	Glutamate ionotropic receptor, NMDA 1 (^{440}**NDTSP**^{444})	Query 2 NDTSP 6 NDTSP Sbjct 440 NDTSP 444	A**NDTSP**MMTKSW peptide may bind to penumbral cells at ischemic brain tissue by mimicking the glutamate ionotropic receptor, NMDA 1 and could be used as a target to deliver NMDA receptors antagonists	100	78	P35438.1
	Voltage-dependent calcium channel, P/Q-type, alpha-1 A (^{2069}**DTSPM**^{2073})	Query 3 DTSPM 7 DTSPM Sbjct 2069 DTSPM 2073	AN**DTSPM**MTKSW peptide may bind to penumbral cells at ischemic brain tissue by mimicking the voltage-dependent calcium channel, P/Q-type, alpha-1 A and could be used as a target to deliver voltage sensitive calcium channels blockers	100	27	P54282.1

Underline indicates identity with the peptide sequence in candidate protein mimics.

Table 4. 3 Core-homing peptide sequences and example of rat proteins containing homologous motifs.

	Example of homologues	Alignment	Comments	Identity (%)	E-value	Accession number

Core	Hypoxia up-regulated mitochondrial movement regulator protein (HUMMR) ([32]**RMSSR**[36])	``Query  7   RMSSR  11``
		``           RMSSR``
		``Sbjct  32  RMSSR  36``
			DS PEYL**RMSSR**A peptide may bind to apoptotic neuronal cells at ischemic brain tissue by mimicking HUMMR protein and could be used as an ischemic zone targeting sequence	100	38	Q8VI64.1

	Sodium/glucose cotransporter 1 (SGLT1) ([129]**PEYLR**[133])	``Query  3   PEYLR  7``
		``           PEYLR``
		``Sbjct  129 PEYLR  133``
			DS**PEYLR**MSSRA peptide may bind to apoptotic neuronal cells at ischemic brain tissue by mimicking SGLT1 protein and could be used as an ischemic zone targeting sequence	100	19	P53790.1
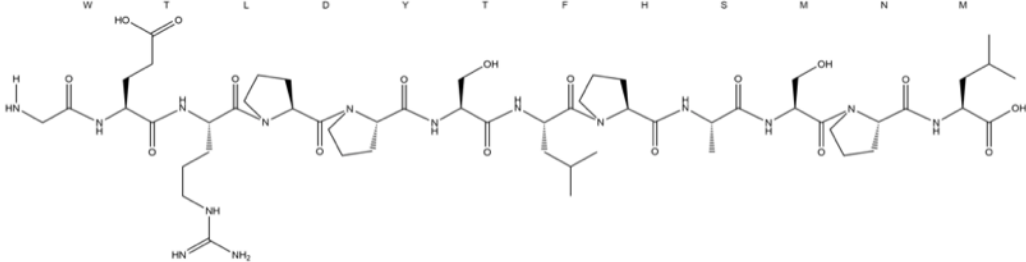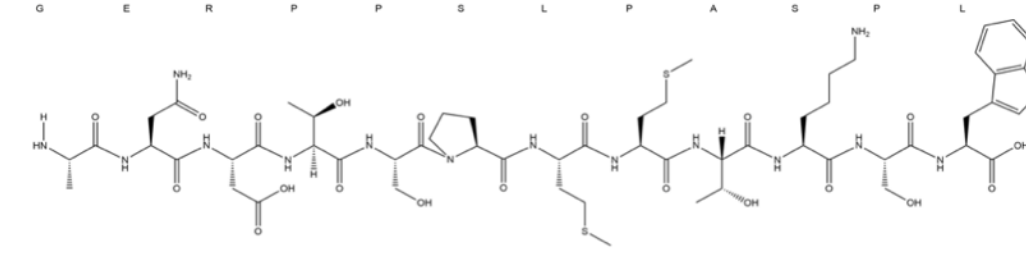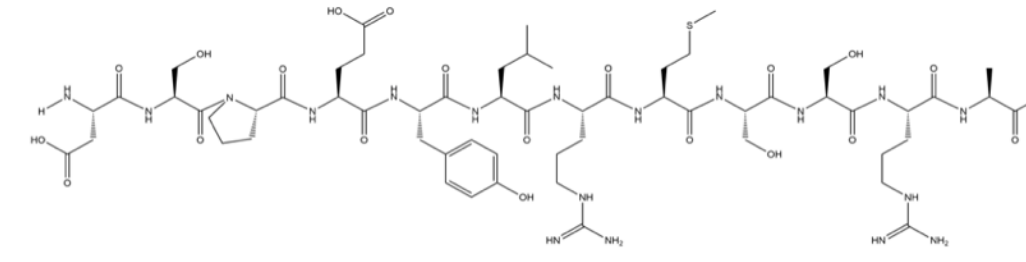
Underline indicates identity with the peptide sequence in candidate protein mimics.

Table 4. 4 Healthy-homing peptide sequences and example of rat proteins containing homologous motifs.

		Example of homologues	Alignment	Comments	Identity (%)	E-value	Accession number
Healthy	HHP1 WTLDYTFHSMNM	Bone morphogenetic protein receptor type-2 (BMPRII) (^{184}**HSMNM**^{188})	Query 8 HSMNM 12 HSMNM Sbjct 184 HSMNM 188	WTLDYTF**HSMNM** peptide may bind to normal neuronal cells by mimicking BMPRII protein and could be used as a target to deliver therapeutics to the brain	100	4.6	O35607.1
	HHP2 GERPPSLPASPL	Synaptotagmin-3 (^{250}**ERPPALP**^{256})	Query 2 ERPPSLP 8 ERPP LP Sbjct 250 ERPPALP 256	G**ERPPSLP**ASPL peptide may bind to normal neuronal cells by mimicking Synaptotagmin-3 protein and could be used as a target to deliver therapeutics to the brain	86%	2.3	P40748
		Neurexin-2-alpha (^{185}**GERPPAL**^{191})	Query 1 GERPPSL 7 GERPP L Sbjct 185 GERPPAL 191	**GERPPSL**PASPL peptide may bind to normal neuronal cells by mimicking Neurexin-2-alpha protein and could be used as a target to deliver therapeutics to the brain	86%	4.6	Q63374.3

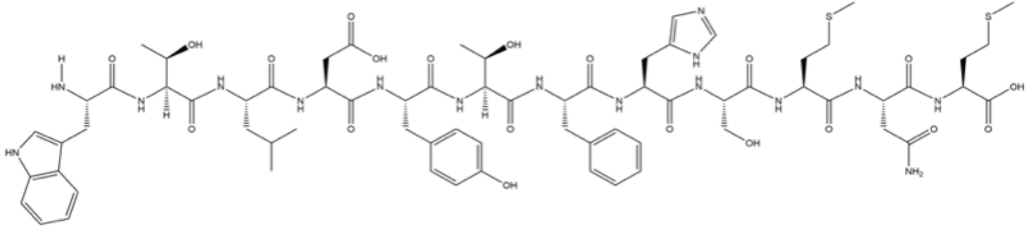Underline indicates identity with the peptide sequence in candidate protein mimics.

Table 4. 5 Identified peptides' chemical structures and characteristics.

Injury type	Sequence and chemical structure	pI	Net charge @ pH 7	% hydrophilic residues
H1		5.08	-0.8	58%
H2		6.00	-0.1	42%
P		5.88	-0.1	58%
C		6.07	-0.1	67%

## 4.5.	Conclusions

4.5.1. Summary and major conclusions

We have developed a new protocol that is an extension of existing techniques for creating ELPs. Our new protocol is designed to improve the overall efficiency of the RDL DNA concatemerization process by using a combination of denaturing metal affinity chromatography and ITC to purify ELPs that would otherwise be unpurifiable using an ITC-only procedure. It does not require the use of large solubility or affinity partners and only requires a short polyhistidine tag, which may not necessarily need to be removed depending on the downstream applications for which the ELPs will be used. This protocol is designed specifically to expand upon ITC-based purifications to allow for the rapid purification of constructs that are: (i) poorly-expressed; (ii) expressed in inclusion bodies or as ELP aggregates; (iii) short constructs with high transition temperatures; and/or (iv) ELPs with strongly hydrophobic guest amino acids.

The effect of drug entrapment on the intrinsic self-assembly and disassembly behavior of ELPs was tested. The results suggest that the nature and hydrophobicity of the guest amino acid position and the ratio of ELP:drug have a significant effect on the particle size and the assembly/disassembly behaviour, especially after drug entrapment. Drug entrapment efficiency was increased as the hydrophobicity of the guest amino acid increased. Moreover, less ELP when mixed with the drug seems to increase the entrapment efficiency as well. Therefore, a certain balance needs to be maintained between the ELP:drug ratio and the choice of the guest amino acid as

together they will have an effect on the phase transition behaviour of ELPs and their drug entrapment capability.

Our results showed that an *in vivo* phage display approach against the HI rat model resulted in identification of new peptides with preferential binding affinity to the core and penumbra cerebrovasculature. An alignment analysis of the identified peptide sequences by using the Clustal W program revealed frequently occurring sequences for the healthy/control group such as WTLDYTFHSMNM, GERPPSLPASPL and a significant occurrence of ANDTSPMMTKSW and DSPEYLRMSSRA sequences in the penumbra and core groups, respectively. Even though the identified brain-homing peptides showed shared homology with several rat proteins, the significance of this homology remains to be ascertained and the exact receptors of those peptides remain to be investigated.

4.5.2. Future directions

These findings reported herein provide evidence for ELPs' capability of loading therapeutics inside the NPs with adequate entrapment efficiency: however, this in some cases comes at the expense of losing the reversibility of its inherited phase transition behaviour. Further in-depth evaluation of the drug entrapment capabilities of multiple ELP constructs would be very beneficial to find the right balance that allow ELPs to load high amount of drug inside the NPs while still retaining their assembly/disassembly characteristic. This would be immensely valuable, especially in hypothermia-triggered drug release applications. Furthermore, the assembly/disassembly behaviour of ELPs should also be evaluated in human plasma in the presence and absence of drug to evaluate if adsorbed plasma proteins on

the surface of ELP NPs would interfere or possibly block the disassembly ability of ELP particles. Future studies examining the in vitro release kinetics of DEX from the drug-loaded ELP NPs are needed. Moreover, evaluation of the localization and *in vivo* release of DEX in an hypoxic/ischemic rat with brain injury will be critical for optimizing the drug delivery system to ensure an enhanced efficacy of the treatment.

Utilizing the variety of the ELP constructs made in this work, a new ELP better suited for drug delivery applications can be developed. Stable spherical micelles in the size range of 50-150 nm can be made by designing an amphiphilic ELP construct via combining small DNA fragments of hydrophobic ELPs (e.g. valine or leucine series) with more hydrophilic ELPs (e.g. alanine series).

Competitive binding of the novel phage-derived peptides at the HI zone to confirm their injury zone specificity can be done using fluorescently labelled peptides to determine their ischemic tissue specificity and the overall biodistribution including HI zone, healthy side of the brain, and their level of uptake by vital organs (heart, kidney, liver, and lungs). Once their HI zone specificity is confirmed, these peptides can be attached to the ELP sequence that forms NPs to develop a targeting drug delivery system that can be tested for targeted delivery of therapeutics to the ischemic zone in the injured brains of newborns.

Altogether, these proposed studies will provide essential information concerning the design of smart stimulus-responsive ELP nanoparticles for systemic delivery of neuroprotective agents. The work presented in this thesis provides a foundation upon which these other studies can be built.

4.5.3. Limitations

An important limitation to the *in vivo* phage display study is that the biodistribution and off-target binding profile of the identified novel vasculature-homing peptides have not been done. After three rounds of biopanning, several novel peptides are shown to be the strongest binders to the tissue of study. Because they survived three cycles of enrichment and have been the most repeated sequences, an assumption can be made about their potential vascular specificity of the tissue of interest, but more experiments are needed to confirm their tissue-specificity. The results reported herein prove these identified peptides are abundant at the vasculature of the tissue of study: however, there is a possibility that these peptides could show a high binding affinity to other areas in the body as well. *In vivo* biodistribution studies will provide a clear picture of where these peptides localize in the body. In addition, competitive binding of the phage-derived peptides at the HI zone using fluorescently labelled peptides can determine their ischemic tissue specificity including HI zone, healthy side of the brain, and vital organs (heart, kidney, liver, and lungs).

References

1. Logitharajah, P., M.A. Rutherford, and F.M. Cowan, *Hypoxic-ischemic encephalopathy in preterm infants: antecedent factors, brain imaging, and outcome.* Pediatr Res, 2009. **66**(2): p. 222-9.

2. Douglas-Escobar, M. and M.D. Weiss, *Hypoxic-ischemic encephalopathy: a review for the clinician.* JAMA Pediatr, 2015. **169**(4): p. 397-403.

3. Rosenbaum, P., et al., *A report: the definition and classification of cerebral palsy April 2006.* Dev Med Child Neurol Suppl, 2007. **109**: p. 8-14.

4. Bax, M., et al., *Proposed definition and classification of cerebral palsy, April 2005.* Dev Med Child Neurol, 2005. **47**(8): p. 571-6.

5. Bax, M.C., *Terminology and classification ofcerebral palsy.* Dev Med Child Neurol, 1964. **6**: p. 295-7.

6. Boyd, R.N., M.E. Morris, and H.K. Graham, *Management of upper limb dysfunction in children with cerebral palsy: a systematic review.* Eur J Neurol, 2001. **8 Suppl 5**: p. 150-66.

7. Boyd, R.N. and R.M. Hays, *Current evidence for the use of botulinum toxin type A in the management of children with cerebral palsy: a systematic review.* Eur J Neurol, 2001. **8 Suppl 5**: p. 1-20.

8. Gage, J.R. and T.F. Novacheck, *An update on the treatment of gait problems in cerebral palsy.* J Pediatr Orthop B, 2001. **10**(4): p. 265-74.

9. Nelson, K.B., *The epidemiology of cerebral palsy in term infants.* Ment Retard Dev Disabil Res Rev, 2002. **8**(3): p. 146-50.

10. Shevell, M.I., et al., *Etiologic determination of childhood developmental delay.* Brain Dev, 2001. **23**(4): p. 228-35.

11. Edwards, A.D., et al., *Neurological outcomes at 18 months of age after moderate hypothermia for perinatal hypoxic ischaemic encephalopathy: synthesis and meta-analysis of trial data.* BMJ, 2010. **340**: p. c363.

12. Nassef, S.K., M. Blennow, and M. Jirwe, *Experiences of parents whose newborns undergo hypothermia treatment following perinatal asphyxia.* J Obstet Gynecol Neonatal Nurs, 2013. **42**(1): p. 38-47.

13. Pulera, M.R., et al., *Apoptosis in a neonatal rat model of cerebral hypoxia-ischemia.* Stroke, 1998. **29**(12): p. 2622-30.

14.   Roth, S.C., et al., *Relation of deranged neonatal cerebral oxidative metabolism with neurodevelopmental outcome and head circumference at 4 years.* Dev Med Child Neurol, 1997. **39**(11): p. 718-25.

15.   Riikonen, R.S., P.O. Kero, and O.G. Simell, *Excitatory amino acids in cerebrospinal fluid in neonatal asphyxia.* Pediatr Neurol, 1992. **8**(1): p. 37-40.

16.   Sweeney, M.I., et al., *Cellular mechanisms involved in brain ischemia.* Can J Physiol Pharmacol, 1995. **73**(11): p. 1525-35.

17.   Zhang, F., et al., *When hypothermia meets hypotension and hyperglycemia: the diverse effects of adenosine 5'-monophosphate on cerebral ischemia in rats.* J Cereb Blood Flow Metab, 2009. **29**(5): p. 1022-34.

18.   Askalan, R., et al., *The effect of postischemic hypothermia on apoptotic cell death in the neonatal rat brain.* Dev Neurosci, 2011. **33**(3-4): p. 320-9.

19.   Askalan, R., et al., *X-linked inhibitor of apoptosis protein expression after ischemic injury in the human and rat developing brain.* Pediatr Res, 2009. **65**(1): p. 21-6.

20.   Manabat, C., et al., *Reperfusion differentially induces caspase-3 activation in ischemic core and penumbra after stroke in immature brain.* Stroke, 2003. **34**(1): p. 207-13.

21.   Novak, C.M., M. Ozen, and I. Burd, *Perinatal brain injury: mechanisms, prevention, and outcomes.* Clin Perinatol, 2018. **45**(2): p. 357-375.

22.   Giussani, D.A., *The fetal brain sparing response to hypoxia: physiological mechanisms.* J Physiol, 2016. **594**(5): p. 1215-30.

23.   Olney, J.W., et al., *The role of specific ions in glutamate neurotoxicity.* Neurosci Lett, 1986. **65**(1): p. 65-71.

24.   Choi, D.W., *Excitotoxic cell death.* J Neurobiol, 1992. **23**(9): p. 1261-76.

25.   Arai, A., et al., *A brief period of hypoxia causes proteolysis of cytoskeletal proteins in hippocampal slices.* Brain Res, 1991. **555**(2): p. 276-80.

26.   Zhang, J., et al., *Nitric oxide activation of poly(ADP-ribose) synthetase in neurotoxicity.* Science, 1994. **263**(5147): p. 687-9.

27.   Stout, A.K., et al., *Glutamate-induced neuron death requires mitochondrial calcium uptake.* Nat Neurosci, 1998. **1**(5): p. 366-73.

28.   Castilho, R.F., M.W. Ward, and D.G. Nicholls, *Oxidative stress, mitochondrial function, and acute glutamate excitotoxicity in cultured cerebellar granule cells.* J Neurochem, 1999. **72**(4): p. 1394-401.

29.   O'Hare, M.J., et al., *Differential roles of nuclear and cytoplasmic cyclin-dependent kinase 5 in apoptotic and excitotoxic neuronal death.* J Neurosci, 2005. **25**(39): p. 8954-66.

30.   Ikonomidou, C. and A.M. Kaindl, *Neuronal death and oxidative stress in the developing brain.* Antioxid Redox Signal, 2011. **14**(8): p. 1535-50.

31.   Favie, L.M.A., et al., *Nitricoxide synthase inhibition as a neuroprotective strategy following hypoxic-ischemic encephalopathy: Evidence from animal studies.* Front Neurol, 2018. **9**: p. 258.

32.   Rousset, C.I., et al., *Mitochondria and perinatal brain injury.* J Matern Fetal Neonatal Med, 2012. **25 Suppl 1**: p. 35-8.

33.   Lu, Y., et al., *Role of mitochondria in neonatal hypoxic-ischemic brain injury.* J Neurosci Rehabil, 2015. **2**(1): p. 1-14.

34.   Thornton, C. and H. Hagberg, *Role of mitochondria in apoptotic and necroptotic cell death in the developing brain.* Clin Chim Acta, 2015. **451**(Pt A): p. 35-8.

35.   Wang, X., et al., *Developmental shift of cyclophilin D contribution to hypoxic-ischemic brain injury.* J Neurosci, 2009. **29**(8): p. 2588-96.

36.   Bernardi, P., et al., *The mitochondrial permeability transition from in vitro artifact to disease target.* FEBS J, 2006. **273**(10): p. 2077-99.

37.   Thornton, C., et al., *Molecular mechanisms of neonatal brain injury.* Neurol Res Int, 2012. **2012**: p. 506320.

38.   Blomgren, K. and H. Hagberg, *Free radicals, mitochondria, and hypoxia-ischemia in the developing brain.* Free Radic Biol Med, 2006. **40**(3): p. 388-97.

39.   Zhu, C., et al., *Cyclophilin A participates in the nuclear translocation of apoptosis-inducing factor in neurons after cerebral hypoxia-ischemia.* J Exp Med, 2007. **204**(8): p. 1741-8.

40.   Hagberg, H., et al., *The role of inflammation in perinatal brain injury.* Nat Rev Neurol, 2015. **11**(4): p. 192-208.

41.   Liu, F. and L.D. McCullough, *Inflammatory responses in hypoxic ischemic encephalopathy.* Acta Pharmacol Sin, 2013. **34**(9): p. 1121-30.

42.   Algra, S.O., et al., *Cerebral ischemia initiates an immediate innate immune response in neonates during cardiac surgery.* J Neuroinflammation, 2013. **10**: p. 24.

43.   Barks, J.D., *Current controversies in hypothermic neuroprotection.* Semin Fetal Neonatal Med, 2008. **13**(1): p. 30-4.

44.   Giesinger, R.E., et al., *Hypoxic-ischemic encephalopathy and therapeutic hypothermia: the hemodynamic perspective.* J Pediatr, 2017. **180**: p. 22-30 e2.

45.   Jacobs, S.E., et al., *Cooling for newborns with hypoxic ischaemic encephalopathy.* Cochrane Database Syst Rev, 2013(1): p. CD003311.

46.   Cilio, M.R. and D.M. Ferriero, *Synergistic neuroprotective therapies with hypothermia.* Semin Fetal Neonatal Med, 2010. **15**(5): p. 293-8.

47.   Ikonomidou, C. and L. Turski, *Why did NMDA receptor antagonists fail clinical trials for stroke and traumatic brain injury?* Lancet Neurol, 2002. **1**(6): p. 383-6.

48.   Costantine, M.M. and N. Drever, *Antenatal exposure to magnesium sulfate and neuroprotection in preterm infants.* Obstet Gynecol Clin North Am, 2011. **38**(2): p. 351-66, xi.

49.   Wilhelm, W., et al., *General anesthesia versus monitored anesthesia care with remifentanil for assisted reproductive technologies: effect on pregnancy rate.* J Clin Anesth, 2002. **14**(1): p. 1-5.

50.   Yamaguchi, M., et al., *The effects of xanthine oxidoreductase inhibitors on oxidative stress markers following global brain ischemia reperfusion Injury in C57BL/6 Mice.* PLoS One, 2015. **10**(7): p. e0133980.

51.   Marro, P.J., O.P. Mishra, and M. Delivoria-Papadopoulos, *Effect of allopurinol on brain adenosine levels during hypoxia in newborn piglets.* Brain Res, 2006. **1073-1074**: p. 444-50.

52.   Rodriguez-Fanjul, J., et al., *Neuroprotection with hypothermia and allopurinol in an animal model of hypoxic-ischemic injury: Is it a gender question?* PLoS One, 2017. **12**(9): p. e0184643.

53.   Benders, M.J., et al., *Early postnatal allopurinol does not improve short term outcome after severe birth asphyxia.* Arch Dis Child Fetal Neonatal Ed, 2006. **91**(3): p. F163-5.

54. Torrance, H.L., et al., *Maternal allopurinol during fetal hypoxia lowers cord blood levels of the brain injury marker S-100B.* Pediatrics, 2009. **124**(1): p. 350-7.

55. Villapol, S., et al., *Melatonin promotes myelination by decreasing white matter inflammation after neonatal stroke.* Pediatr Res, 2011. **69**(1): p. 51-5.

56. Jou, M.J., et al., *Melatonin protects against common deletion of mitochondrial DNA-augmented mitochondrial oxidative stress and apoptosis.* J Pineal Res, 2007. **43**(4): p. 389-403.

57. Pandi-Perumal, S.R., et al., *Melatonin antioxidative defense: therapeutical implications for aging and neurodegenerative processes.* Neurotox Res, 2013. **23**(3): p. 267-300.

58. Seabra, M.L., et al., *Randomized, double-blind clinical trial, controlled with placebo, of the toxicology of chronic melatonin treatment.* J Pineal Res, 2000. **29**(4): p. 193-200.

59. Hendaus, M.A., F.A. Jomha, and A.H. Alhammadi, *Melatonin in the management of perinatal hypoxic-ischemic encephalopathy: light at the end of the tunnel?* Neuropsychiatr Dis Treat, 2016. **12**: p. 2473-2479.

60. Robertson, N.J., et al., *Melatonin augments hypothermic neuroprotection in a perinatal asphyxia model.* Brain, 2013. **136**(Pt 1): p. 90-105.

61. Weichhart, T., et al., *The anti-inflammatory potency of dexamethasone is determined by the route of application in vivo.* Immunol Lett, 2010. **129**(1): p. 50-2.

62. Paragliola, R.M., et al., *Treatment with synthetic glucocorticoids and the hypothalamus-pituitary-adrenal axis.* Int J Mol Sci, 2017. **18**(10).

63. Sônia Maria Alvarenga Anti1, R.D.N.G., Wiliam Habib Chahade, *Antiinflamatórios hormonais: Glicocorticóides.* Einstein, 2008. **6**(1): p. S159-S65.

64. Newton, R., *Molecular mechanisms of glucocorticoid action: what is important?* Thorax, 2000. **55**(7): p. 603-13.

65. Norris, J.W., *Steroids may have a role in stroke therapy.* Stroke, 2004. **35**(1): p. 228-9.

66. Gomes, J.A., et al., *Glucocorticoid therapy in neurologic critical care.* Crit Care Med, 2005. **33**(6): p. 1214-24.

67.   Fischer, S., et al., *In vitro effects of dexamethasone on hypoxia-induced hyperpermeability and expression of vascular endothelial growth factor.* Eur J Pharmacol, 2001. **411**(3): p. 231-43.

68.   Sandercock, P.A. and T. Soane, *Corticosteroids for acute ischaemic stroke.* Cochrane Database Syst Rev, 2011(9): p. CD000064.

69.   Longui, C.A., *Glucocorticoid therapy: minimizing side effects.* J Pediatr (Rio J), 2007. **83**(5 Suppl): p. S163-77.

70.   Subiros, N., D.G. Del Barco, and R.M. Coro-Antich, *Erythropoietin: still on the neuroprotection road.* Ther Adv Neurol Disord, 2012. **5**(3): p. 161-73.

71.   Juul, S., *Neuroprotective role of erythropoietin in neonates.* J Matern Fetal Neonatal Med, 2012. **25 Suppl 4**: p. 105-7.

72.   McPherson, R.J. and S.E. Juul, *Recent trends in erythropoietin-mediated neuroprotection.* Int J Dev Neurosci, 2008. **26**(1): p. 103-11.

73.   Juul, S.E., et al., *High-dose erythropoietin for asphyxia and encephalopathy (HEAL): A randomized controlled trial - background, aims, and study protocol.* Neonatology, 2018. **113**(4): p. 331-338.

74.   Anderson, R.E., W.K. Tan, and F.B. Meyer, *Brain acidosis, cerebral blood flow, capillary bed density, and mitochondrial function in the ischemic penumbra.* J Stroke Cerebrovasc Dis, 1999. **8**(6): p. 368-79.

75.   Kurzepa, J., et al., *The significance of matrix metalloproteinase (MMP)-2 and MMP-9 in the ischemic stroke.* Int J Neurosci, 2014. **124**(10): p. 707-16.

76.   Panagiotou, S. and S. Saha, *Therapeutic benefits of nanoparticles in stroke.* Front Neurosci, 2015. **9**: p. 182.

77.   Lv, W., et al., *Bioengineered boronic ester modified dextran polymer nanoparticles as reactive oxygen species responsive nanocarrier for ischemic stroke treatment.* ACS Nano, 2018.

78.   Han, L., et al., *Targeted drug delivery to ischemic stroke via chlorotoxin-anchored, lexiscan-loaded nanoparticles.* Nanomedicine, 2016. **12**(7): p. 1833-1842.

79.   Guo, X., et al., *Thrombin-responsive, brain-targeting nanoparticles for improved stroke therapy.* ACS Nano, 2018. **12**(8): p. 8723-8732.

80.   Kojima, C., et al., *The synthesis and evaluation of polymer prodrug/collagen hybrid gels for delivery into metastatic cancer cells.* Nanomedicine, 2013. **9**(6): p. 767-75.

81.   Callahan, D.J., et al., *Triple stimulus-responsive polypeptide nanoparticles that enhance intratumoral spatial distribution.* Nano Lett, 2012. **12**(4): p. 2165-70.

82.   Zhang, J., et al., *Glycyrrhetinic acid-mediated polymeric drug delivery targeting the acidic microenvironment of hepatocellular carcinoma.* Pharm Res, 2015. **32**(10): p. 3376-90.

83.   Sun, Y., et al., *Synthesis and characterization of pH-sensitive poly(itaconic acid)-poly(ethylene glycol)-folate-poly(l-histidine) micelles for enhancing tumor therapy and tunable drug release.* J Colloid Interface Sci, 2015. **458**: p. 119-29.

84.   Hu, J., et al., *pH-responsive and charge shielded cationic micelle of poly(L-histidine)-block-short branched PEI for acidic cancer treatment.* J Control Release, 2013. **172**(1): p. 69-76.

85.   Ouahab, A., et al., *Novel pH-sensitive charge-reversal cell penetrating peptide conjugated PEG-PLA micelles for docetaxel delivery: In vitro study.* International Journal of Pharmaceutics, 2014. **466**: p. 233-245.

86.   Zhao, Y., et al., *Tumor-specific pH-responsive peptide-modified pH-sensitive liposomes containing doxorubicin for enhancing glioma targeting and anti-tumor activity.* Journal of Controlled Release, 2016. **222**: p. 56-66.

87.   Johnson, R.P., et al., *Poly(PEGA)-b-poly(L-lysine)-b-poly(L-histidine) hybrid vesicles for tumoral pH-triggered intracellular delivery of doxorubicin hydrochloride.* ACS Appl Mater Interfaces, 2015. **7**(39): p. 21770-9.

88.   Han, Q., et al., *Switchable liposomes: targeting peptides functionalized and pH-Triggered cytoplasmic delivery.* ACS applied materials & interfaces, 2016: p. 6-11.

89.   Chen, P., et al., *pH-Responsive chimaeric pepsomes based on asymmetric Poly(ethylene glycol)-b-Poly(L-leucine)-b-Poly(L-glutamic acid) triblock copolymer for efficient loading and active intracellular delivery of doxorubicin hydrochloride.* Biomacromolecules, 2015. **16**: p. 1322-1330.

90.   Hu, J., et al., *Design of tumor-homing and pH-responsive polypeptide–doxorubicin nanoparticles with enhanced anticancer efficacy and reduced side effects.* Chem. Commun., 2015. **51**: p. 8-11.

91.   Callahan, D.J., et al., *Triple stimulus-responsive polypeptide nanoparticles that enhance intratumoral spatial distribution.* Nano Letters, 2012. **12**(4): p. 2165-2170.

92.   Seib, F.P., et al., *pH-dependent anticancer drug release from silk nanoparticles.* Adv Healthc Mater, 2013. **2**(12): p. 1606-11.

93.   Wu, H., et al., *Injectable and pH-responsive silk nanofiber hydrogels for sustained anticancer drug delivery.* ACS Appl Mater Interfaces, 2016. **8**(27): p. 17118-26.

94.   Urry, D.W., *Entropic elastic processes in protein mechanisms. I. Elastic structure due to an inverse temperature transition and elasticity due to internal chain dynamics.* J Protein Chem, 1988. **7**(1): p. 1-34.

95.   Urry, D.W., et al., *Temperature of polypeptide inverse temperature transition depends on mean residue hydrophobicity.* Journal of the American Chemical Society, 1991. **113**(11): p. 4346-4348.

96.   Ge, X., et al., *Self-cleavable stimulus responsive tags for protein purification without chromatography.* J Am Chem Soc, 2005. **127**(32): p. 11228-9.

97.   Cole, M.A., et al., *Stimuli-responsive interfaces and systems for the control of protein-surface and cell-surface interactions.* Biomaterials, 2009. **30**(9): p. 1827-50.

98.   Chilkoti, A., M.R. Dreher, and D.E. Meyer, *Design of thermally responsive, recombinant polypeptide carriers for targeted drug delivery.* Adv Drug Deliv Rev, 2002. **54**(8): p. 1093-111.

99.   Bidwell, G.L., 3rd, et al., *A thermally targeted elastin-like polypeptide-doxorubicin conjugate overcomes drug resistance.* Invest New Drugs, 2007. **25**(4): p. 313-26.

100.   Urry, D.W., et al., *Biocompatibility of the bioelastic materials, Poly(GVGVP) and its γ-irradiation cross-linked matrix: summary of generic biological test results.* Journal of Bioactive and Compatible Polymers, 1991. **6**(3): p. 263-282.

101.   Yao, X.L. and M. Hong, *Structure distribution in an elastin-mimetic peptide (VPGVG)3 investigated by solid-state NMR.* Journal of the American Chemical Society, 2004. **126**(13): p. 4199-4210.

102.   Hong, M., et al., *Structure of an elastin-mimetic polypeptide by solid-state NMR chemical shift analysis.* Biopolymers, 2003. **70**(2): p. 158-168.

103.   Li, N.K., et al., *Molecular description of the LCST behavior of an elastin-like polypeptide.* Biomacromolecules, 2014. **15**(10): p. 3522-30.

104.   Reichheld, S.E., et al., *Direct observation of structure and dynamics during phase separation of an elastomeric protein.* Proceedings of the National Academy of Sciences, 2017: p. 201701877.

105.   Rauscher, S., et al., *Proline and glycine control protein self-organization into elastomeric or amyloid fibrils.* Structure, 2006. **14**(11): p. 1667-1676.

106.   Kumashiro, K.K., et al., *Backbone motion in elastin's hydrophobic domains as detected by 2H NMR spectroscopy.* Biopolymers, 2012. **97**(11): p. 882-888.

107.   Muiznieks, L.D. and F.W. Keeley, *Proline periodicity modulates the self-assembly properties of elastin-like polypeptides.* Journal of Biological Chemistry, 2010. **285**(51): p. 39779-39789.

108.   Fujita, Y., M. Mie, and E. Kobatake, *Construction of nanoscale protein particle using temperature-sensitive elastin-like peptide and polyaspartic acid chain.* Biomaterials, 2009. **30**: p. 3450-3457.

109.   Ghoorchian, A., et al., *Size and shape characterization of thermoreversible micelles of three-armed star elastin-like polypeptides.* The Journal of Physical Chemistry B, 2013. **117**(29): p. 8865-8874.

110.   MacEwan, S.R., et al., *Phase behavior and self-assembly of perfectly sequence-defined and monodisperse multiblock copolypeptides.* Biomacromolecules, 2017. **18**(2): p. 599-609.

111.   Osborne, J.L., R. Farmer, and K.A. Woodhouse, *Self-assembled elastin-like polypeptide particles.* Acta Biomater, 2008. **4**(1): p. 49-57.

112.   Nicolini, C., et al., *Characterization of the temperature- and pressure-induced inverse and reentrant transition of the minimum elastin-like polypeptide GVG(VPGVG) by DSC, PPC, CD, and FT-IR spectroscopy.* Biophysical Journal, 2004. **86**(March).

113.   McDaniel, J.R., D.C. Radford, and A. Chilkoti, *A unified model for de novo design of elastin-like polypeptides with tunable inverse transition temperatures.* Biomacromolecules, 2013. **14**(8): p. 2866-2872.

114.   Urry, D.W., et al., *Hydrophobicity scale for proteins based on inverse temperature transitions.* Biopolymers, 1992. **32**(9): p. 1243-50.

115.   Girotti, A., et al., *Influence of the molecular weight on the inverse temperature transition of a model genetically engineered elastin-like pH-responsive polymer.* Macromolecules, 2004. **37**(9): p. 3396-3400.

116.   Meyer, D.E. and A. Chilkoti, *Quantification of the effects of chain length and concentration on the thermal behavior of elastin-like polypeptides.* Biomacromolecules, 2004. **5**: p. 846-851.

117.   MacKay, J.A., et al., *Quantitative model of the phase behavior of recombinant pH-responsive elastin-like polypeptides.* Biomacromolecules, 2010. **11**(11): p. 2873-2879.

118.   Meyer, D.E. and A. Chilkoti, *Purification of recombinant proteins by fusion with thermally-responsive polypeptides.* Nat Biotechnol, 1999. **17**(11): p. 1112-5.

119.   Meyer, D.E. and A. Chilkoti, *Genetically encoded synthesis of protein-based polymers with precisely specified molecular weight and sequence by recursive directional ligation: examples from the elastin-like polypeptide system.* Biomacromolecules, 2002. **3**(2): p. 357-67.

120.   Bataille, L., et al., *Expression and purification of short hydrophobic elastin-like polypeptides with maltose-binding protein as a solubility tag.* Protein Expr Purif, 2015. **110**: p. 165-71.

121.   Bataille, L., et al., *Recombinant production and purification of short hydrophobic Elastin-like polypeptides with low transition temperatures.* Protein Expr Purif, 2016. **121**: p. 81-7.

122.   Smith, G.P., *Filamentous fusion phage: novel expression vectors that display cloned antigens on the virion surface.* Science, 1985. **228**(4705): p. 1315-7.

123.   Huang, J.X., S.L. Bishop-Hurley, and M.A. Cooper, *Development of anti-infectives using phage display: biological agents against bacteria, viruses, and parasites.* Antimicrob Agents Chemother, 2012. **56**(9): p. 4569-82.

124.   Jonczyk, E., et al., *The influence of external factors on bacteriophages--review.* Folia Microbiol (Praha), 2011. **56**(3): p. 191-200.

125.   Nicol, C.G., et al., *Use of in vivo phage display to engineer novel adenoviruses for targeted delivery to the cardiac vasculature.* FEBS Lett, 2009. **583**(12): p. 2100-7.

126.   Kehoe, J.W. and B.K. Kay, *Filamentous phage display in the new millennium.* Chem Rev, 2005. **105**(11): p. 4056-72.

127. Smith, G.P. and V.A. Petrenko, *Phage display.* Chem Rev, 1997. **97**(2): p. 391-410.

128. Deng, X., et al., *Advances in the T7 phage display system (Review).* Mol Med Rep, 2018. **17**(1): p. 714-720.

129. Kolonin, M., R. Pasqualini, and W. Arap, *Molecular addresses in blood vessels as targets for therapy.* Curr Opin Chem Biol, 2001. **5**(3): p. 308-13.

130. Ruoslahti, E., *Vascular zip codes in angiogenesis and metastasis.* Biochem Soc Trans, 2004. **32**(Pt3): p. 397-402.

131. Babickova, J., et al., *In vivo phage display--a discovery tool in molecular biomedicine.* Biotechnol Adv, 2013. **31**(8): p. 1247-59.

132. D'Onofrio, N., et al., *Vascular-homing peptides for targeted drug delivery and molecular imaging: meeting the clinical challenges.* Biochim Biophys Acta, 2014. **1846**(1): p. 1-12.

133. Pasqualini, R. and E. Ruoslahti, *Organ targeting in vivo using phage display peptide libraries.* Nature, 1996. **380**(6572): p. 364-6.

134. Li, J., L. Feng, and X. Jiang, *In vivo phage display screen for peptide sequences that cross the blood-cerebrospinal-fluid barrier.* Amino Acids, 2015. **47**(2): p. 401-5.

135. Akita, N., et al., *Identification of oligopeptides binding to peritoneal tumors of gastric cancer.* Cancer Sci, 2006. **97**(10): p. 1075-81.

136. Wan, X.M., et al., *Identification of nose-to-brain homing peptide through phage display.* Peptides, 2009. **30**(2): p. 343-50.

137. Chen, Y., et al., *Transdermal protein delivery by a coadministered peptide identified via phage display.* Nat Biotechnol, 2006. **24**(4): p. 455-60.

138. Enback, J. and P. Laakkonen, *Tumour-homing peptides: tools for targeting, imaging and destruction.* Biochem Soc Trans, 2007. **35**(Pt 4): p. 780-3.

139. Ruoslahti, E., S.N. Bhatia, and M.J. Sailor, *Targeting of drugs and nanoparticles to tumors.* J Cell Biol, 2010. **188**(6): p. 759-68.

140. Ruoslahti, E. and D. Rajotte, *An address system in the vasculature of normal tissues and tumors.* Annu Rev Immunol, 2000. **18**: p. 813-27.

141. Li, J., et al., *Identification of peptide sequences that target to the brain using in vivo phage display.* Amino Acids, 2012. **42**(6): p. 2373-81.

142.   van Rooy, I., et al., *Identification of peptide ligands for targeting to the blood-brain barrier.* Pharm Res, 2010. **27**(4): p. 673-82.

143.   Fan, X., et al., *An in vivo approach to structure activity relationship analysis of peptide ligands.* Pharm Res, 2007. **24**(5): p. 868-79.

144.   Kolonin, M.G., et al., *Synchronous selection of homing peptides for multiple tissues by in vivo phage display.* FASEB J, 2006. **20**(7): p. 979-81.

145.   Hong, H.Y., et al., *Detection of apoptosis in a rat model of focal cerebral ischemia using a homing peptide selected from in vivo phage display.* J Control Release, 2008. **131**(3): p. 167-72.

146.   Zhao, Y., et al., *Dual targeted nanocarrier for brain ischemic stroke treatment.* J Control Release, 2016. **233**: p. 64-71.

147.   United States Pharmacopeial, C., *The United States Pharmacopeia 2011 : USP 34 ; The national formulary : NF 29*. 2010, Rockville, MD: United States Pharmacopeial Convention.

148.   Harmonisation, I.C.o., *Validation of analytical procedures: text and methodology Q2(R1). Proceedings of the International Conference on Harmonisation of Technical Requirements for Registration of Pharmaceuticals for Human Use.* Geneva, Switzerland, April 25–27, 2005.

149.   Stationery, O., *British pharmacopoeia 2007*. 2006, London: The Stationery Office.

150.   Nguyen A., A.E.A., Yager J.Y., *Unilateral common carotid artery ligation as a model of perinatal asphyxia: the original Rice–Vannucci model*, in *animal models of neurodevelopmental disorders*. 2015, Humana Press, New York, NY.

151.   Work, L.M., et al., *In vivo biopanning: A methodological approach to identifying novel targeting ligands for delivery of biological agents to the vasculature.* Methods Mol Med, 2005. **108**: p. 395-413.

152.   Lee, C., A. Levin, and D. Branton, *Copper staining: a five-minute protein stain for sodium dodecyl sulfate-polyacrylamide gels.* Anal Biochem, 1987. **166**(2): p. 308-12.

153.   McPherson, D.T., J. Xu, and D.W. Urry, *Product purification by reversible phase transition following Escherichia coli expression of genes encoding up to 251 repeats of the elastomeric pentapeptide GVGVP.* Protein Expr Purif, 1996. **7**(1): p. 51-7.

154. Wentzell, L.M., T.J. Nobbs, and S.E. Halford, *The SfiI restriction endonuclease makes a four-strand DNA break at two copies of its recognition sequence.* J Mol Biol, 1995. **248**(3): p. 581-95.

155. Nobbs, T.J., et al., *DNA excision by the Sfi I restriction endonuclease.* J Mol Biol, 1998. **281**(3): p. 419-32.

156. Wentzell, L.M. and S.E. Halford, *DNA looping by the Sfi I restriction endonuclease.* J Mol Biol, 1998. **281**(3): p. 433-44.

157. Williams, S.A. and S.E. Halford, *SfiI endonuclease activity is strongly influenced by the non-specific sequence in the middle of its recognition site.* Nucleic Acids Res, 2001. **29**(7): p. 1476-83.

158. Chow, D.C., et al., *Ultra-high expression of a thermally responsive recombinant fusion protein in E. coli.* Biotechnol Prog, 2006. **22**(3): p. 638-46.

159. Bornhorst, J.A. and J.J. Falke, *Purification of proteins using polyhistidine affinity tags.* Methods Enzymol, 2000. **326**: p. 245-54.

160. Bessa, P.C., et al., *Thermoresponsive self-assembled elastin-based nanoparticles for delivery of BMPs.* J Control Release, 2010. **142**(3): p. 312-8.

161. Herrero-Vanrell, R., et al., *Self-assembled particles of an elastin-like polymer as vehicles for controlled drug release.* J Control Release, 2005. **102**(1): p. 113-22.

162. Clancy, B., R.B. Darlington, and B.L. Finlay, *Translating developmental time across mammalian species.* Neuroscience, 2001. **105**(1): p. 7-17.

163. Wu, H., et al., *Melatonin attenuates neuronal apoptosis through up-regulation of K(+) -Cl(-) cotransporter KCC2 expression following traumatic brain injury in rats.* J Pineal Res, 2016. **61**(2): p. 241-50.

164. Jaenisch, N., O.W. Witte, and C. Frahm, *Downregulation of potassium chloride cotransporter KCC2 after transient focal cerebral ischemia.* Stroke, 2010. **41**(3): p. e151-9.

165. Martin-Aragon Baudel, M.A., A.V. Poole, and M.G. Darlison, *Chloride co-transporters as possible therapeutic targets for stroke.* J Neurochem, 2017. **140**(2): p. 195-209.

166. Garthwaite, G., G.D. Williams, and J. Garthwaite, *Glutamate toxicity: An experimental and theoretical analysis.* Eur J Neurosci, 1992. **4**(4): p. 353-360.

167. Choi, D.W., J.Y. Koh, and S. Peters, *Pharmacology of glutamate neurotoxicity in cortical cell culture: attenuation by NMDA antagonists.* J Neurosci, 1988. **8**(1): p. 185-96.

168. Li, Y., et al., *HUMMR, a hypoxia- and HIF-1alpha-inducible protein, alters mitochondrial distribution and transport.* J Cell Biol, 2009. **185**(6): p. 1065-81.

169. Li, Y. and D.A. Rempe, *During hypoxia, HUMMR joins the mitochondrial dance.* Cell Cycle, 2010. **9**(1): p. 50-7.

170. Vemula, S., et al., *A functional role for sodium-dependent glucose transport across the blood-brain barrier during oxygen glucose deprivation.* J Pharmacol Exp Ther, 2009. **328**(2): p. 487-95.

171. Charytoniuk, D.A., et al., *Distribution of bone morphogenetic protein and bone morphogenetic protein receptor transcripts in the rodent nervous system and up-regulation of bone morphogenetic protein receptor type II in hippocampal dentate gyrus in a rat model of global cerebral ischemia.* Neuroscience, 2000. **100**(1): p. 33-43.

172. Sudhof, T.C., *alpha-Latrotoxin and its receptors: neurexins and CIRL/latrophilins.* Annu Rev Neurosci, 2001. **24**: p. 933-62.

173. Butz, S., et al., *The subcellular localizations of atypical synaptotagmins III and VI. Synaptotagmin III is enriched in synapses and synaptic plasma membranes but not in synaptic vesicles.* J Biol Chem, 1999. **274**(26): p. 18290-6.

174. Huang, J., et al., *SAROTUP: scanner and reporter of target-unrelated peptides.* J Biomed Biotechnol, 2010. **2010**: p. 101932.

175. Duchrow, T., et al., *Enhancing navigation in biomedical databases by community voting and database-driven text classification.* BMC Bioinformatics, 2009. **10**: p. 317.

Appendix 1

A Detailed and High-Yield Protocol for the Concatemerization, Expression and Purification of Marginally Soluble, Short Elastin-Like Polypeptides

Published as a supplementary protocol to "Bahniuk MS, Alshememry AK, Unsworth LD. High-yield recombinant expression and purification of marginally soluble, short elastin-like polypeptides. BioTechniques. 2016 Dec;61(6):297-304."

Appendix 1: A Detailed and High-Yield Protocol for the Concatemerization, Expression and Purification of Marginally Soluble, Short Elastin-Like Polypeptides

Markian S. Bahniuk[1,2,¶,*], Abdullah K. Alshememry[2,3,¶], Larry D. Unsworth[1,2,4,*]
1 Department of Biomedical Engineering, University of Alberta, Edmonton, Alberta, Canada
2 National Institute for Nanotechnology, National Research Council, Edmonton, Alberta, Canada
3 Faculty of Pharmacy and Pharmaceutical Sciences, University of Alberta, Edmonton, Alberta, Canada
4 Department of Chemical & Materials Engineering, University of Alberta, Edmonton, Alberta, Canada
¶ These authors contributed equally to the manuscript.
* Corresponding Authors

LEGEND

⇨ *ATTENTION*

* *HINT*

🖐 *REST*

REAGENTS

Syntheic DNA encoding for a short repeat of ELPs (Integrated DNA Technologies, Coralville, Iowa, USA)

XL10 Gold competent *Escherichia coli* cells (Agilent Technologies, Santa Clara, California, USA)

Ampicillin (ThermoFisher, Waltham, Massachusetts, USA)

Agarose for plates and electrophoresis gels (EMD Millipore, Etobicoke, Ontario, Canada)

Bacto-tryptone (BD Biosciences, San Jose, California, USA)

Yeast extract (BD Biosciences, San Jose, California, USA)

Glycerol (EMD Millipore, Etobicoke, Ontario, Canada)

NaCl (ThermoFisher, Waltham, Massachusetts, USA)

KCl (ThermoFisher, Waltham, Massachusetts, USA)

$MgSO_4$ (ThermoFisher, Waltham, Massachusetts, USA)

Glucose (ThermoFisher, Waltham, Massachusetts, USA)

Plasmid miniprep kit (Qiagen, Toronto, Ontario, Canada)

MinElute gel extraction kit (Qiagen, Toronto, Ontario, Canada)

EcoRI (New England Biolabs, Ipswich, Massachusetts, USA)

HinDIII (New England Biolabs, Ipswich, Massachusetts, USA)

NdeI (New England Biolabs, Ipswich, Massachusetts, USA)

BamHI (New England Biolabs, Ipswich, Massachusetts, USA)

BglI (New England Biolabs, Ipswich, Massachusetts, USA)

PflMI (New England Biolabs, Ipswich, Massachusetts, USA)

SfiI (New England Biolabs, Ipswich, Massachusetts, USA)

pUC19 cloning vector (Bio Basic, Markham, Ontario, Canada)

T4 DNA ligase enzyme (Invitrogen, Carlsbad, California, USA)

Ligase buffer (Invitrogen, Carlsbad, California, USA)

Antarctic phosphatase (New England Biolabs, Ipswich, Massachusetts, USA)

OneTouch BL21(DE3) competent *Escherichia coli* cells (Invitrogen, Carlsbad,
California, USA)

Glacial Acetic Acid (Sigma-Aldrich, St. Louis, Missouri, USA)

Tris-base (Invitrogen, Carlsbad, California, USA)

Ethylenediaminetetraacetic acid (EDTA) (ThermoFisher, Waltham, Massachusetts,
USA)

Ethidium bromide (Sigma-Aldrich, St. Louis, Missouri, USA)

pET-25b(+) expression vector (EMD Millipore, Etobicoke, Ontario, Canada)

Terrific broth rich media (TB) (ThermoFisher, Waltham, Massachusetts, USA)

L-proline (Sigma-Aldrich, St. Louis, Missouri, USA)

Isopropyl β-D-1-thiogalactopyranoside (IPTG) (ThermoFisher, Waltham,
Massachusetts, USA)

Copper chloride (Sigma-Aldrich, St. Louis, Missouri, USA)

40% Acrylamide:Bis Acrylamide, 29:1 Solution (Bio-Rad Laboratories, Hercules, California, United States)

Sodium dodecyl sulfate (SDS) (ThermoFisher, Waltham, Massachusetts, USA)

Ammonium persulfate (APS) (Bio-Rad Laboratories, Hercules, California, United States)

Tetramethylethylenediamine (TEMED) (EMD Millipore, Etobicoke, Ontario, Canada)

Tricine (ThermoFisher, Waltham, Massachusetts, USA)

Ammonium acetate (VWR International, Radnor, Pennsylvania, USA)

Glycine (Bio-Rad Laboratories, Hercules, California, United States)

Precision Plus Protein™ Dual Color Standards (Bio-Rad Laboratories, Hercules, California, United States)

Methanol (Sigma-Aldrich, St. Louis, Missouri, USA)

Urea (ThermoFisher, Waltham, Massachusetts, USA)

Imidazole (Sigma-Aldrich, St. Louis, Missouri, USA)

NaH_2PO_4 (EMD Millipore, Etobicoke, Ontario, Canada)

NaOH (ThermoFisher, Waltham, Massachusetts, USA)

REAGENT SETUP

Ligase buffer needs to be thoroughly mixed, aliquoted, stored frozen and used only once. Great care must be taken to thaw the ligase buffer at room temperature and mix very thoroughly to ensure any precipitants are fully resolubilized.

500 mM and 1 M Proline stock solutions are made and aliquoted to 1 mL and 10 mL, respectively and then stored frozen and used once.

Urea solutions need to be filtered and made fresh to avoid the risk of them carbamylating the ELP samples.

PROCEDURE

DESIGN AND INITIAL PROCESSING OF A NEW ELP GENE

1. Order a gene coding for 10 repeats of VPGLG (L_{10}) from a DNA synthesis company. Note that due to its length, the L_{10} was provided in the pIDTblue plasmid. The exact sequence of this gene is detailed in Supplementary Figure 1.

⇨ *ATTENTION* : The protocol will refer to the doubling of L_{10} to L_{20} and the

expression of L_{20} simply as examples. This protocol is applicable to all ELP sequences.

2. Transform the pIDTblue-L_{10} plasmid into XL10 Gold *Escherichia coli* (*E. coli*). Begin by thawing an aliquot of competent cells on ice for 20 minutes. Add 2 µL of 0.5 ng/µL plasmid to the competent cells and stir gently with a pipette tip. Incubate the cells on ice for 30 minutes, then 42°C for exactly 30 seconds, and then back on ice for 2 minutes. Add 900 µL of super optimal broth with catabolite repression (SOC) media to the cell aliquots and incubate at 37°C with 225 rpm rotation for one hour. Hold the microcentrifuge tubes horizontally in the shaking incubator to allow for better mixing. After this recovery period, plate various volumes of the cell

solution on LB agar plates supplemented with 100 µg/mL ampicillin and grow overnight at 37°C.

3. Roughly 16 hours later remove the plates from heat and store at 4°C for use in the afternoon. Pick individual colonies and grow them up in 5mL liquid cultures of LB broth and 100 µg/mL ampicillin at 37°C and 225 rpm overnight.

4. About 16 hours later remove the liquid cultures from the incubator and use a portion of the liquid culture to make glycerol stocks by combining 1mL of the resulting bacterial solution with 450 µL of sterile 80% glycerol. This can be kept at -80°C and used multiple times to generate new liquid cultures as needed.

✋ *REST:* **Once a glycerol stock is made, this is often a convenient pause point.**

These stocks can be stable for years with proper storage. This type of rest point occurs multiple times in this protocol.

5. Process the remaining liquid culture using a miniprep kit to yield a solution of purified pIDTblue-L_{10} plasmid. Measure the purity and concentration of this solution using a spectrophotometer, ideally one designed to use low sample volumes such as a NanoDrop. If yields are low, larger initial volumes of liquid culture can be used.

✋ *REST:* **Purified DNA can be frozen at -20°C for weeks without any**

deleterious effects. There are multiple places throughout this protocol where this rest point may be applied.

6. Extract the L_{10} gene from the purified plasmid by double digesting with EcoRI and HinDIII. Add 0.5 µL of each 20 U/µL enzyme to 2-3 µg of DNA in the manufacturer-recommended buffer in a final reaction volume of 20 µL and incubate at 37°C for 2 hours. Purify the gene by running the digest on a 2% agarose gel using Tris-acetate-EDTA running buffer then separate the 196 base pair (bp) band using a gel extraction kit. Kits designed to use a minimal amount of elution solution such as the Qiagen MinElute kit are recommended as they minimize sample dilution. Ethidium bromide is used to visualize sample bands in DNA gels though other options are available.

* *HINT*: **For all restriction enzyme digest reactions, be sure to add the**

enzyme(s) last and gently mix the final solution to ensure complete dispersion of the enzyme(s).

7. Prepare a pUC-19 cloning vector for the newly purified L_{10} gene. Digest 1.5-2.0 µg of the plasmid with 0.5 µL each of 20 U/µL EcoRI and HinDIII like with the pIDTblue-L_{10} plasmid and purify by running the digest on 1% agarose gel and extracting the 2635 bp linearized plasmid using a gel extraction kit.

8. Ligate the L_{10} sequence into the pUC19 vector by combining 20 fmol of insert with 10 fmol of vector, heat the DNA mixture at 65°C for 5 minutes to ensure the sticky ends are fully available, then add ligase buffer from a fresh aliquot as well as 0.5 µL of 1 U/µL T4 DNA ligase enzyme and ultrapure water to reach a final reaction volume of 10 µL. Incubate the ligase reaction at 16°C for 20 minutes. In order to

reduce the number of incorrect background colonies, add 0.5 µL of 20 U/µL BamHI

enzyme after the ligation reaction and incubate at 37°C for 10 minutes.

9. Add 2 µL of the ligase reaction to 100 µL of chemically competent XL10 gold *E.

coli* and transform as described above. Grow up multiple transformed colonies in

liquid culture and purify with a miniprep kit as mentioned previously.

10. Confirm correct insertion of L_{10} into pUC19 by isolating plasmid DNA from

multiple transformed colonies then digesting both pIDTblue-L_{10} and putative pUC19-

L_{10} plasmids with BglI and NdeI. Add 0.5 µL of 10 U/µL BglI and 0.5 µL of 20 U/µL

NdeI enzymes to about 750 ng of DNA, in supplier-recommended buffer conditions

for a final reaction volume of 20 µL and incubate at 37°C for 1 hour. When run on an

agarose gel, a successful pUC19-L_{10} vector will result in plasmid fragments of 67,

334, 1051 and 1379 bp. An unmodified pUC19 would digest into fragments of 62,

1056 and 1568 bp. pIDTblue-L_{10} would show a banding pattern of 178, 212, 1276

and 1436 bp.

RECURSIVE DIRECTIONAL LIGATION (RDL)

11. Prepare the pUC19-L_{10} vector for RDL by digesting 1.5-2.0 µg of it with 0.5 µL

of 10 U/µL PflMI restriction enzyme in the recommended buffer conditions with a

final volume of 20 µL for 4 hours at 37°C. The L_{10} insert is prepared in the same

fashion except that the DNA is digested with both 10 U/µL PflMI and 10 U/µL BglI.

12. Purify the vector using a 1% agarose gel electrophoresis followed by a gel

extraction. A correct vector digest yields one band on the DNA gel corresponding to

the size of the vector as opposed to an uncut vector which will run smaller than its actual length.

13. Redigest the purified linear vector with PflMI as described above to minimize the amount of uncut vector present in the sample. No agarose gel purification or extraction is necessary after this second restriction digest.

14. To abate the amount of vector reclosure during the upcoming ligation reaction, the vector DNA can be dephosphorylated so that it cannot be ligated closed on itself. Treat the twice-digested vector with Antarctic phosphatase. Add 2.3 µL of the provided 10X buffer to the 20 µL digest reaction along with 1 µL of the 5U/µL phosphatase enzyme. Incubate this reaction at 37°C for one hour then 65°C for 5 minutes to inactivate the phosphatase.

15. Purify and extract the insert similarly to the vector, but using a 2% gel. The insert digest contains multiple fragments, with bands of 170, 1118 and 1371 bp corresponding to vector fragments. In the case of L_{10}, the DNA fragment of interest had a molecular weight of 165 bp. Do not dephosphorylate the insert.

16. Ligate the linearized and dephosphorylated pUC19-L_{10} with the L_{10} gene insert using an insert:vector ratio of 50:10 fmol. We have found that this ratio does allow for the occasional double insertion which may be useful in some RDL situations. Heat the DNA mixtures at 65°C for 5 minutes to ensure the sticky ends of the sequences are open for ligation to one another. Afterwards, add ligase buffer from a freshly thawed aliquot in addition to 0.5 µL of 1U/µL T4 DNA ligase and ultrapure water to bring the reaction to a final volume of 10 µL. Allow the ligation reaction to proceed for 20 minutes at 16°C.

17. Use the ligation reaction to transform 100 µL of XL10-gold cells as described in step 2 in the "Initial Processing of a New ELP Gene" section.

18. In addition to the ligation reaction above, control reactions can be set up periodically to assess the number of vector-only transformations that may otherwise obscure the correct clones resulting from RDL. One of these controls involved replacing the insert and ligase with water to estimate how much of the pUC19-L_{10} remained uncut through the vector preparation procedure. Another control only replaces the insert with water to examine the degree of vector reclosure in the ligation reaction.

19. Grow up some of the resulting bacterial colonies in 5 mL liquid cultures with 100 µg/mL ampicillin at 37°C and 225 rpm overnight and collect the plasmids using a miniprep kit. In order to screen the DNA for correct oligomerization of the L_{10} gene into L_{20}, digest roughly 750 ng of the plasmids with 0.5 µL each of 10 U/µL PflMI and BglI in a final reaction volume of 20 µL at 37°C for one hour then separate the fragments by 2% agarose electrophoresis. A successful RDL reaction resulting in L_{20} is illustrated by an apparent doubling of the length of the ELP gene from 165 to 330 bp. This result is illustrated in Figure 1.

20. Once correct clones have been identified, glycerol stocks can be made of them as described in Step 4 of the "Initial Processing of a New ELP Gene" section.

21. From this point on the RDL procedure can be repeated using the pUC19-L_{20} for further concatemerization.

EXPRESSION VECTOR MODIFICATION

22. Digest roughly 2 µg of expression plasmid pET-25b(+) with 0.5 µL each of 20 U/µL EcoRI and NdeI in EcoR1 buffer in a final reaction volume of 20 µL at 37°C for 4 hours. The digest can be confirmed by running a portion on a 0.8% agarose gel. This plasmid digestion does not require purification due to a post-ligation restriction digest detailed below.

23. Our modifying sequence was of sufficient length that it could only be obtained as part of a plasmid and is referred to as pIDT-mod. As such, upon its receipt it should be first transformed into XL10-Gold cells as detailed in Step 2 of the "Initial Processing of a New ELP Gene" section. The sequence of the expression vector modifier is given in Supplementary Figure 2.

24. Grow up a successfully transformed colony of pIDT-mod in 5mL of LB with 100 µg/mL ampicillin at 37°C and 225 rpm overnight and extract and purify the plasmid using a Qiagen miniprep kit.

25. Digest approximately 4 µg of the purified pIDT plasmid using 0.5 µL each of 20 U/µL EcoRI and NdeI in EcoR1 buffer in a final reaction volume of 20 µL at 37°C for 4 hours.

26. Separate the digest reactions on a 2% agarose gel and collect the 293 bp band using a gel extraction kit.

27. Combine the linearized vector and insert at a 20:10 fmol insert:vector ratio and heat at 65°C for 5 minutes. Use 0.5 µL of 1U/µL T4 DNA ligase, ligase buffer and ultrapure water to a final volume of 10 µL. Allow the ligation reaction to proceed at 16°C for 20 minutes. After the ligation, add 0.5 µL of 20 U/µL BamHI and incubate

the solution at 37°C for 10 minutes. This "killer cut" serves to cleave only DNA with the original undesired EcoRI to NdeI sequence present in pET-25b(+). This effectively eliminates the generation of *E. coli* colonies containing the original vector, as any remaining pET-25b(+) will be linearized and thus will not be able to transform *E. coli* whereas the modified expression vector lacks a BamHI cut site and will remain circular.

28. Use 2 µL of the ligation reaction to transform 100 µL of XL10-gold cells as described previously in step 2 of the "Initial Processing of a New ELP Gene" section.

29. To screen for correct expression vector modification, perform BamHI and SfiI single digest reactions. Collect plasmid from the previous transformation by growing up individual colonies in 5mL liquid culture with 100 µg/mL ampicillin at 37°C and 225 rpm overnight and collect the plasmids using a miniprep kit. Digest about 500ng of plasmid using either 0.5 µL of 20 U/µL BamHI at 37°C or by 0.5 µL of 20 U/µL SfiI at 50°C in the manufacturer-recommended buffer for 1 hour. BamHI will not cut the correctly modified plasmid and SfiI should linearize the majority of it. For the original pET-25b(+), the opposite is true.

⇨ *ATTENTION*: SfiI digests must be carried out at the non-standard reaction

temperature of 50°C. The enzymatic activity at 37°C is greatly reduced. This applies to all SfiI reactions in the protocol.

CLONING AN ELP GENE INTO A MODIFIED EXPRESSION VECTOR

30. Digest 1.5-2.0 µg of the modified expression vector with 0.5 µL of 20 U/µL SfiI enzyme in the recommended buffer up to a final volume of 20 µL for 4 hours at 50°C.

Note that this enzyme requires a non-standard incubation temperature for full activity. This reaction can be done multiple times in parallel to increase the final yield of the linearized plasmid.

31. Run the digest reaction on a 0.8% agarose gel to separate the linearized vector from the undigested vector and SfiI recognition site spacer sequence. Extract the 5530 bp band representing the linearized modified expression using a gel extraction kit.

32. Redigest the extracted DNA with SfiI again using the same conditions as Step 30. No agarose gel electrophoresis or extraction is necessary after this second digest. This additional digest step will significantly decrease the likelihood of getting incorrect clones after transformation with the ELP gene.

33. Dephosphorylate the doubly-digested vector using Antarctic phosphatase to significantly reduce the likelihood of reclosed vector clones. 2.3 µL of the 10X dephosphorylation buffer is added to the 20 µL SfiI digest reaction along with 1 µL of the 5 U/µL phosphatase enzyme. Incubate this reaction at 37°C for one hour then 65°C for 5 minutes in order to inactivate the phosphatase.

34. Prepare the ELP insert by first digesting about 4 µg of the pUC-L$_{20}$ plasmid with 0.5 µL each of 10 U/µL PflMI and BglI using manufacturer-recommended buffer conditions in a final reaction volume of 20 µL at 37°C for 4 hours. This reaction can be done multiple times in parallel to increase final yields.

35. Purify the ELP insert by running the digest reaction on a 2% agarose gel. This gel percentage may change depending on the size of the ELP gene. The digestion will yield multiple bands. Bands of 170m 118 and 1371 bp are fragments of the pUC

vector and should not be isolated. The L_{20} gene will present as a band at 330 bp. Collect this band from the gel using a gel extraction kit.

36. Ligate the ELP L_{20} gene and modified expression vector together using a 50:10 fmol ratio. The ligation and transformation procedure is identical to that of steps 16 and 17 of the "Recursive Directional Ligation" procedure above except that between the ligation and transformation steps include a killer cut using SfiI. Add 0.5 µL of 20 U/µL SfiI enzyme to the ligation reaction and incubate at 50°C for 10 minutes to reduce the number of vector-only colonies. This killer cut will linearize remaining modified expression vector plasmids which would otherwise result in false positive transformants.

37. Screen the colonies produced by the ligation and transformation procedure by NdeI and EcoRI double digest. Begin by growing the colonies in 5 mL LB with 100 µg/mL ampicillin overnight at 37°C and 225 rpm. Extract the DNA using a miniprep kit. Digest about 750 ng of each plasmid with 0.5 µL each of 20 U/µL NdeI and EcoRI in the manufacturer recommended buffer and a final reaction volume of 20 µL at 37°C for 1 hour.

38. Run the resulting DNA fragments using agarose gel electrophoresis. For the L_{20} gene the DNA fragment that would confirm successful ligation would be 407 bp. A 2% agarose gel would be appropriate for these conditions. Longer ELP constructs would result in larger bands which may require a lower percentage agarose gel. The other DNA fragment that is generated is 5453 bp in length. If a colony contains a modified expression vector (*ie.* an empty vector clone) then an NdeI and EcoRI double digest will result in bands of 293 and 5453 bp.

TRANSFORMING *E. coli* BL21(DE3) WITH AN ELP EXPRESSION PLASMID

39. Thaw one 50 µL aliquot of OneTouch BL21 (DE3) *E. coli* cells on ice for 20 minutes. Meanwhile, dilute a solution of purified ELP expression plasmid to 10 ng/µL. After the cells are thawed, add 2 µL of this plasmid solution to and stir gently using the pipette tip. Thaw the cells on ice for 20 minutes before adding the DNA. Incubate the cells and DNA on ice for a minimum of 30 minutes then heat shock at 42°C for exactly 30 seconds. Leave the cells on ice for 2 minutes to recover then add 900 µL of SOC media and incubate the cells at 37°C and 225 rpm for one hour. Plate various volumes of the cell solution on LB plates containing 100 µg/mL ampicillin and grown overnight at 37°C.

40. The next morning remove the plates from the heat and leave at 4°C. Grow liquid cultures using 5mL of LB with 100 µg/mL ampicillin at 37°C and 225 rpm overnight, purify the plasmid using a Qiagen miniprep kit and send the resulting DNA for sequencing. Use standard T7 promoter and terminator primers for Sanger sequencing. Given the highly repetitive and GC-rich DNA sequences of the ELP gene, the PCR reaction may require modifications to work properly. The sequencing reactions and any necessary adjustments in the PCR reaction were addressed by the Molecular Biology Service Unit at the University of Alberta.

41. Once correct clones have been identified, glycerol stocks can be made up as in Step 4 of the "Initial Processing" section.

ELP EXPRESSION

42. In the afternoon, prepare a starter culture of 50 mL of terrific broth media (TB) containing 50 µL of 100 mg/mL ampicillin (100 µg/mL final concentration) and 1 mL of 500 mM proline (10 mM final concentration) by adding filter sterilized ampicillin and proline to autoclaved and cooled TB. Inoculate from previous glycerol stock using sterile disposable inoculating loop.

43. Incubate in a shaking incubator at 37°C, 225 rpm for ~16 hours.

44. The next morning use the starter culture to inoculate 1 L of rich TB media supplemented with 10 mL of 1 M proline (10 mM proline final concentration) and 1 mL of 100 mg/mL ampicillin (100 µg/mL final concentration) by adding filter sterilized ampicillin and proline to autoclaved and cooled TB. Then incubate at 37°C to an optical density at 600nm (OD_{600}) of 0.8.

45. Induce cell expression using 1 mL of 2 M Isopropyl β-D-1-thiogalactopyranoside (IPTG) (2m M final concentration) then incubate at 37°C, 225 rpm for 24 hours.

46. Collect cell pellet by centrifugation at 3000 g at 4°C, for 20 mins. Discard the supernatant and weigh the wet pellet then store it at -80°C until further use.

✋ *REST:* **The bacterial pellets can remain frozen for a few months with no side effects.**

DENATURING POLYACRYLAMIDE GEL ELECTROPHORESIS (SDS-PAGE)

47. To make the 20% separating gel layer, mix 5 mL of 3M Tris, 0.4% SDS, pH 8.45 with 7.6 mL of 40% acrylamide (acrylamide/bis-acrylamide 29:1 ratio). Also add 3 g of glycerol then add 12.4 mL of Milli-Q water. Ensure the glycerol is well-mixed by

inverting the tube several times. Just before pouring the gel add 50 µL of 10%

ammonium persulfate and 20 µL of tetramethylethylenediamine (TEMED). Then

immediately pour the mixture in the casting frame and allow it to solidify for 45

minutes. These volumes are sufficient to produce four gels using the Bio-Rad Mini-

Protean Tetra Cell system and may need to be adjusted for other gel equipment.

48. To make the 5% stacking gel layer, mix 1.25 mL of 3M Tris, 0.4% SDS, pH 8.45

with 625 µL of 40% acrylamide (acrylamide/bis-acrylamide 29:1 ratio). Then add 3.1

mL of Milli-Q distilled water. Invert the tube several times to ensure even mixing.

Immediately before casting the stacking gel add 23 µL of 10% ammonium persulfate

and 10 µL of TEMED. Then immediately pour the mixture in the casting frame and

allow it to solidify for 45 minutes.

49. Once the gel has run to completion (typically the gel is stopped when the sample

dye runs off the bottom of the gel) transfer the gel to a container and wash with an

excess of MilliQ water twice for 5 minutes each with rocking.

50. Incubate the gel for 10 minutes in 50-100 mL of 0.19M Tris, 0.1% SDS buffer at

pH 8.8 with rocking.

51. After discarding the buffer, pour 50 mL of 0.3M $CuCl_2$ on the gel and incubate

for 10 minutes with rocking.

52. Dispose of the copper solution then wash the gel again with an excess of MilliQ

water twice for 5 minutes each.

METAL AFFINITY CHROMATOGRAPHY

53. Prepare a fresh and filter sterilized denaturing lysis solution (8 M urea, 10 mM Tris, 115 mM monosodium phosphate, pH 8.0) and denaturing washing solution (8 M urea, 10 mM Tris, 115 mM monosodium phosphate, pH 6.3).

* *HINT*: **Keep these solutions warm in order to increase the dissolution rate of the solid urea.**

54. Thaw the cell pellets by immersing them in water at room temperature.

55. Add 25 mL of lysis buffer, ensuring complete resuspension of the pelleted *E. coli*.

56. Incubate the lysis reaction at room temperature with rocking for 1 hour. Then incubate at 4°C for 30 minutes with rocking to allow time for any ELPs to fully solubilize.

57. During the incubation period, equilibrate a 1.5 mL Ni-NTA column by washing with 1.5 column volumes of MilliQ water followed by washing with 1.5 column volumes of denaturing lysis solution.

58. Transfer solution of lysed cells to an appropriate centrifuge tube and spin at 20,000 g, 4°C for 30 min.

59. Decant the crude soluble lysate into a new tube then filter sterilize it to remove any small insoluble particles. Remove and save a 50 μL sample for SDS-PAGE analysis.

60. Transfer the nickel beads into the soluble lysate tube.

61. Incubate the lysate and nickel beads at 4°C with rotation or rocking overnight.

62. Start the next day by making the buffered imidazole solutions (31 mM, 62 mM, 125 mM, 250 mM, 500 mM, 2 M) using 25 mM Tris, 50 mM NaCl buffer at pH 8.0.

63. Ideally in a 4°C cold room, transfer the soluble lysate and column material mixture back into the nickel column, being careful to recollect as much of the column material as possible.

64. Add three column volumes of denaturing wash solution and keep the flow through for SDS-PAGE analysis. This should be done at room temperature to avoid urea crystallization in the wash solution. This wash should be repeated a total of two times.

65. Move the column back into the cold room (if applicable) and repeat the same wash procedure three times using 25 mM Tris, 50 mM NaCl buffer at pH 8.0. This serves to both wash the protein on the column and remove the urea from the previous lysis and wash solutions.

66. Begin the elution by adding two column volumes of 31 mM buffered imidazole and collect the flow through. Repeat the elution step using progressively higher imidazole concentrations such as 62 mM, 125 mM, 250 mM, 500 mM and 2 M. This is most useful when first processing an unfamiliar ELP. Once it is known what imidazole concentration(s) elute the ELP, the gradient approach may not be necessary.

67. After elution samples are collected, keep them at 4°C until further purified using

ITC. Sample eluents processed on SDS-PAGE can be seen in Figures 2 and 3.

INVERSE TEMPERATURE CYCLING (ITC)

68. Run the nickel chromatography eluents on SDS-PAGE and choose those with

relatively strong ELP bands for ITC purification. Depending on the construct, simply

warming the various eluents to 37°C may cause those containing ELP to turn cloudy.

While this is a convenient alternative, running eluents on SDS-PAGE is a much better

method of identifying ELP-containing eluents but will require more time. This may

be unfavourable for solution-unstable constructs.

69. Before combining the eluents, save 50 μL from each for SDS-PAGE analysis.

70. Combine ELP-containing eluents then induce the ELP transition by incubating the

solution at 37°C water bath for 15 minutes. Again, depending on the ELP construct

being produced, a higher temperature and/or supplementary NaCl may be necessary

to trigger the ELP phase transition. This may require some experimentation for new

constructs. Figures 2 and 4 illustrate the visual change that may be observed for ELPs undergoing assembly.

71. Transfer samples from the water bath to a pre-warmed centrifuge and immediately spin them down at 20,000g at 37°C for 15 minutes. Collect the soluble fraction and replace it with equivalent volume of pre-chilled phosphate-buffered saline (PBS), pH 7.4. Lower volumes could be used if concentrating the sample is desired.

* *HINT:* **The ELP pellet may not be visible in all cases.**

72. Resuspend the ELP pellets using bath sonication on ice for 30 minutes to ensure maximal pellet resuspension and ELP resolubilization.

73. After sonication, transfer samples immediately to a pre-chilled centrifuge and spin them down at 20,000 g at 4°C for 15 min. Transfer the ELP-containing supernatant to a clean tube and then resuspend any remaining pellet in pre-chilled PBS. It can be useful to screen the final pellet on SDS-PAGE to see if any ELP was not solubilized or if any contaminating protein carried over.

* *HINT:* **It may be possible in some circumstances to recover more ELP from the sample tube by repeating the resuspension step. However, any additional ELP will likely be significantly more dilute than the first resuspension.**

74. Run samples on SDS-PAGE to assess their purity. If one round of ITC isn't sufficient, repeat a second round of ITC. If the ELPs were concentrated during the

first round of ITC, the temperature and amount of NaCl necessary to trigger the phase transition may be decreased. Note: Since the phase transition can be triggered at room temperature for some ELP constructs, samples should be kept in ice as often as possible. Sample results demonstrating a successful ITC purification can be seen in Figure 3.

75. Determine the ELP product concentrations based on their absorbance at 280 nm. Dilute the ELP solutions as necessary to ensure they will not become cloudy during the absorbance measurement. The Beer-Lambert law can be used to convert absorbance at 280 nm to protein concentration in conjunction with an extinction coefficient calculated using the ProtParam tool from ExPASy. Note that other conventional protein quantification methods may not be applicable to ELPs due to the assays being dependent upon side chain chemistries. ELPs have significantly fewer reactive side chains than common standard curve proteins such as bovine serum albumin or immunoglobulin G so these methods would significantly underestimate the concentration of ELP solutions.

76. Aliquot samples into small volumes then immediately flash freeze them with liquid nitrogen then store at -80 °C.
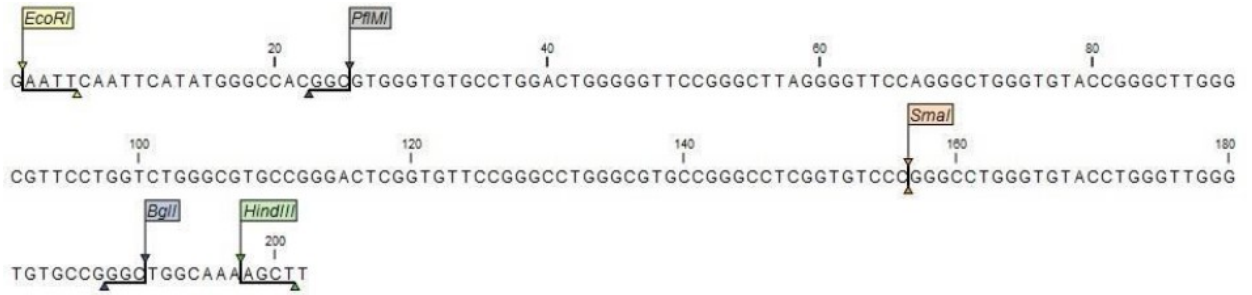
FIGURES

Figure Appendix 1. 1 Sequence of an elastin-like polypeptide gene encoding (VPGLG)₁₀.

This sequence is used as the basis for recursive directional ligation (RDL) showing all the relevant restriction enzyme cut sites necessary for cloning and gene concatemerization.
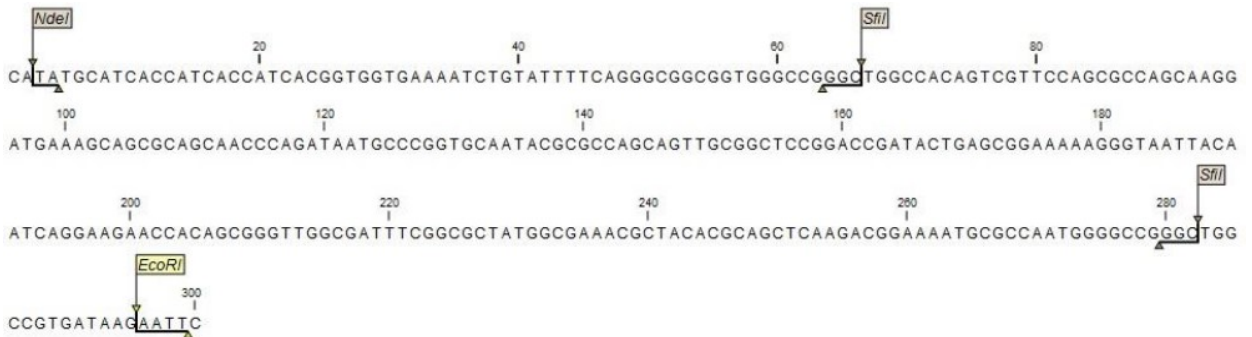

Figure Appendix 1. 2 Sequence of the expression vector modifying DNA sequence.

This DNA sequence shows the relevant restriction enzyme sites for modification of the expression vector and insertion of the ELP gene. Note that the DNA sequence between the two SfiI cut sites is purified away and does not end up in the final ELP gene but is vital for efficient SfiI cleavage.

RECIPIES

Super Optimal Broth with Catabolite Repression (SOC) (100 mL)

Ingredient	Volume	Final Concentration
Tryptone	2 g	2% (w/v)
Yeast Extract	0.5 g	0.5% (w/v)
NaCl	0.05 g	10 mM
250 mM KCl	1 mL	2 mM
ddH$_2$O	98 mL	N/A

Adjust pH to 7.0

Add dd H$_2$O to a final volume of 100mL

Autoclave and allow to cool to less than 50°C

Add sterilized MgCl$_2$ and glucose

1 M MgCl$_2$	1 mL	10 mM
2 M glucose	1 mL	20 mM

Terrific Broth (TB) (1 L)

The sterile potassium phosphate solution must be added after the rest of the media

has been autoclaved

Tryptone	12 g	1.2% (w/v)
Yeast Extract	24 g	2.4% (w/v)
Glycerol	4 mL	0.4% (v/v)

Add ddH$_2$O to a final volume of 900 mL

Autoclave and allow to cool

Add 100 mL of potassium phosphate solution

Potassium phosphate solution for TB (100 mL)

K_2HPO_4	12.5 g	0.72 M
KH_2PO_4	2.3 g	0.17 M

Dissolve in ddH_2O to a final volume of 100 mL and autoclave

Copper Staining Buffer for SDS-PAGE (1 L)

Tris base (or acid)	23.0 g (29.9 g)	0.19M	10% SDS	10 mL
	0.1% (w/v)			

Use either tris base or acid-not both

Add ddH_2O to a final volume of ~990 mL

Adjust solution pH to 8.8

Add ddH_2O to a final volume of 1 L

10% Sodium Dodecyl Sulfate (SDS) (100 mL)

SDS	10 g	10% (w/v)

Add ddH_2O to a final volume of 100 mL

Denaturing Lysis Solution (125 mL)

*The urea will dissolve much faster if the solution is heated

Urea	60.1 g	8 M
$NaH_2PO_4 \cdot H_2O$	1.73 g	100 mM

Tris base   0.15 g   10 mM

Add ~80mL H_2O

Adjust pH to 8.0

Add H_2O to a final volume of 125 mL

Filter sterilize

Denaturing Wash Solution (125 mL)

* *The urea will dissolve much faster if the solution is heated*

Urea   60.1 g   8 M

$NaH_2PO_4 \cdot H_2O$ 1.73 g   100 mM

Tris base   0.15 g   10 mM

Add ~80mL H_2O

Adjust pH to 6.3

Add H_2O to a final volume of 125 mL

Filter sterilize

25 mM Tris, 50 mM NaCl Buffer (200 mL)

Tris base   606 mg   25 mM

NaCl   584 mg   50 mM

Add dd H_2O to a final volume of ~190 mL

Adjust pH to 8.0

Add dd H_2O to a final volume of 200 mL

Filter sterilize

TROUBLESHOOTING

-Inefficient restriction enzyme cleavages:

Prepare DNA using XL10 Gold *E. coli* or non-methylating cell lines such as GM2929.

Prepare multiple parallel digests to increase the total amount of digested DNA.

-Insufficient amounts of purified DNA after agarose gel extractions:

Ensure gel extraction kit and procedure is working properly.

Perform multiple parallel digests and serially elute the products with the extraction kit.

-No colonies after cloning:

Ensure correct antibiotics were used on the agarose plates.

Double check DNA molar ratios are correct.

Check that only the vector DNA was dephosphorylated.

Make sure the phosphatase enzyme is deactivated completely.

Confirm transformation procedure is working.

Confirm ligase enzyme and buffer are working.

-Many colonies after cloning but few or none contain the insert of interest:

Confirm vector DNA has been linearized correctly.

Ensure phosphatase enzyme is working properly.

Ensure DNA molar ratios are correct.

-No or poor expression levels:

Confirm DNA sequence is correct.

Ensure ELP is not in the insoluble cell lysate and unintentionally discarded before purification.

Vary expression conditions including induction, OD_{600}, expression time and expression temperature to optimize ELP expression levels.

-Poor metal-affinity purification results:

Confirm ELP expression.

Ensure matrix is clean and/or charged.

Increase binding time.

Consult the QIAexpressionist manual for further suggestions.

-Additional ELP is present in the urea washes:

Nickel column may be saturated. Consider using a larger column volume.

Add ~3 mM imidazole to lysis and wash buffers to reduce nonspecific binding.

-Incomplete resolubilization of purified ELP during the ITC procedure:

Proper temp for cold spin

ELP may be too concentrated. Dilute before heating to trigger phase transition.

-ELP separates out of solution despite storing at 4°C:

Store flash frozen immediately upon purification.

Dilute ELP to lower concentration before storage at 4°C.

-Sample for A_{280} measurements turn cloudy:

Dilute sample further before taking measurements.

EQUIPMENT

DNA electrophoresis tank (VWR International, Radnor, Pennsylvania, USA)

UVP ChemDocIt T52 gel imaging system (UVP, Upland, California, USA)

Shaking incubator for liquid cell culture (New Brunswick Scientific, Edison, New Jersey, USA)

Variable temperature heat block/water bath (VWR International, Radnor, Pennsylvania, USA)

Pipettors for handling down to 0.5µL liquid volumes and disposable tips (VWR International, Radnor, Pennsylvania, USA)

Nanodrop spectrophotometer (ThermoFisher, Waltham, Massachusetts, USA)

MilliQ lab water system (EMD Millipore, Etobicoke, Ontario, Canada)

BioMate 3 UV spectrophotometer (ThermoFisher, Waltham, Massachusetts, USA)

Temperature-controlled high-speed centrifuge (Eppendorf, Hamburg, Germany)

Ni-NTA Superflow Columns (Qiagen, Toronto, Ontario, Canada)

Thermo Barnstead Labquake™ Tube Shaker/Rotators (ThermoFisher, Waltham, Massachusetts, USA)

Rapid-flow filters (ThermoFisher, Waltham, Massachusetts, USA)

Water bath (ThermoFisher, Waltham, Massachusetts, USA)

Branson 2800 Ultrasonic Cleaner (Branson Ultrasonics, Danbury, Connecticut, United States)

Mini-PROTEAN® Tetra Cell (Bio-Rad Laboratories, Hercules, California, United States)

EQUIPMENT SETUP

Before use, drain the storage solution from the nickel-NTA columns then was them two times with twice the column volume of ultrapure water, then twice with twice the column volume of denaturing wash buffer.

Wash nickel columns after use by incubating them with 0.5 M NaOH for 30 min, then drain the column and add the storage solution and keep at 4°C.

During the ITC procedure, pre-heating and pre-chilling the centrifuge in advance is essential to ensure the centrifuge reaches the appropriate temperature.